

Assessment of podocyte injury using two novel glomerular markers

Inauguraldissertation

zur

Erlangung der Würde eines Doktors der Philosophie

vorgelegt der

Philosophisch-Naturwissenschaftlichen Fakultät

der Universität Basel

VON

Valérie DUBOST

aus

Frankreich, Bartenheim

Basel, 2017

Originaldokument gespeichert auf dem Dokumentenserver der Universität Basel
edoc.unibas.ch

Genehmigt von der Philosophisch-Naturwissenschaftlichen Fakultät

auf Antrag von

Prof. Dr. Alex Odermatt

Dr. med. Pierre Moulin

Prof. Dr. med. Luigi Terracciano

Basel, September 20th, 2016

Prof. Dr. J. Schibler
Dekan

Acknowledgements

I would like to thank Dr. Pierre Moulin and Prof. Dr. Alex Odermatt for their support and advices during the entire thesis.

I am grateful to the Novartis Preclinical Safety Management (Page Bouchard, Salah-Dine Chibout and André Cordier) for giving me the opportunity to conduct my research and providing the resources for my thesis.

Many thanks to my colleagues Daniel Stiehl and Elaine Tritto for advising with the genomic profiling analysis as well as Willi Frieauff and Arno Doelemeyer for sharing their image analysis expertise.

A special thanks to Emre Cörek who developed the fingerprint analysis, successfully applied in this work.

I would further like to thank to David Feldman and Mauricio Avigdor for their support and assistance with the animal models.

I would like to express my warmest gratitude towards Magdalena Westphal, Magali Jivkov for being a big help in preparing tissue sections and stainings, and Katy Darribat and Walyd Khenoussi for their patience with the dissection of the glomeruli. My special thanks to Virginie Riebel and Marianne Uteng, who offered their expertise with the cell cultures and implementation of the podocytes culture.

Last but not least I would like to thank Diethilde Theil for the critical review of the manuscript and providing a very accurate view on science.

Assessment of podocyte injury using two novel glomerular markers

Table of Contents

Acknowledgements	3
1. Summary	7
2. Introduction	8
2.1 Functional anatomy of the nephron and glomerulus	8
2.2 Podocytes alteration and proteinuria	13
2.3 An approach to better characterize podocytes lesions	18
3. Animal models with proteinuria	20
3.1 Model of albumin overload	21
3.2 Model of immune deposition nephrotoxicity	22
3.3 Model of drug-induced nephrotoxicity	23
3.3.1 Glomerular toxicant	23
3.3.1 Tubular toxicant	24
4. Material and Method	25
4.1 Method for Laser capture microdissection of glomeruli	25
4.2 GeneChip® arrays process	25
4.3 Method for GeneChip® arrays analysis	26
4.4 Animal study design for Rat albumin overload model	27
4.5 Animal study design for rat Passive Heymann nephritis model	27
4.6 Animal study design using nephrotoxicants	28
4.7 Normal tissue for localization	28
4.8 Immunohistochemistry	29
4.9 <i>In situ</i> hybridization	30
4.10 Immunohistochemistry and <i>in situ</i> hybridization on frozen tissues	31

4.11	Image analysis	32
4.11.1	Scanning of slides and detection of kidney sections	32
4.11.2	The image analysis platform	32
4.11.3	Optical density of ISH signal in glomeruli.....	33
4.12	Method for culture of primary podocytes.....	34
4.12.1	Drug treatment of the primary culture of rat podocytes	35
4.12.2	Characterization of the primary podocytes using immunofluorescence	37
4.13	Dosage of urinary proteinuria or albuminuria	38
4.13.1	Albumin overload and PHN studies	38
4.13.2	Puromycin aminonucleoside (PAN) and Cisplatin studies	38
4.14	Method for the fingerprint analysis.....	39
5.	RESULTS.....	40
5.1	Identification of glomerular specific markers.....	40
5.1.1	Role and function of Semaphorin 3G.....	44
5.1.2	Role and function of Cystatin C.....	46
5.1.3	The tubular injury marker KIM-1	47
5.2	Expression of Sema3G, CYTC and KIM-1 in normal kidney.....	49
5.2.1	Embryonic expression of Sema3G and CYTC	49
5.2.2	Expression of Sema3G in rat adult normal kidney.....	51
5.2.3	Expression of CYTC in rat adult normal kidney	53
5.2.4	Expression of KIM-1 in rat adult normal kidney.....	56
5.3	Cross-species expression of Sema3G and CYTC.....	57
5.3.1	Localization of Sema3G in kidney of mouse / dog / monkey / human.....	57
5.3.2	Localization of CYTC in kidney of mouse / dog / monkey / human	58
5.4	Expression of Sema3G and CYTC in rat models of podocytes injuries.....	62
5.4.1	Results of the Albumin overload model	62
5.4.2	Results of the Passive Heymann nephritis model.....	71
5.4.3	Results of the nephrotoxicity models	78
5.5	<i>In vitro</i> studies using toxicant	97
5.6	Comparative summary of the animal models results.....	110
6.	Discussion.....	111

6.1	Sema3G as marker of podocyte adaption and injury	112
6.2	Cystatin C as marker of podocyte injury	114
6.3	A tubular injury marker associated to podocyte injury evaluation	116
6.4	A pattern of tissue injury to explore glomerular damages?	118
7.	Future outlook	121
8.	Conclusion	123
9.	Supplementary data	124
10.	Bibliography	134
11.	Curriculum Vitae of Valérie DUBOST	140

1. Summary

The glomerular filtration barrier is an efficient filtration system, which ensures proper function of the kidney by avoiding proteinuria. At the same time, this barrier is also the most vulnerable component of the kidney. The podocyte, a terminal differentiated cell, is the key player in maintaining integrity. Most of the kidney diseases initiate from injuries of the podocytes, which lead to effacement with slit diaphragm disruption, followed ultimately by cell detachment and loss. Such a lesion can only be detected by electron microscopy.

The goal of the present work was to identify early marker(s) of podocyte injury, which are uniquely expressed in these cells and are very sensitive to stress or any other type of insults. With such marker at hand, early evaluation of podocyte injury and disease progression to the entire nephron can be explored.

By applying gene expression profile analysis on laser capture microdissected glomeruli two novel podocytes markers, Semaphorin-3G (Sema3G) and Cystatin C (CYTC) could be identified. Their specific expression in podocytes was further confirmed by the use of *in situ* hybridization and immunohistochemistry on rat kidney tissue sections.

In a next step, modulation of Sema3G and CYTC was further assessed in models of podocyte injury (functional and structural impairment and drug-induced toxicity models).

Sema3G is a very sensitive marker to podocyte adaption and injury, which was down regulated in all animal models tested except functional injury model. In the opposite, CYTC was upregulated only in the drug-induced toxicity model.

By combining the *in situ* localization of these newly characterized markers with the well validated kidney injury molecule -1 (KIM-1), it was possible to follow the sequence of events from early podocyte injury to entire proximal tubule damage. Hence, this represents a valuable tool for exploring the pathogenesis of glomerulopathy.

2. Introduction

1.1 Functional anatomy of the nephron and glomerulus

The urinary system is composed of a pair of kidneys and ureters, the bladder, and the urethra. This system accomplishes a variety of functions contributing to maintain body homeostasis.

The role of the kidneys is to excrete water-soluble metabolites (e.g. urea) and regulate the fluid and electrolyte balance of the body. They are the site of production of renin, a hormone and enzyme that participates to the regulation of the blood pressure by cleaving the circulating angiotensinogen into angiotensin I. The kidneys also produce erythropoietin, a cytokine that stimulates the production of erythrocytes.

Anatomically, the kidney is composed of a cortex and a medulla that are further divided into sub parts. The functional unit of the kidney is the nephron and is composed of the following elements:

- renal corpuscle
- proximal convoluted tubule
- thin and thick limbs of the nephron loop (loop of Henle)
- distal convoluted tubule
- collecting tubule

An illustration is shown in Figure 1.

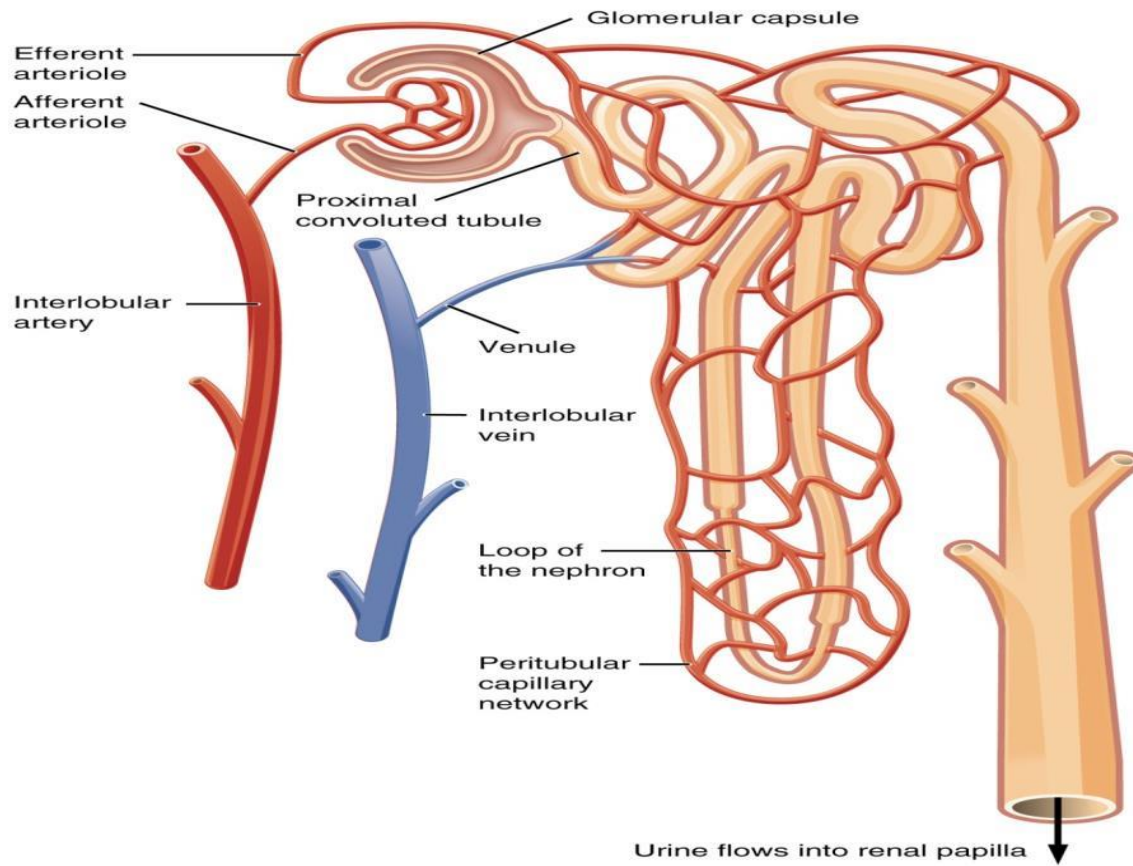


Figure 1: The structure of kidney nephron. Source: “Blood Flow in the Nephron” by Phil Schatz. License: CC BY 4.0 or Wikipedia, the free encyclopedia.

The nephron is starting with a structure called the renal corpuscle which is the initial blood-filtering unit and is composed of two parts: the glomerulus and the Bowman’s capsule. The glomerulus is a tuft of small blood vessels (capillaries) and is inserted into the Bowman’s capsule. The inner layer (visceral layer) of the capsule closely envelops the glomerular capillaries and is composed of highly specialized epithelial cells called podocytes (Figure 2), whereas the outer layer (parietal layer) consists of a simple squamous epithelium supported externally by a basal lamina and a thin layer of reticular fibers. Between the two capsular layers is the urinary space (also called the capsular space) which receives the fluid filtered through the capillary wall and the visceral layer.

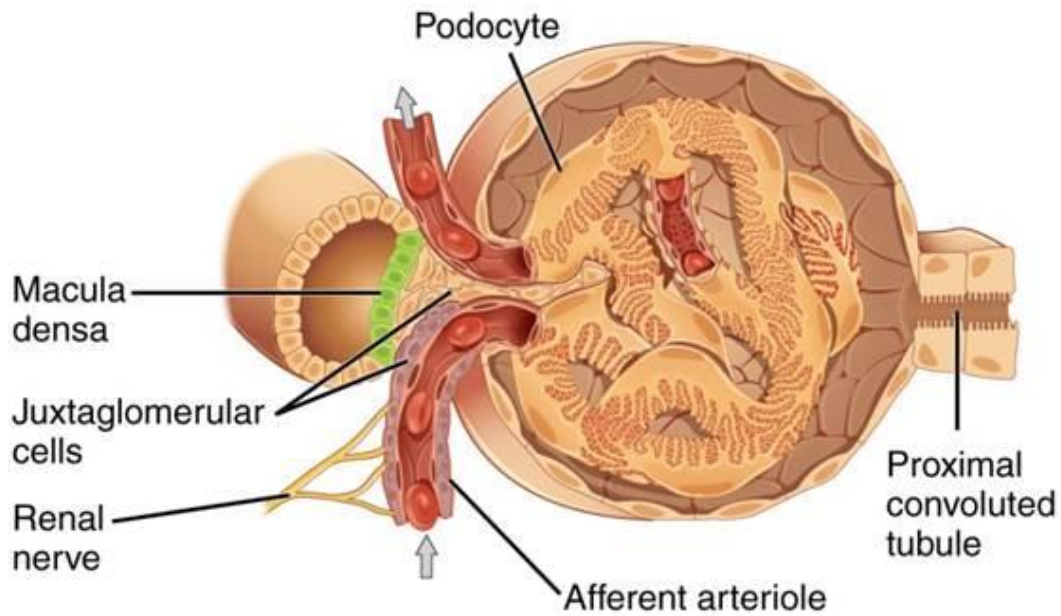


Figure 2: The renal glomerulus. Source: Wikipedia, the free encyclopedia.

The main function of the glomerulus is to constitute an efficient filtration barrier. This barrier is composed of the glomerular endothelial cells, the glomerular basement membrane and the podocytes.

The capillary loops of the glomerulus are covered by these specialized endothelial cells with large fenestrae. In between the capillaries, modified smooth muscle cells called mesangial cells, regulate blood flow by their contractile activity and secrete extracellular matrix, prostaglandins and cytokines.

Between the highly fenestrated endothelial cells of the capillaries and the podocyte there is a thick glomerular basement membrane (GBM). This membrane is the most significant part of the filtration barrier separating the blood in the capillaries from the urinary space. This GBM is formed by the apposition of basal laminae produced by the capillaries and the

podocytes and composed of three layers: lamina rara externa, lamina densa, and lamina rara interna. The lamina rara externa is adjacent to the podocyte processes. The lamina densa is the central layer composed mainly of type IV collagen and the lamina interna is adjacent to the endothelial cells.

The podocytes have a large cell body from which arise several primary processes that give raised to secondary cytoplasmic processes. These are three morphologically and physiologically different segments: the cell body, the major process and the foot processes. The cell body of the podocyte is not in direct contact with the basement membrane of the capillaries whereas each foot process is. The foot processes arise from the split of the major processes and contain an actin-based cytoskeleton that is linked to the GBM. The podocytes form a highly branched interdigitating network: the foot processes of one podocyte are connected 2 by 2 with the foot processes of an adjacent podocyte and this arrangement forms a filtration slit called the slit diaphragm. The slit diaphragm is a highly specialized type of intercellular junction made of modified adherent junctions and constitutes the final barrier avoiding protein loss during the filtration process. (Junqueira's Basic Histology book. 12th edition. 2009). One of the most important components of the slit diaphragm is a large transmembrane protein called nephrin.

This glomerular barrier is permeable to water, ions and small molecules. It filters molecules circulating in the bloodstream into the Bowman's space and allows discrimination among various protein molecules based on their size (e.g. albumin or protein with molecular weight higher than 70 kilodaltons) and their charge (e.g. negatively charged molecules). The barrier prevents the passage of large molecules into the Bowman's space and keeps them in the blood stream. The molecules that pass through the filtration barrier enter the Bowman's space and flows into the lumen of the proximal convoluted tubule and became the glomerular filtrate. The rate at which the glomerulus filters the plasma is called the glomerular filtration rate (GFR). It is important to notice that the filtration rate is much higher than the flow in systemic capillaries because the glomerular capillaries are connected at both ends to high-resistance arterioles, the afferent arteriole and the efferent arteriole. This anatomical feature creates a high hydrostatic pressure in the glomerular capillaries, which is one of the forces that favor filtration through the

Bowman's capsule. The glomerular filtrate exits the glomerulus through the proximal convoluted tubule and is then further processed along the nephron to form the urine (Boron WF., Boulapep E: Medical Physiology (2nd ed.). 2012)

The general anatomy of the kidney varies between the different species, in particular between human and rodents. These inter-species differences have to be taken into account during the test of new drugs and in particular when trying to interpret the significance for humans for drug induced phenomenon observed in kidneys of laboratory rats. At the morphological level, the rat kidney is composed of one single lobe whereas human kidney contains a minimum of 8 to 11 cone-shaped renal lobes, each composed of a central conical medullary pyramid surrounded by a cap of cortex. In the rat, the glomerular filtration rate can be variable when this parameter stays absolutely stable in human. The rat has also the ability to concentrate urine about twice more than in human. This peculiarity of rat renal physiology is an evolutionary adaptation to a dry climate. The osmotic ratio (urine/plasma) for man is 4.2 whilst is 8.9 for rat. The difference in urine concentration capacity is the result of functional anatomical differences between the two species. Compared to the cortex, the relative medullary thickness of the human kidney is 3.0 with 14% long-looped nephrons, whereas the relative medullary thickness of the rat kidney is 5.8 with 25% long-looped nephrons (*M. Suckow, S. Weisbroth: The Laboratory Rat. 2005*).

In addition to the morphological and anatomical differences, the rat shows some specific biochemical characteristics and can for example very easily eliminate cholesterol from the plasma using muricholic acids, which are a group of bile acids found mainly in mice and rats and at low concentrations in other species.

The alpha-2 microglobulin induced nephropathy is also a known example of rat specific pathology. This protein belongs to the lipocalin family which is characterized by the ability to bind a range of small hydrophobic molecules and to form complexes with soluble macromolecules. They act in the general clearance of endogenous and exogenous compounds (Flower 1996). The alpha 2-microglobulin nephropathy is an important toxicological syndrome that occurs in male rats following exposure to a number of

important industrial and environmental chemicals. This protein is produced in large amounts by the liver of male rat and reversibly binds to chemicals (and/or their metabolites). The complex formed is resistant to proteolytic hydrolysis and lead to accumulation in renal lysosomes before creating a subsequent cytotoxicity and cell death (Swenberg, Short et al. 1989). This is an example of syndrome highly species and sex specific that is important to know and to take in consideration when the rat data are analyzed to determine the relevance for human risk assessment.

1.2 Podocytes alteration and proteinuria

The glomerular filtration barrier is very sophisticated and an efficient filtration device but at the same time, it is also the most vulnerable component of the kidney.

As any other cell, the podocyte needs to maintain homeostasis that requires permanent adjustment based on the variations of neighbors cells, metabolism variations ... etc. In case of physiologic stress and pathologic stimuli, all the cells need to adapt reaching a new steady state that allows their survival and function. This adaption is a reversible functional and structural response and may consist of an increase in cell size (hypertrophy) and functional activity, an increase in cell number (hyperplasia), a decrease in the size and the metabolic activity (atrophy) or a change in the phenotype of the cells (metaplasia). When the stress stimulus is eliminated, the cell can return to the original state without having suffered any harmful consequences. If the limits of the adaptive response are exceeded or if the cells are exposed to injurious agent, there is an injury. The cell injury is reversible up to a certain point, but if the stimulus persists or is severe enough, the cell suffers irreversible injury and ultimately cells death. (Robbins & Cotran Pathologic Basis of Disease (8th Edition), 2009).

The podocyte is a terminal differentiated neuron-like epithelial cell which has a very limited capacity of division and replacement. The podocyte main function in the kidney is to maintain the glomerular basement membrane filtration mechanism and is playing a key role to ensure the proper selectivity of the filter. Therefore, it is crucial that the podocyte

ensures a continuous performance. However, if the stress persists or is intense enough, the podocyte can irreversibly suffer and shed into the urine or show signs of chronic degeneration.

The main adaptation mechanism of the podocyte is hypertrophy and was studied by Wiggins et al. in 2005 (Wiggins, Goyal et al. 2005) in the aging rat. They showed that the podocyte is compensating its low capacity to divide by hypertrophy. They could recognize 5 stages in the hypertrophy process in the way of glomerulosclerosis. The stage 1 has been defined as the normal podocytes, stage 2 a non-stressed podocytes hypertrophy, stage 3 an adaptive podocytes hypertrophy, stage 4 decompensated podocytes hypertrophy and stage 5 podocytes depletion. Only stage 4 and 5 are associated with proteinuria (functional changes) but changes in the podocytes biology start earlier at stage 3 (e.g. increase desmin).

Aside from aging and in a more general situation, the glomerular response to podocyte injury has recently to reviewed by Nagata M. (Nagata 2016). The podocytes can be exposed to several type of stress such as mechanical, oxidative or immunological. The protective response of the podocyte to injury such as ischemia, chemical substances and inflammatory cells can be the production of reactive oxygen species (ROS) (Diamond, Bonventre et al. 1986, Chen, Meng et al. 2013). Another adaptive response of the podocyte against stress is upregulation of several proteins including for instance vimentin and desmin (Shimojo 1998). Occasionally other molecule can be transiently expressed e.g. Notch (Niranjan, Bielez et al. 2008).

In an injured podocyte, cell death mechanisms are possible and the autophagy process is particularly important for post mitotic cells with highly branched cellular processes like podocytes or neuronal cells. Autophagosomes have been found in normal (resting) podocytes of mouse (Mizushima, Yamamoto et al. 2004) and human (Sato, Adachi et al. 2006) which implies a high level of basal autophagy activity in the podocytes.

In their mini-review, T. Weide and T. Huber (Weide and Huber 2011) focused on autophagy as a critical mechanism to maintain glomerular homeostasis. The efficiency of autophagy

seems to counterbalance intracellular oxidative stress. Under pathological conditions, the loss of autophagy appears to increase dramatically the susceptibility to glomerular disease: reduction of the basal level of autophagy flux promotes cytoplasmic accumulation damaged organelles and protein aggregates, leading of oxidative stress, ER stress, inflammation and apoptosis. Therefore, defective autophagy in podocytes accelerates glomerular damage after the induction of glomerular injuries by PAN (Fougeray and Pallet 2015).

When the podocyte injury reaches a certain level of severity, it has some clinical consequences including proteinuria and decreased renal function which account for the vast majority of end-stage kidney diseases. The glomerular proteinuria is associated with loss of albumin and high molecular weight proteins. When the podocytes are injured, the foot processes simplify or lose their normal interdigitating pattern (referred to as effacement of the foot processes) and the slit diaphragm is disrupted. These changes are associated with a reorganization of the actin cytoskeleton (Mundel and Reiser 2010) (see Figure 3).

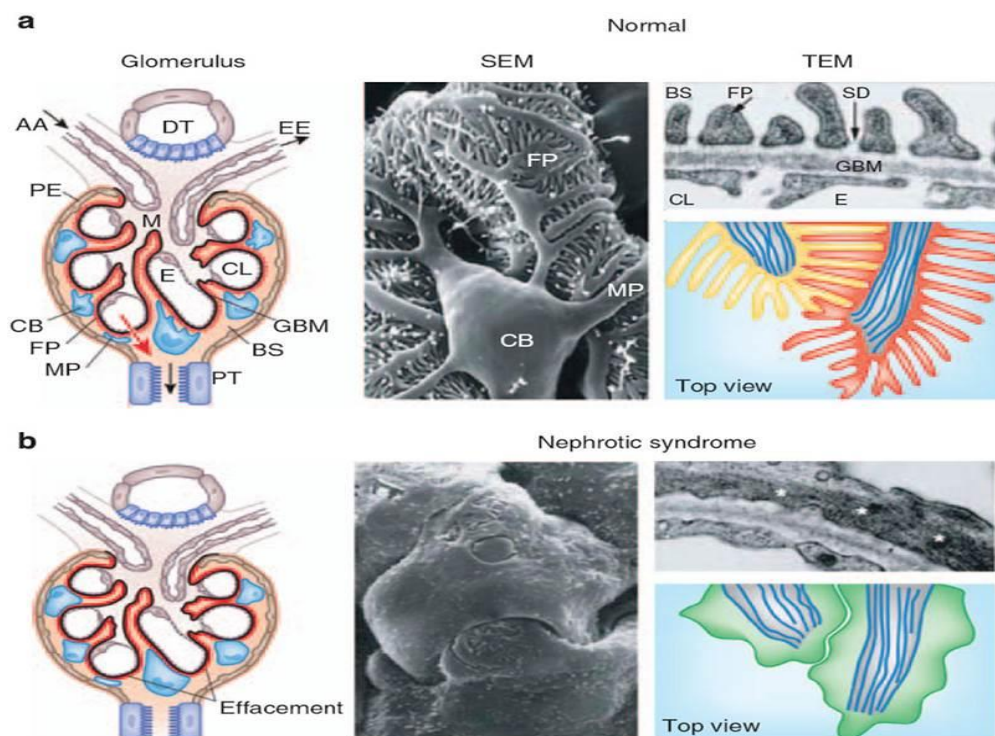


Figure 3: Foot effacement process following podocyte injury. Source: Mundel and Reiser, 2010.

When the proteinuria persists, proteins leaking through the filter are damaging the tubules, impairing their function. As the function of the tubules worsens, the blood flow to the affected nephrons is reduced. Simultaneously, damaged podocytes are producing cytokines that modulate the activity and the phenotype of endothelial and mesangial cells in the glomerulus. The combination of these two phenomena leads to glomerulosclerosis and to further reduction of the renal function (Shankland 2006). The foot process effacement is usually considered irreversible at this stage.

Several diseases are associated with alteration of the glomerular barrier (and/or podocytes alteration). Their etiology is variable:

- Immunological mechanisms underlie most forms of glomerulonephritis and/or glomerular disorders: either antibodies react with antigens in the glomerular basement membrane (e.g. anti-GBM; Heymann nephritis) or the antibodies react with non-glomerular antigen in the circulation to form an immune complex that are deposited in the glomerulus.
- Epithelial cells injury induced by certain mediators: cells and molecules related to acute and chronic inflammation are involved and an inflammation reaction occurs in the glomeruli.
- Abnormality of the structure of the GBM: Genetic predisposition: e.g. hereditary nephritis including X-linked nephritis; or non-enzymatic glycosylation of GBM proteins in diabetes.
- Drug induced glomerulopathies are rare, in comparison to other causes of drug induced kidney injury (Izzedine, Launay-Vacher et al. 2006). The most common underlying mechanism is immune activation as seen in drug-induced, ANCA-associated vasculitis (AAV), drug-induced lupus (DIL), and drug-associated membranous nephropathy (MN) (Hogan, Markowitz et al. 2015). However, there is an increasing number of reports of direct drug-induced podocytopathy such as minimal-change disease (MCD) and focal and segmental glomerulosclerosis (FSGS) (Markowitz, Bomback et al. 2015).

Although severe glomerular lesions result in proteinuria, they are not the only cause that can induce this phenomenon. There is a tubular proteinuria, overflow proteinuria or

exercise-induced proteinuria. The classification is based on the amount of protein, the type of protein (albumin or low molecular weight proteins) or the underlying pathological damage. As example, the tubular proteinuria occurs most commonly in disease processes affecting the tubulo-interstitial component of the kidney and low molecular proteins such as beta-2 microglobulin, which are normally completely reabsorbed by proximal tubules will be present in the urine. The overflow proteinuria results from an increased excretion of low molecular weight proteins in the urine (e.g. production of paraprotein in case of multiple myeloma). In this case, the proteinuria results from the amount of filtered protein exceeding the reabsorption capacity of the proximal tubule. Similarly the exercise-induced proteinuria results from an increased urinary excretion of proteins from plasma origin during the physical exercise. This proteinuria is transient and is not associated with any particular renal disease. In spite of the different type of proteinuria, the proteinuria associated to glomerular barrier remains of particularly importance regarding the kidney function and kidney diseases.

2.3 An approach to better characterize podocytes lesions

A Predictive Safety Testing Consortium composed of pharmaceutical industry, academic partners and health authorities was built some years ago, with the aim to evaluate biomarkers of kidney injury for potential regulatory use in drug safety assessment (Dieterle, Sistare et al. 2010). Although seven markers were identified and accepted by health authorities as renal biomarkers for detection of acute drug-induced renal toxicity (Dieterle, Perentes et al. 2010), glomerular diseases and podocyte injury which is playing an important role in progressive renal dysfunction were not explored.

Currently, the gold standard method to detect podocyte abnormalities requires electron microscopy. Immunohistochemistry, for specific markers has been considered as a complementary method (e.g. desmin or Angiotensin-Like-4), but so far, only advanced stages of podocyte damage were detectable (Herrmann, Tozzo et al. 2012, Li, Chen et al. 2015).

The focus of the present work was to detect the podocyte injury and the integrity of filtration barrier function in the context of renal toxicity. To better understand alteration of podocyte in glomerular disease, it would require improved *in situ* tools, which detect and differentiate podocyte adaptation (stage of reversible injury) from non-reversible injury and monitor the onset and progression of damage in the entire nephron.

The present study aimed at identifying podocyte markers that can be used for studying the podocyte *in-situ*. A stepwise molecular approach was carried out, which led to the identification of new podocyte injury markers.

- At first, gene expression profiling was conducted from laser captured microdissected glomeruli from healthy rat kidney sections and novel markers were identified
- Then, the presence of newly identified markers (Sema3G and CYTC) was further explored by immunohistochemistry and *in-situ* hybridization of rat kidney sections.

- Next, the in situ modulation of the Sema3G and CYTC were further studied in several podocyte injury animals model
- Finally, the interplay of Sema3G and CYTC and potential tubular injury related to the barrier dysfunction was explored by assessing KIM-1 expression and modulation.

This approach is suitable for early detection of podocyte dysfunction and for evaluating the impact of injury on the entire nephron. Such a tool is applicable in the context of investigative toxicological studies, animal models or human clinical case studies. In preclinical toxicology studies, detection of early alterations and understanding of lesion progression, are a prerequisite and indispensable for renal safety assessment in support of the development of new drugs.

3. Animal models with proteinuria

A very comprehensive review of the different rodent models to study podocytes diseases have been published by Pippin J.W in 2009 (Pippin, Brinkkoetter et al. 2009). This review was very useful to select the models that would support the best our goal to study the different case of podocyte injury and proteinuria.

The choice of the rodent models is recommended by the author because of their low cost and maintenance. The choice of the rat is related to the fact that the models are well-defined in this species and that the rat is the species used for toxicological study. However, a word of caution would be that the reactivity and sensitivity of this species has the disadvantage to be strain dependent.

The animal model needs to have the podocytes as the primary cells undergoing acquired forms of injury and respond to changes. Care should be taken to avoid models where endothelial cells, parietal epithelial cells, GBM or mesangial cells are targeted and podocytes then respond to that injury in a second step.

All the models chosen summarize different cases of podocyte injury and may be representative of the human pathology but not always and in this case would exhibit a specific response of the podocytes to injury.

The selected models are:

- a model of albumin overload that don't reproduce an precise human pathology but allows to study the slit diaphragm abnormality. This is a functional impairment model where the damage on podocyte depends from the dose and duration of albumin injection. With short treatment, the podocyte remains intact and there is no cellular stress visible. The foot process effacement is reversible.
- a model of immune deposition that reproduce the human membranous nephropathy. This model will represent a model of structural impairment. The podocyte is lying on an irregular glomerular basement membrane, affecting its stability. In this situation of stress, the podocyte is in adaptive stage (reversible injury)

- a model of drug-induced toxicity using a glomerular toxicant (e.g. puromycin aminonucleoside) that will be compared to a tubular toxicant (e.g. cisplatin). With puromycin aminonucleoside (PAN), the podocyte is affected by a direct drug-induced toxicity and the foot process effacement is associated with cytoskeletal changes and apoptosis. The injury is irreversible,

3.1 Model of albumin overload

The glomerulus is restricting the passage of albumin and many other plasma proteins by forming a selective barrier based on the size and the charge of the molecules. This barrier is composed by the fenestrated glomerular endothelium, the glomerular basement membrane, but the slit diaphragm between podocytes foot processes is the major component of the size-selective filtration barrier. The podocytes are located on the extra-capillary side of the glomerular basement membrane and are normally protected from high concentration of plasma proteins. In case of filtration machinery damage, albumin and other protein will permeate the impaired slit diaphragm or effaced foot process and podocytes will be exposed to elevated concentrations. The model of albumin overload is a useful model to study the response of a podocytes submitted to a temporary functional impairment situation and to study the related molecular/cellular events. This model is not really representing a specific human disease entity.

An *in vivo* model of albumin overload was first described by Davies and Brewer in 1977 (Davies and Brewer 1977). They could observe that rats injected intraperitoneally with 1 g of bovine serum albumin (BSA) daily for 5 days develop heavy proteinuria and there is swelling and loss of the foot processes of the glomerular epithelial cells. Proteinuria persists when the injections of BSA are stopped. The persisting proteinuria is caused by glomerular damage resulting from disruption and necrosis of the glomerular epithelial cells leading to complete sclerosis of glomeruli. The presence of macromolecules abnormally filtered into the proteinuric proximal tubule is also causing a dysregulation of the signaling and the phenotype of the proximal tubule epithelial cells (Baines and Brunskill 2008). The

albumin is endocytosed by the cells of this segment and will increase the production of proinflammatory cytokines and profibrogenic cytokines (Eddy and Giachelli 1995).

Such a model can also be used to verify the accuracy of urinary biomarkers in case of proteinuria, in particular low molecular weight markers normally reabsorbed by the proximal epithelial cells in a receptor mediated transport (e.g. case of the cystatin C in competition with albumin on the same megalin receptor) (Nejat, Hill et al. 2012).

Several version of the albumin overload protocol exist, starting with the type and the species of the protein injected (serum albumin versus globulin), the dosage administrated (from 1 to 15 mg/day/g), the route of administration (intra-peritoneal versus intravenous), the duration (3-5 days until several weeks) and the rat strain. The different rat strains were tested by Lawrence et al (Lawrence and Brewer 1981) and according to their results, the injury seems the most severe in male Wistar rats and mildest in male Sprague-Dawley rats. The amount of BSA administered correlates with the severity of the glomerular injury and the magnitude of proteinuria. By reducing the albumin injection to 2-days only, Yoshida et al (Yoshida, Nagase et al. 2008) showed that it is possible to induce podocyte injury and apoptosis with a massive urinary proteinuria but without cytotoxic effect of the albumin.

It has been demonstrated that the podocyte injury was then induced via TGF-B1/p38 MAPK pathway and was accompanied by albumin deposition and an increase of apoptosis (Yoshida, Nagase et al. 2008).

3.2 Model of immune deposition nephrotoxicity

The rat model of passive Heymann nephritis is the most widely studied model of podocyte injury.

This model is a passive model of immunization, that utilizes antiserum against a podocyte antigen generated in another animal (often rabbits, goats or sheep), which is injected into a rat or mouse to elicit immune complex formation. The initial period of a passive model (5 to 7 days) is referred as the heterologous phase because it relies on the binding of the antibody injected from a foreign source to its target in the host (rat or mouse). Subsequently the host develops its own immune response to the deposited heterologous

antibody and starts the autologous phase of disease.

The first model was described by Heymann et al in 1959 (Heymann, Hackel et al. 1959), using kidney extracts with Freund's adjuvant which correspond to an active immune model. Later, an insoluble subfraction from rat proximal tubule brush borders termed fraction 1A (FxA1) was isolated and used to produce antibodies (Edgington, Glassock et al. 1967, Edgington, Glassock et al. 1968). The targets of the FxA1 antibody is a 600-kDa membrane bound glycoprotein called megalin and a 45-kDa protein called receptor associated protein (RAP).

Generally male rats are used and antibody is administered intravenously or intraperitoneally. Controls are done using pre-immune IgG from sheep or saline.

After injection, the anti-FxA1 antibodies bind to megalin which is expressed on podocytes' foot processes. The antibody is capped and shed into the sub-epithelial space where it deposits. It accumulates until obliteration of the slit diaphragm. Sublethal complement activation occurs on affected podocytes, causing damage and intracellular signaling activation. Four to seven days after injection proteinuria occurs and persists throughout the autologous phase of the model. The only histological changes are GBM thickening and foot effacement process that can be observed by electron microscopy.

The PHN model has been proved to be very relevant to human disease and closely follows the pathogenesis of human membranous nephropathy.

3.3 Model of drug-induced nephrotoxicity

3.3.1 Glomerular toxicant

The puromycin aminonucleoside (PAN) nephrosis is the experimental prototype for the human minimal change disease (MCD) or the focal segmental glomerulosclerosis (FSGS).

The podocyte is the primary target of the puromycin aminonucleoside (PAN), therefore the rat PAN model became a powerful tool for investigating podocytes pathophysiology.

Puromycin is an aminonucleoside antibiotic produced by the bacterium *Streptomyces*

alboniger that causes premature chain termination during translation taking place in the ribosome. PAN causes direct DNA damage via the production of reactive oxygen species. Many administration routes can be used (subcutaneous, intraperitoneal or intravenous) but this is the cumulative PAN exposure which is critical and determine whether rats develop histological features of MCD or FSGS and the progression of the glomerular lesions from podocytes effacement to glomerular scarring. Between 2 and 4 days following PAN administration, podocytes' foot processes disorganize into broad expanses of epithelial cytoplasm. Podocytes show typical flattening and loss of foot process. After this pre-proteinuric phase, podocyte detachment and proteinuria occur simultaneously. Proteinuria develops between day 4 and 6, peak around day 8 and normalized at 4 weeks. This PAN rat model affords the opportunity to evaluate serial changes in the podocytes

3.3.1 Tubular toxicant

Cisplatin (cis-diamminedichloroplatinum[II]) is widely used for chemotherapy to efficaciously treat various cancers. But the cisplatin therapy is limited by cellular resistance and severe side-effects in normal tissues, like nephrotoxicity, ototoxicity... (Pabla and Dong 2008). Nephrotoxicity primarily occurs in kidney proximal tubule epithelial cells. Cisplatin is cleared by the kidney through glomerular filtration but the uptake of cisplatin in renal tubular cells is high, leading to cisplatin accumulation and tubular cell injury and death. Two different membrane transporters have been identified to be able to transport cisplatin, Ctr1 and OCT2. Ctr1 is highly expressed in adult kidney and is localized to the basolateral membrane of the proximal tubule (Pabla, Murphy et al. 2009) but OCT2 has been identified as the major determinant of the cisplatin-induced tubular toxicity (Yonezawa, Masuda et al. 2005).

One single injection of cisplatin by intraperitoneal injection (3 mg/kg) is enough to induced nephrotoxicity in male rats and represent of good model of tubular toxicity for comparison to a glomerulus specific toxicant.

4. Material and Method

4.1 Method for Laser capture microdissection of glomeruli

All chemicals and material for Laser capture microdissection (LCM) were provided by Applied Biosystems, Rotkreuz, Switzerland.

LCM was performed on 10 µm thickness frozen section of OCT embedded normal rat kidney. The tissue samples were thawed in the cryostat chamber for 30 min before the cut and the optimal temperature for sectioning was obtained at -16°C. The sections were collected on PEN membrane glass slides, fixed with ethanol 75% for 30 sec, hydrated in water for 15 sec, then stained with cresyl violet containing 10U/ml of protector RNase inhibitor, washed in water before deshydration in increasing concentration of ethanol until xylene and air dried. All these steps were performed under RNase-free conditions and using the Histogene® LCM frozen kit according to the manufacturer's instructions.

LCM was performed using the Veritas™ system with CapSure® Macro LCM Caps using a pulse power of 70mW, 2500 µsec pulse duration.

A minimum area of 250 000 µm² area was captured for glomerulus and cortex region without glomerulus. RNA was isolated using the Picopure® RNA Isolation kit following manufacturer instructions, concentrated in a volume of 11µL and checked with Agilent 2100 BioAnalyser with RNA 6000 Picochip. (Agilent Technologies AG, Switzerland) for quantification and integrity check.

4.2 GeneChip® arrays process

Total RNA extracted from the LCM glomeruli and from the primary culture of rat podocytes was further processed for GeneChip® experiments which were conducted at CIToxLAB (Evreux, France) using the Rat Genome Rat230 2.0 Arrays (Affymetrix, Inc., Santa Clara, CA, USA).

Target preparation was performed with a starting amount of approximately 2 ng of total

RNA for the laser captured glomeruli and with a starting amount between 6 and 90 ng for the cultured podocytes, unless otherwise specified using the NuGEN Ovation^{Pico} WTA system according to manufacturer's instruction (NuGEN Technologies Inc.). Briefly, cDNA generated by single primer isothermal amplification (SPIA) was fragmented and labeled using the Encore Biotin module (NuGEN Technologies Inc.). SPIA cDNA size distribution (before and after fragmentation) was confirmed by agarose-gel electrophoresis. Approximately 4.55 µg of biotinylated cDNA was hybridized for 18 hours at 45°C on an array. The array was washed and stained on Affymetrix Fluidics Workstation 450 and scanned on Affymetrix Scanner 3000 according to the manufacturer's technical manual. The scanned image was converted into numerical values of the signal intensity (Signal) and into categorical expression level measurement (Absolute Call) using the Affymetrix's MAS 5.0 algorithm. The software scaled the average intensity of each chip to a target intensity of 150.

4.3 Method for GeneChip® arrays analysis

Microarray expression data were analyzed using a Novartis internal analytical software tool (COMPARE 4.7.4. software). An initial filtering of data for each of the experiments was done to remove any probe sets that had a mean raw expression value below the fixed threshold according to the goal of the experiment (e.g. probe sets with a raw expression value (MAS 5.0) <1'000 were filtered out for the laser captured glomeruli analysis in order to restrict the analysis to very highly expressed transcripts). The probe sets were also selected to have at least 50% of present call in any given group, and probe sets without annotation were eliminated.

Gene signatures relating to relevant biological processes were established using COMPARE based on similarity measures across genes and knowledge of the biological function of the gene product. For finding transcripts with similar pattern of expression across groups of an experimental setup, a transcript of interest was defined and Pearson correlation coefficient

was used against the entire data set. For clustering analysis, Pearson coefficient for the similarity measure and a complete linkage algorithm were used.

Signatures were scored as the geometric mean of the fold changes of each transcript present in the signature.

4.4 Animal study design for Rat albumin overload model

Podocyte injury induced by albumin overload was performed in male Harlan Sprague-Dawley rat following a slightly modified experimental method as described by Yoshida et al, 2008 (Yoshida, Nagase et al. 2008).

After seven days of acclimation, rats were placed in metabolic cages for sham urine collection then returned in home cages. BSA was dissolved in the morning of the injection with the goal to deliver 8.5 mg/g dose without exceeding the NACUC dosing limit.

Animals were injected intra-peritoneal with BSA (n=5) or with saline solution (n=3) for 4 consecutive days and placed in metabolic cages after the injection of day 3. Urine was collected at day 4. Rats were also sacrificed at day 4 and kidney tissue was collected either in 10% neutral buffered formalin solution for further paraffin embedding or frozen in isopentane until OCT embedding.

This study was performed at Novartis Pharma Inc, East Hanover, NJ, USA in compliance with the Novartis Animal Care and Use Committee.

4.5 Animal study design for rat Passive Heymann nephritis model

Male Sprague-Dawley rats with a body weight between 176 and 191g were injected intravenously either with normal sheep serum (n=6) or with 0.5 ml/100g anti-Fx1A antiserum (n=8). Antiserum against Fx1A as well as the sheep serum was purchased from Probetex (San Antonio, TX, USA). Rats were euthanized on day 14 and kidney tissue was collected and frozen in isopentane until OCT embedding.

Urine was collected on days 6 and 13 and harvested for determining urinary excretion of

albumin.

This study was performed at Novartis Pharma Inc, East Hanover, NJ, USA in compliance with the Novartis Animal Care and Use Committee.

4.6 Animal study design using nephrotoxicants

Two different animal studies were design for testing a known glomerular toxicant puromycin aminonucleoside (PAN) and a tubular toxicant Cisplatin. In each study, Wistar Han male rats of 11-12 weeks old were used. Rats were randomly assigned to treatment (n=6) and control group (n=6). In the PAN study, animals were treated daily by intraperitoneal injection at 40mg/kg/day. Control animals were treated with isotonic purified solution (0.9% NaCl). Animals were sacrificed after 3, 7 and 14 days. For each time point, urine collection was performed and kidney was collected, fixed in 10% buffered formalin for 48-72 hours maximum before being processed for paraffin embedding.

In the Cisplatin study, animals were treated only once by intraperitoneal injection at 3 mg/kg under a dosage volume of 10 ml/kg. Control animals received isotonic saline solution (0.9%NaCl) under the same experimental conditions. On completion of the treatment period (days 3, 7, 14), samples collection and tissue processing was collected the same way as for the PAN study.

These two studies were performed at the contract research organization CIToxLab (Evreux, France) in compliance with Animal Health regulations, in particular with the Council Directive No. 86/609/EEC of 24th November 1986.

4.7 Normal tissue for localization

Rat, mouse, dog and monkey (Cynomolgus monkey) kidney tissues were provided by the Molecular localization lab of Novartis Pharma AG, Department of Pre-Clinical safety (Discovery and investigative Pathology section) and belong to the lab tissue collection. The tissues samples were usually collected from untreated and/or reserve animals of

investigative toxicology animal studies performed in conformity with the Swiss Animal Welfare Law.

Human kidney tissue samples were coming from two female healthy donors (Caucasian ethnicity) and were purchased from The International Institute for the Advancement of Medicine (IIAM, Edison, NJ, USA). The use of these human samples comply with Swiss Human Research Act (HRA) as well as any relevant laws, regulations, Novartis policies, contents of the informed consent (IC), ethics committee (EC)/ institutional review boards (IRB) approval, and/or regulatory authority approval, and with additional requirements and standards as described in the NIBR Guidance Document on Human Tissue.

4.8 Immunohistochemistry

Immunohistochemistry (IHC) for CYTC was performed using commercially available antibodies from Abcam (Abcam Ltd, Cambridge, UK). The rabbit polyclonal antibody ab33487 was used until being discontinued by the provider, and then replaced by the rabbit monoclonal antibody ab109508 with similar results.

For Sema3G, no good and specific antibody working for immunohistochemistry were found therefore all the analysis were performed only at mRNA level using *in situ* hybridization.

The IHC for neuropilin 2 (NRP2) was done using a rabbit monoclonal antibody from Cell Signaling Technology (reference 3366, clone D39A5).

For all staining, the IHC was performed using the fully automated instrument Ventana Discovery® XT (Roche Diagnostics Schweiz AG, Rotkreuz, Switzerland) with Roche reagents. Formalin fixed paraffin embedded sections were de-paraffinized and rehydrated under solvent-free conditions (EZprep solution) followed by demasking step performed by heat retrieval cycles in a citrate or Tris-EDTA based buffer (CC1 solution or RiboCC solution, option standard). Subsequently slides were blocked for endogenous avidin/biotin activity. The rabbit polyclonal anti-Cystatin C was diluted at 1/50 and incubated for 60min at room temperature, whilst the rabbit monoclonal anti-Cystatin C was diluted at 1/10'000 and incubated for 3 hours. The anti-NRP2 antibody was diluted at 1/50 and incubated for 1hour. A short post-fixation (glutaraldehyde at 0.05%) was done before applying a biotin

conjugated donkey anti-rabbit at 1/500 for 16 min (Jackson Immunoresearch Inc.). Detection was performed with a streptavidin-biotin peroxydase detection system DABMap® Kit following the manufacturer recommendations. The NRP2 antibody required a detection using a ready to use polymer anti-rabbit (UltraMap®-anti-rabbit-HRP conjugated) followed by the ChromoMap® detection kit. All slides were counter stained with Hematoxylin and bluing reagent, dehydrated and mounted using Pertex™ (Biosystems Switzerland AG, Nunningen, Switzerland).

4.9 *In situ* hybridization

Template for Sema3G, CYTC and KIM-1 riboprobe synthesis was generated by RT-PCR on RNA from kidney tissue using self-priming oligonucleotide primers flanked in 5' with SP6- and T3-promoter recognition sequences (primer sequences available in Table 1 of the supplementary data). The purified PCR product was transcribed using T3-RNA polymerase (anti-sense) and SP6-RNA polymerase (sense) at 37°C for 2 hours using dNTP containing Digoxigenin-UTP according to the manufacturer recommendations (Roche Diagnostics Schweiz AG, Rotkreuz, Switzerland). The quality and quantity of the riboprobe was evaluated using the 2100 BioAnalyzer (Agilent Technologies, Palo Alto, CA). As control of quality and specificity, the purified PCR products were submitted for double strand sequencing and Blast to the expected sequence (performed by Solvias AG, Kaiseraugst, Switzerland). From the primer design step, all the probes were also carefully verified for Blast and alignment homologies and in particular the rat semaphorin 3G probe that was tested against semaphoring 3A which is known to be highly expressed in the rat kidney.

ISH was performed using the fully automated instrument Ventana Discovery® XT (Roche Diagnostics Schweiz AG, Rotkreuz, Switzerland). All chemicals were also provided by Roche Diagnostics. Briefly, formalin fixed paraffin embedded sections were de-paraffinized and rehydrated under solvent-free conditions (EZprep solution). Pretreatment steps were done with the RiboMap™ kit following the manufacturer's instructions. Cell conditioning

(demasking) was performed by heat retrieval cycles in RiboCC solution using option mild followed by a complementary enzymatic digestion (Protease 3 for 16 minutes at 37°C). Hybridization was performed adding to each slide 200 µl of RiboHybe solution containing a DIG-riboprobe and was incubated for 6 hrs. After hybridization sections were washed 3 times with saline-sodium citrate buffer. The details for probes concentrations and hybridization temperatures are summarized in Table 2 of the supplementary data.

DIG-label probe detection was performed using an Alkaline Phosphatase-conjugated sheep anti-digoxigenin antibody (Roche Diagnostics) diluted 1/500 in antibody diluent. Antibody incubation was carried out for 32 min at 37°C followed by chromogenic detection using BlueMap™ Kit with a substrate incubation time of 6 hrs. Counterstaining using ISH nuclear fast red was performed for 4 min. Sections were mounted in glycerol-gelatin mounting medium (Sigma-Aldrich Chemie GmbH, Buchs, Switzerland).

4.10 Immunohistochemistry and *in situ* hybridization on frozen tissues

For the animal model with PHN, only frozen tissues were available and some slight adjustments of the protocols had to be performed.

In this case, cryosections of 10 µm were performed and collected on superfrost plus slides. After 30 min drying, the slides were immersed in Shandon™ Formal-Fixx™ solution (reference 9990244, Thermo Scientific, Switzerland) for 3 days before transfer in the Ventana autostainer and run with the same protocol as FFPE material.

Also for the model of PHN, one additional molecular marker was run to verify the complement deposition after treatment of the animals with the anti-FxA1 antibody. The staining was performed by immunofluorescence (IF) using a rabbit polyclonal antibody anti-C3c from Dako (Dako Schweiz AG, Baar, Switzerland, article number F0201)

The IF was performed manually on frozen sections that were fixed for 10 min in acetone. Blocking of non-specific background was performed for 30 min using Image-iT FX blocking reagent (Invitrogen; Catalog N°: I36933) then sections were washed in IHC amplification buffer (ProHisto; Catalog N°: AA4) three times for 5 min. The rabbit anti-c3 complement

FITC-conjugated antibody was diluted at 1/10. After incubation, the slides were washed again in IHC amplification buffer before being counterstained with DAPI/NucBlue fixed cell stain (Molecular probes; Catalog n°: R37606) for 2 min. Reaction was stopped in distilled water and slides were mounted with FluoroMount Prolong gold antifade reagent (LifeTechnologies; catalog N°: P36930) before fluorescence microscopic observation.

4.11 Image analysis

4.11.1 Scanning of slides and detection of kidney sections

Slides were scanned using the Aperio scanscope AT Turbo slide scanner (Leica, Muttenez, Switzerland) using the 40x magnification.

4.11.2 The image analysis platform

For the detection of glomeruli and the quantitative RNA ISH evaluation based on image analysis of the generated images, we used the proprietary image analysis platform ASTORIA (Automated Stored Image Analysis) which had been developed (at Novartis AG Basel) using Microsoft Visual Studio 2010, and consists of collections of many algorithms and modules based on functions from Matrox MIL V9 libraries (Matrox Inc, Quebec, Canada) to support the specific analysis of a variety of applications from histological image analysis. ASTORIA provides a simple user interface that allows the selection of algorithms and adjustable parameter sets, together with the specification of folders containing tif images to be processed. System requirements are a MIL V9 runtime license from Matrox (Matrox Inc, Quebec, Canada). ASTORIA generates ASCII text result files comprising measurement data such as median, mean and standard deviation for the objects' optical density, and more metadata, for each sample analyzed, and also tables with individual morphometric and densitometric data for each glomerulus.

4.11.3 Optical density of ISH signal in glomeruli

Forty glomeruli per slide were manually outlined by a human operator. For each image of manually outlined glomerulus, the following sequence of steps was performed:

1. Specific extraction of blue ISH signal spots to support optimum segmentation of the glomeruli: top hat on smoothed Green channel of RNA ISH image (2) and subsequent iterated top hat based segmentation loop using the top hat gray image as basis. By looping through a range of top hat binarization thresholds leads to a growing collection of RNA ISH positive areas, referred internally as to “plaques”.
2. Morphological processing of “RNA ISH plaque” objects followed by a connector transformation, linking objects that are sufficiently close to each other and indicative for belonging to the same glomerulus, after elimination of white spaces, to avoid linking across the Bowman’s space.
3. Closing holes of connected objects and creation of convex hull in order to identify spatially overlapping objects.
4. Separation of touching “convex hull” objects and morphometric classification (area, roundness, elongation...)
5. Locally refined removal of “white space”
6. Final sequence of morphological transformations (closing holes, separation, opening, size filter)
7. Final individual analysis of objects: optical density measurement for valid glomeruli.
8. “Specific optical density” which has been described to reflect the amount of protein (antigen) concentration, based on measuring and using the staining intensity of an appropriate antibody in a non-linear way (Rahier, Stevens et al. 1989, Ruifrok and Johnston 2001) was measured for each glomerulus, using the Green channel image of the RNA ISH image. In our case, the “specific optical density” reflects the amount of mRNA concentration. For the specimen background reference necessary for OD measurement, a ring around each glomerulus was determined through several dilations and subtraction of the glomerulus mask.

9. For each sample, a text file containing a table with entries of morphometric and densitometric values for each object considered to be a valid glomerulus was generated, providing the basis for further statistical analysis.

4.12 Method for culture of primary podocytes

Isolation and primary culture of the rat podocytes was done accordingly to the improved method described by Katsuya K et al. in 2006 (Katsuya, Yaoita et al. 2006).

Male Wistar adult rats of weight between 250 and 400 g were anaesthetized with a pentobarbital solution at 75 mg/kg by an intra-peritoneal injection of 1.5 ml/kg.

A perfusion of the kidney was performed by inserting a catheter below the renal arteries into the aorta, before cutting the vena cava and perfusing the kidney with Hank's Balanced Salt Solution (HBSS)-/- using a peristaltic pump injecting 12 ml of solution in 2 min. The HBSS-/- solution was then replaced by a perfusion solution containing 15 ml of HBSS + 0.9 ml of Dynabeads M-450 tosylactivated deactivated (2.4×10^7 beads) (reference 140-13, Life Technologies AG, Switzerland) and 15 mg of iron powder (reference 44890, Sigma-Aldrich, Buchs, Switzerland) for additional 2 min.

The perfused kidneys were then carefully removed from the abdominal cavity and put in a petri dish containing HBSS. Only the kidney cortex was kept, cut in small pieces and placed in a digestion solution based on collagenase A at 1 mg/ml (reference 11088793001, Roche Diagnostics, Rotkreuz, Switzerland) and deoxyribonuclease I at 10'000 U (reference 4536282001, Roche Diagnostics, Rotkreuz, Switzerland) in 25 ml of HBSS.

The enzymatic digestion will take place under stirrer (helical tool) at 37°C rotation at 4-5 rpm for 60 minutes. At the end of the digestion, the collagenase-digested tissue will be filtered through a 100 µm cell stainer, wash in HBSS -/- and distributed in 15 ml tubes. The tubes are then placed in to the Dyna Mag2- magnet in order to recover the glomerulus containing the magnetic beads previously perfused and blocked in the glomerular capillaries. The liquid is discarded. The magnetic isolated glomeruli were washed 4x times with 5 ml of PBS. The suspension was filtered through a 70 µm cell stainer and was reversed in a petri dish before being again submitted to the DynaMag2 magnet. The

isolated glomeruli were collected and put in DMEM/F12 based culture medium with fetal bovine serum and Penicilline-streptavidin. The obtained glomeruli were counted and seeded between 7'000 and 10'000 glomeruli per well using 6-well plates coated with collagen I (reference 356400, Becton Dickinson, Allschwil, Switzerland).

The 6-well plates were put in incubator at 37°C and not touched for 4 days in order to obtain glomeruli attachment to the plate and favors the cellular outgrowths.

After 4-days, the cells were rinsed with TrypLE express (trypsin based solution, reference 12604013, Life Technologies, Switzerland) and incubated with this solution for 2 to 4 minutes. Cells were scraped and transferred in 15 ml tubes containing 2-3 ml of culture medium, centrifuged at 250 rpm for 5 min. Supernatant was discarded and the pellet was suspended in fresh medium and submitted to magnetic isolation to remove the remaining glomeruli and collect only the isolated cells (podocytes). The cells were counted in haemometer counting chamber with trypan blue. Density was adjusted to 30'000 cells/well using a 96-wells plate coated with collagen I (reference 336407, Becton Dickinson, Allschwil, Switzerland).

4.12.1 Drug treatment of the primary culture of rat podocytes

The drug treatment was performed the day after the seeding.

A preliminary step of dose range finding was necessary to determine an appropriate treatment dose for Puromycin aminonucleoside (PAN) that avoided cell toxicity (reference P7130, Sigma-Aldrich, Buchs, Switzerland). The first panel of concentrations tested for PAN was between 0, 25, 50, 100 and 150µg/ml (Figure 4) and was then further refined with lower concentrations between 0 and 2 µg/ml (Figure 4). For cisplatin (reference C2210000, Sigma-Aldrich, Buchs, Switzerland), increasing concentration from 0, 1.5, 3, 6, 12, 25, 50 and 100 µM were tested without any problems of viability. The dose of 50 µM was chosen for cisplatin and two concentrations of PAN were defined as low dose (0.1µg/ml) and high dose (1 µg/ml).

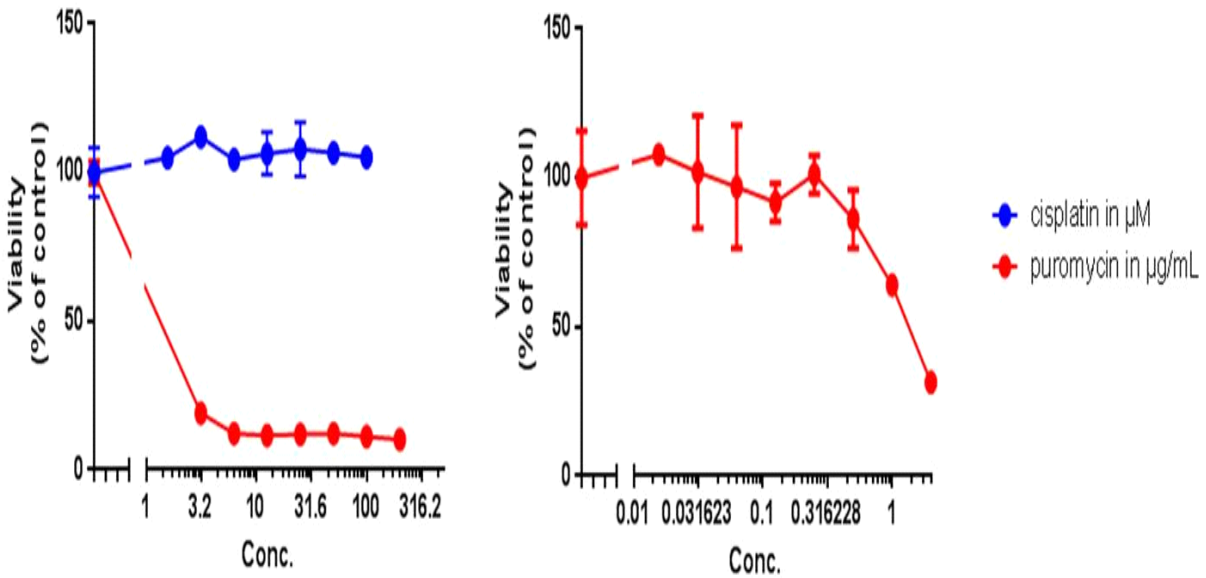


Figure 4: Viability test results after treatment of the primary podocytes with increasing concentrations of PAN and cisplatin.

The compounds were diluted in such a way that 50 μ L of culture medium from each well can be exchange with 50 μ L of diluted compounds.

Compounds were incubated for different end points: 3h, 6h, 24h and 48h. Then, an aliquot of supernatant was collected for the viability test and the cells were washed with PBS before being lysed with 30 μ l of QIAzol Lysis Reagent (reference 79306, Qiagen, Hombrechtikon, Switzerland) stored at -80°C until further processing for RNA extraction using the Qiagen RNAeasy mini-kit (reference 74104, Qiagen, Hombrechtikon, Switzerland) following the provider instructions.

The extracted RNAs were processed for GeneChip® experiments as already described previously.

4.12.2 Characterization of the primary podocytes using immunofluorescence

Aside from the treatments, some of the cells were plated on chamber slides and incubated the same way as the treated samples. No drug treatment was applied on it. At the end of the experiment, the cells were washed with PBS and fixed in PFA 4% in PBS for 10 minutes at room temperature. After the fixation, the cells were washed again in PBS and permeabilized with a Triton-X100 solution at 0.25% in PBS at room temperature for 15 minutes. Before applying the primary antibodies, a blocking step of 30 minutes was performed using Image IT fix signal enhancer solution (reference I36933, Invitrogen, Switzerland). The primary antibodies rabbit anti-podocin (reference P0372, Sigma) and mouse anti-synaptopodin (clone Q1D4, reference 65294, Progen) were diluted at 1/500 and 1/50 respectively in amplifying antibody dilution buffer (ready to use solution reference AA3, ProHisto) and were incubated overnight at 4°C. The next day, a goat anti-rabbit Alexa-488 conjugated (reference A21206, Invitrogen) diluted at 1/200 was mixed with a goat anti-mouse Alexa-546 conjugated (reference A21123, Invitrogen) diluted at 1/200 and applied for 30 minutes at room temperature. The slides were mounted in Prolong gold anti-fade reagent (reference P369303, Invitrogen) after a 2 minutes counterstaining using NucBlue fixed cell stain (reference R37606, Invitrogen).

These two markers podocin and synaptopodin were used as specific markers of podocytes, considering that the podocin is a marker of podocytes foot process membrane marker and synaptopodin is specific of mature podocytes.

These two markers in combination with a morphological examination of the cells shape should allow a determination if the isolation process and culture generated proper podocytes or not.

4.13 Dosage of urinary proteinuria or albuminuria

4.13.1 Albumin overload and PHN studies

In these two studies, determination of the presence of albumin in urine samples was performed at Novartis Pharma Inc, East Hanover, NJ, USA, at the same place as the animal studies occur.

The animals were individually kept in metabolism cages for urine collection at day 4 (albumin overload study) and day 7 and 14 (PHN study). Urine samples were harvested and analyzed by immunoassay using a coating albumin antibody detected by an HRP-based chromogenic detection. The results are expressed in total albumin excretion in micrograms.

4.13.2 Puromycin aminonucleoside (PAN) and Cisplatin studies

For these two studies, total protein quantification was done in urine samples.

The analyses were conducted at the contract research organization CIToxLab (Evreux, France) at the same place as the animal studies occur.

The urine was collected from 2:00 to 8:00 pm and from 8:00 pm to 6:00 am on days 2/3, 6/7 and 13/14 on fasted animals. For this purpose, the animals were individually placed in metabolism cages. During urine collection, the animals had free access to water but not to food.

The urine was collected in tubes without thymol crystals and kept at approximately +4°C during the collection period. Urine fractions of 2 ml were centrifuged at +4°C for 30 minutes at 10,000 g. before to be subjected to urine analysis.

Total proteins were measured on the automatic analyzer ADVIA 1650 (Bayer HealthCare) using the Pyrogallol red method. Results were expressed in g/L.

4.14 Method for the fingerprint analysis

Using the Definiens software (Definiens AG, Munich, Germany), the digitally scanned slides from the KIM-1 in-situ hybridization staining results were used to process the images in a standardized way. Definiens was used to make an evaluation of a phenomenon which is segmental and focal. The goal is to look at an entire kidney section and identify where is located the primary lesions. The idea is to combine and/or overlap stained area with morphological area. Therefore, the following morphological regions have been defined: cortex; inner medulla; outer medulla. The limit between outer medulla and cortex was defined by the different tissue structure and with help of the interlobular rays. Staining results were then measured to provide data on the total amount of stained tissue as well as stain relative area versus unstained area.

These results should illustrate the place where the tubular injury starts and how it progress in the different situation of injuries induced in the rat models tested.

5. RESULTS

4.15 Identification of glomerular specific markers

The evaluation of new potential podocytes lesion markers starts by identifying a marker that would be specific for the glomerulus and may be used as indicator of podocyte dysfunction.

Glomeruli of normal rat kidney tissue sections (average of 50 glomeruli/rat; n=5 rats) were isolated by laser capture microdissection and compared to remaining cortical tissue devoided of glomeruli. Total RNA was extracted from these samples and a differential genomic profile was generated between the two tissue preparations.

With the data set, the goal was to perform a very stringent analysis that can eliminate all transcripts expressed in both tissues (glomerulus and cortex) and to isolate a pure set of glomerulus specific genes. The threshold for the average expression level was put high (average expression value [MAS 5.0] of >1'000) in order to retain only robustly expressed genes and eliminate genes weakly expressed and/or expressed in different cells types within the glomerulus. Using this expression level filter, from the 31042 probe sets of the chips, 5% of probe sets (1696) were pre-filtered. Probe sets without annotation were also removed. The remaining number of probe sets was then 1450. The fold change comparison between the two groups considered only probe sets with a minimal up or down-regulation of 1.5-fold and differences of group means were further tested by T-Test (alpha 0.05). At this point, we find a limited group of 1020 probe set. We still wanted genes strongly discriminating glomerulus from cortex, therefore the log₂ Fold change value was chosen at 2.0 (or more) between the two groups. The final list contains 127 probe sets and is available in the Supplementary data part (Supplementary Table 3). The transcripts that fulfill the selection are visualized by blue circles (upper left corner) in the scatter plot correlation picture in Figure 5.

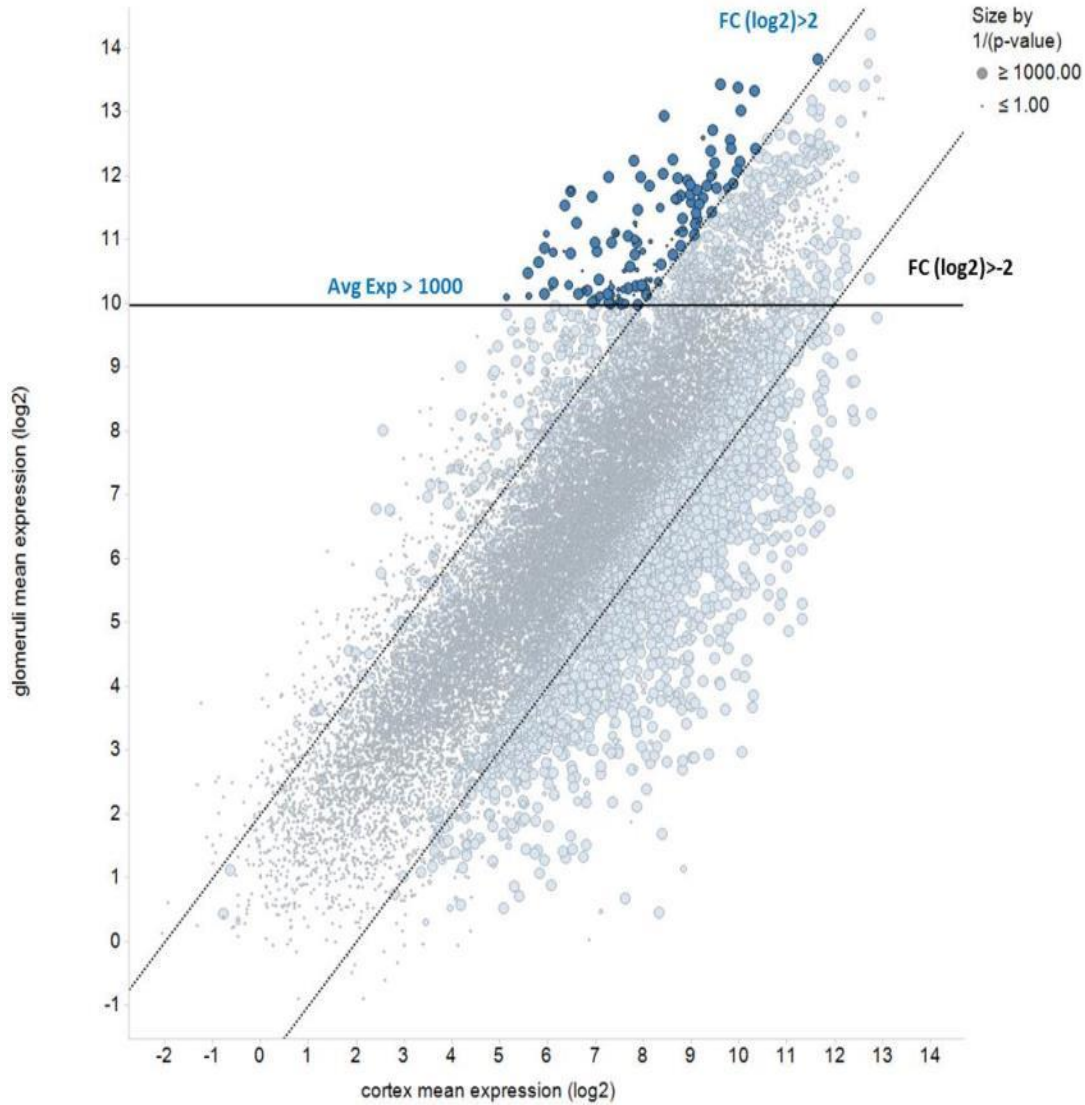


Figure 5: Scatter plot correlation between kidney cortex expressed genes versus glomerular expressed genes. Data are given as mean expression levels (\log_2) of individual features gene per tissue including all annotated probe sets. The expression threshold for average expression >1000 (MAS 5.0) is indicated by a horizontal line. Dotted lines indicate \log_2 -transformed fold changes (FC) thresholds of $> |2|$. Features gene level with an average expression value >1000 in glomerulus and at least 4-fold enriched expression over kidney cortex are marked by filled blue circles.

The heat map visualization confirm the very high specific expression of these genes in glomeruli compared to the cortex tissue (Figure 6)

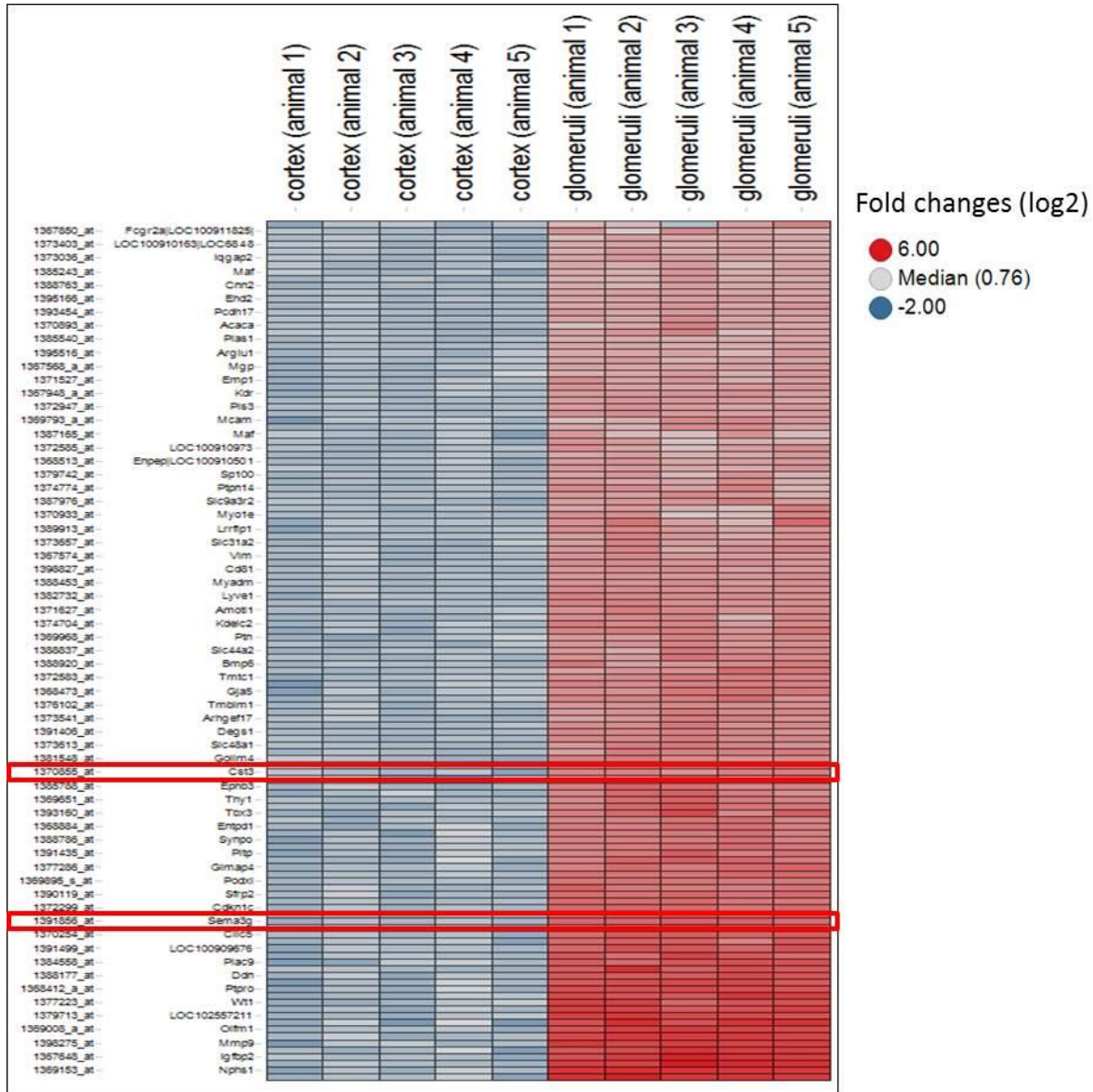


Figure 6: Heat map visualization of the glomerulus specific genes. Fold changes (log₂) for individual samples were calculated as compared to average expression levels for each probe set across the 5 cortex samples. Animal numbers indicate samples derived from the same individual.

The list of 127 glomerulus specific probe sets is expected to contain a mix of genes expressed in the different cell types present in the glomerulus, namely podocytes, endothelial cells, mesangial cells and eventually some infiltrating cells. The vast majority of these 127 transcripts are mainly podocytes-related genes and it was possible to identify some well-known molecules already described to be expressed in these cell like synaptopodin, nephrin, WT1, some integrins, podocalyxin-like gene, tight junction protein 1 (ZO1), dendrin (Patrakka and Tryggvason 2010, Greka and Mundel 2012). In the opposite, some genes well-known to be expressed in podocytes were missing among these podocin (Nphs2) which is unfortunately not covered by the Rat230 2.0 Arrays or TRPC6 which is detected by the array but that was eliminated from the results because its expression was below the expression threshold we applied.

We found then some genes related to endothelial cells, like Lyve-1 or endothelial PAS domain protein 1. Finally, Th1 expression was found, this gene is one well known and used marker for mesangial cells (Ricono, Xu et al. 2003). The presence of potential macrophage can be expected and in fact some CD68 expression was detected. Renin expression was also detected. The fact that this gene is known to be in the juxta-glomerular apparatus (but not in the glomerulus *per se*), confirms that the precision of laser microdissection was sufficient to enrich the data set in glomerulus specific genes, but eventually included adjacent tissue as e.g. juxta-glomerular apparatus.

In the list of 127 transcripts containing glomerulus specific gene we compiled, there were two genes that drawn our attention, Sema3G and Cst3. These two genes ranked respectively the second and fourth in terms of highest glomerular mean expression in log2 scale. When assessing the expression of these 2 genes in the single animals used for this analysis, the expression data confirmed that both genes are expressed at high level in the glomerulus of normal kidney (both with average expression [MAS 5.0] around 10'000) with strong reproducibility between the donors (see data details in Figure 7).

At the time this work was started, an overview of the literature told us that none of them were precisely described in the literature for being involved in any podocytes-related function. Sema3G seems to be effectively expressed in endothelial cells but is mainly

described as guidance molecule (see role and function below) and Cst3 is a well-known biomarker of kidney function but is supposed to be only filtered by the glomerulus and not synthesized by the cells of the glomerulus.

This choice was driven by the fact that these two genes were ranked as even more glomerular specific genes as synaptopodin or the podocalyxin-like genes and their presence among podocyte-specific genes should be in direct relation with this cell and is certainly involved in the podocyte function.

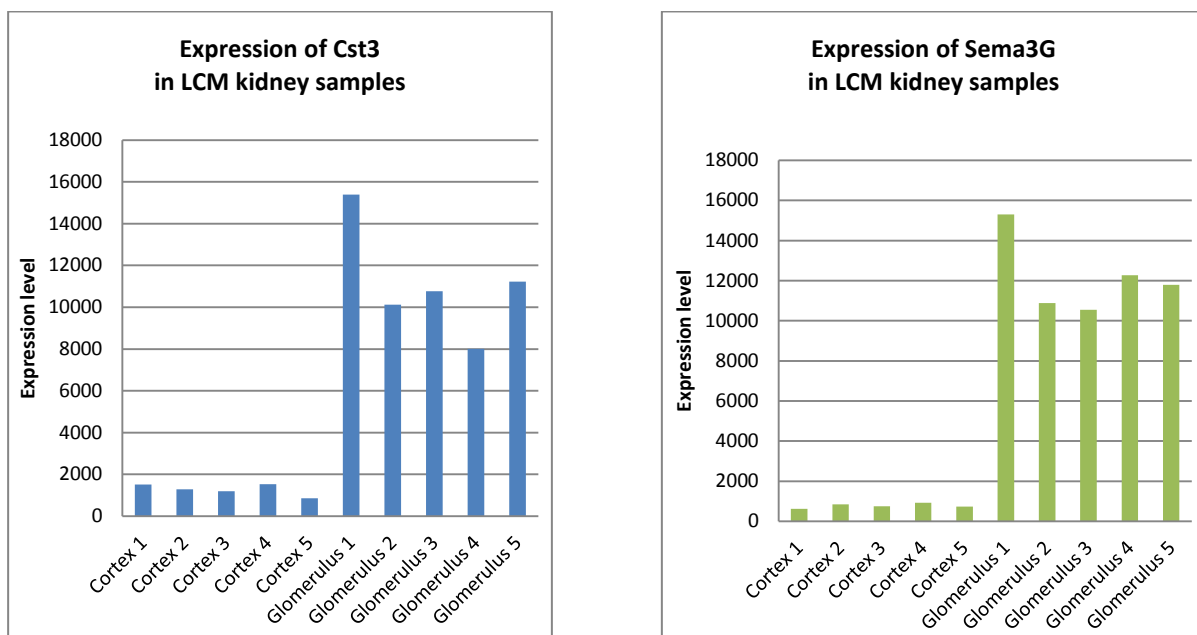


Figure 7: Comparison of Sema3G and CYTC expression levels in the glomerulus versus the cortex samples for each single animal

4.15.1 Role and function of Semaphorin 3G

Semaphorin 3G (Sema3G) belongs to the semaphorin family that is a large gene family with seven classes. The class 3 semaphorins are composed of semaphorin domain, an immunoglobulin domain and a highly basic carboxyl terminus. Class 3 semaphorins are

secreted proteins and regulate signaling pathways that control many processes like cell adhesion, cytoskeletal dynamics, migration, survival and proliferation of cells. Semaphorin 3A was the first identified semaphorin in vertebrates on the basis of its ability to induce the collapse of axonal growth cones of the dorsal root ganglion (DRG) (Luo, Raible et al. 1993, Behar, Mizuno et al. 1999).

In the opposite, Sema3G is the most recent and unknown semaphorin of the class 3. It was identified in 2005 in mouse and was shown by Northern blot to be expressed in adult tissue mainly in lung and kidney, moderately in the heart and placenta and slightly in brain. Some expression was also detected by *in situ* hybridization in kidney at E17 (Taniguchi, Masuda et al. 2005). In 2006, Takemoto et al. by screening a large-scale sequenced cDNA library from mouse glomeruli at different stages of development, they could find Sema3G within the 300 glomerular cell enriched transcripts and within five novel podocytes transcript in the E18.5 kidney, without investigating further this marker (Takemoto, He et al. 2006).

Initially, Sema3G has been mainly described for its role as repulsive axon guidance signaling molecule (Yu and Moens 2005) but it also has been characterized as attractive and repulsive regulators of angiogenesis exerting an autocrine effect of on endothelial cells and a paracrine effects on smooth muscle cells (Kutschera, Weber et al. 2011). Sema3G specifically was mentioned in the class-3 semaphorins as inhibitors of tumor progression, being the only class-3 semaphorin to have a prognostic value in adult gliomas (Karayan-Tapon, Wager et al. 2008). Recently Sema3G was identified as a PPAR-gamma downstream effector which is centrally involved in regulating endothelial cells migration (Liu, Li et al. 2015).

The receptor of Sema3G is mainly neuropilin-2 that dimerize with plexin, and it is also mainly described for its role in axonal growth and guidance and in physiological and pathological angiogenesis.

Some other class 3 semaphorin family members like Sema3A and 3F have been described to be expressed in podocytes, and Sema3A has been shown to regulate the expression and interactions of slit-diaphragm proteins and decreases podocyte survival (Guan, Villegas et

al. 2006). Now, Sema3G has just been confirmed as novel podocyte gene and that the knockout of this gene doesn't show glomerular defects but aberrant foot process by EM (Ishibashi, Takemoto et al. 2016).

4.15.2 Role and function of Cystatin C

Cystatin C (CYTC) is a low molecular weight (13-kD) molecule and consists of 120 amino acid residues with two disulfide bridges and belongs to family 2 of the cystatin superfamily. CYTC is produced by all nucleated cells (Mussap and Plebani 2004). CYTC is an endogenous cysteine proteinase inhibitor and is considered as the physiologically most important inhibitor, regulating activities of endogenous cysteine proteinases such as cathepsins B, H, L and S in the extracellular environment. Considering that cysteine cathepsins play fundamental roles in multiple biological processes such as protein turnover, pro-protein processing, antigen presentation and apoptosis, the role of CYTC is related to many pathological processes such as cardiovascular disease and apoptosis (Shi, Sukhova et al. 1999, Turk, Stoka et al. 2012).

CYTC is mainly used as a biomarker of kidney function. Due to its low molecular weight, CYTC is filtered from the blood by the glomerulus then reabsorbed through a megalin-mediated endocytosis Ca⁺ dependent manner (Kaseda, Iino et al. 2007) and metabolized by proximal tubule cells (PTC). Under normal conditions, the production of CYTC is constant and its reabsorption by the PTCs is complete and no CYTC can be found in the urine. Because of these properties, CYTC became an interesting marker for clinical use and a potential alternative to creatinine measurement. It could replace or supplement serum creatinine to estimate the glomerular filtration rate (GFR). GFR based on serum creatinine level are limited by their dependence on muscle mass and CYTC level has the advantage not to be influenced by this muscle mass. The performance of cystatin C alone or the combination creatinine-cystatin C compared to creatinine-based estimating equations in chronic and acute kidney disease has been intensively studied (Inker and Okparavero 2011). However, it seems that at the end, models based on cystatin C alone are not superior

to those based on creatinine, but models based on both markers can improve GFR estimation in the reference range (Eriksen, Mathisen et al. 2012).

In preclinical studies, urinary CYTC has also been proposed for potential detection of both glomerular and proximal renal damage and was within the seven biomarkers endorsed by the FDA and EMEA for acute kidney injury (Dieterle, Perentes et al. 2010). Recently this marker was also tested in rat models of anti-glomerular basement membrane glomerulonephritis and Zucker diabetic fatty (ZDF) rats and it was shown that urinary CYTC can be a useful marker of renal damage (Togashi, Imura et al. 2013, Togashi and Miyamoto 2013). The limitation for the usage of CYTC as a trustful urinary marker has been pointed out by Nejat M. in 2012 (Nejat, Hill et al. 2012). CYTC reabsorption is receptor-mediated using megalin (Kaseda, Iino et al. 2007) but the same receptor is also used by albumin. They could demonstrate that in case of increased albuminuria, the absorption of CYTC can be reduced by competitive inhibition.

Aside from these different roles of CYTC, it was never described and studied in details what is the role and regulation of CYTC into the glomerular compartment and how this expression is regulated in this part of the kidney under different toxicological and/or pathological conditions.

4.15.3 The tubular injury marker KIM-1

In all the coming work, KIM-1 is going to be the tubular injury marker systematically associated to the two glomerular markers Sema3G and CYTC in order to have an indicator of nephrotoxicity.

KIM-1 has been described for the first time in 1996 by Ichimura et al. (Ichimura, Bonventre et al. 1998). KIM-1 is also called Hepatitis A virus cellular receptor 1 (HAVCR1) (Kaplan, Totsuka et al. 1996) and T cell Immunoglobulin mucin (TIM-1). KIM-1 is a type I cell membrane glycoprotein with a six cysteine immunoglobulin like domain and a mucin domain.

In the normal kidney KIM-1 is expressed at very low level but as soon as the kidney gets injured by toxicants or ischemia, it is immediately upregulated in the cells which are dedifferentiated and undergoing replication. KIM-1 has been identified as an important player in the restoration of the morphological integrity and function to postischemic kidney (Ichimura, Bonventre et al. 1998). Additionally, KIM-1 possesses a single transmembrane domain and undergoes membrane-proximal cleavage by metalloproteinase, which leads to the release of soluble KIM-1 ectodomain into the urine. The constitutive cleavage of KIM-1 is mediated by ERK activation, and is accelerated by p38 MAP kinase activation (Zhang, Humphreys et al. 2007). This shed ectodomain of KIM-1, released in the lumen, is heavily glycosylated and stable and appears in the urine after injury. KIM-1 is a phosphatidylserine receptor which recognizes apoptotic cells directing them to lysosomes. It also serves as a receptor for oxidized lipoproteins and hence is important for uptake of components of the tubular lumen which may be immunomodulatory and/or toxic to the cell. Data suggest that KIM-1 expression is protective during early injury, whereas in chronic disease states, prolonged KIM-1 expression may be maladaptive and may represent a target for therapy of chronic kidney disease (Bonventre 2014). KIM-1 has been qualified by the United States Food and Drug Administration and the European Medicines Agency for preclinical assessment of nephrotoxicity. But recent data suggest the importance to monitor KIM-1 for early diagnosis and clinical course not only in patients with various forms of AKI and other renal diseases but also in patients with cardiorenal syndrome, heart failure, cardiopulmonary bypass, cardiothoracic surgical interventions in the pediatric emergency setting, and so forth (Medic, Rovcanin et al. 2015).

4.16 Expression of Sema3G, CYTC and KIM-1 in normal kidney

In order to confirm the expression of Sema3G and CYTC in podocytes, we proceed with their mRNA and protein localization using respectively *in-situ* hybridization and immunohistochemistry on tissue sections of rat kidney.

4.16.1 Embryonic expression of Sema3G and CYTC

The localization of Sema3G and CYTC in the rat embryonic kidney was done by *in situ* hybridization using rat embryos at the stage of E15 days post coitum (dpc), when cortical and medullary regions are reasonably well-defined. In the cortical region, substantial numbers of primitive glomeruli can be found. More centrally, the medullary region principally contains undifferentiated mesenchyme tissue with a few interspersed collecting tubules.

Expression of Sema3G was visible in what was identified as primitive glomeruli, in the cells that surround the structure. Some faint signal was sometime visible in the structure close to the glomerulus and identified as a primitive tubule but was more likely background.

No other organ in this section seems to express Sema3G, with the exception of the endothelial cells of some blood vessels in the embryonic lung. This result is in agreement with the previous observation done by Taniguchi et al. where Sema3G was detected in mouse kidney, lung and cerebellum at E17dpc (Taniguchi, Masuda et al. 2005). The cerebellum region was not available on the section and therefore the expression in this tissue couldn't be confirmed.

Similarly, *in situ* hybridization with the CYTC probe gave some positive signal in the primitive glomeruli (at the same location as the Sema3G). Additionally, some signal could be found in the brain, potentially in the pons but the precise region was difficult to identify on this section. Some isolated circulating cells were also positive.

The literature review could not find any previously described expression of CYTC in embryonic kidney. All published data are describing either the detection of CYTC in serum as marker of renal function assessment (Bokenkamp, Dieterich et al. 2001) or the

expression of CYTC in blastocysts for supporting the embryonic implementation (Baston-Buest, Schanz et al. 2010). No description of the tissue distribution of CYTC could be found.

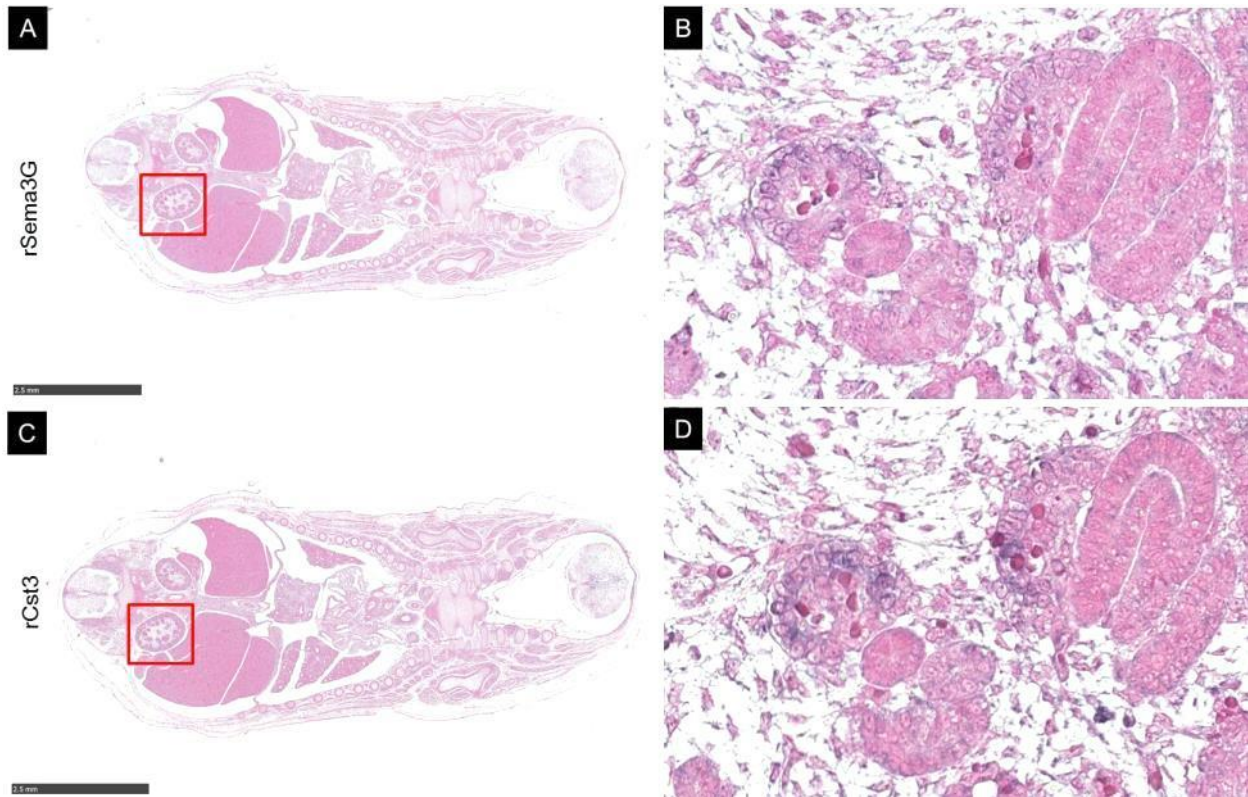


Figure 8: Expression of Sema3G (A and B) and CYTC (C and D) by ISH in rat embryo at E15dpc (Blue: NBT substrate for ISH; Red: counterstaining). (A)(C) are low magnification (x1.25) of the entire embryo and (C)(D) are high magnification (x40) of the kidney. Staining for Sema3G and CYTC in the primitive glomerulus can be observed.

Summary of Sema3G/CYTC embryonic expression

Expression for Sema3G and CYTC could be detected as early as E15 dpc in the primitive glomerulus of rat.

Additionally some blood vessel seems to express Sema3G. CYTC was also found in nervous tissue and isolated circulating cells.

4.16.2 Expression of Sema3G in rat adult normal kidney

The expression of Sema3G in rat adult kidney was investigated using *in situ* hybridization. In normal rat kidney, a strong expression of Sema3G was found in the podocytes (Figure 9A). Podocytes are easily identifiable (also without an H&E staining) based on their size, round shape, and location on the internal layer of the Bowman's space.

In the rest of the kidney, some expression could be found in the endothelial cells of some arteries. The signal intensity was clearly weaker and not all vessels were positive (Figure 9B). No other region of the kidney showed any signal.

As the neuropilin receptor 2 (NRP2) has been described as the main receptor of Sema3G (Taniguchi, Masuda et al. 2005), we localize also NRP2 by immunohistochemistry as complementary information. NRP2 has been found not to be expressed in the podocytes of the glomerulus but in the parietal epithelial cells of the Bowman's capsule. We could otherwise notice some expression in the endothelial cells in the vessel at proximity of the glomerulus, apparently veins or lymphatics but the endothelial cells of the arteries remains negative (Figure 10).

The results on the ligand-receptor localization bring already some information about the mode of action of the Sema3G molecule that certainly acts in a paracrine manner in glomerulus and autocrine in the vascular bed outside of the glomerulus.

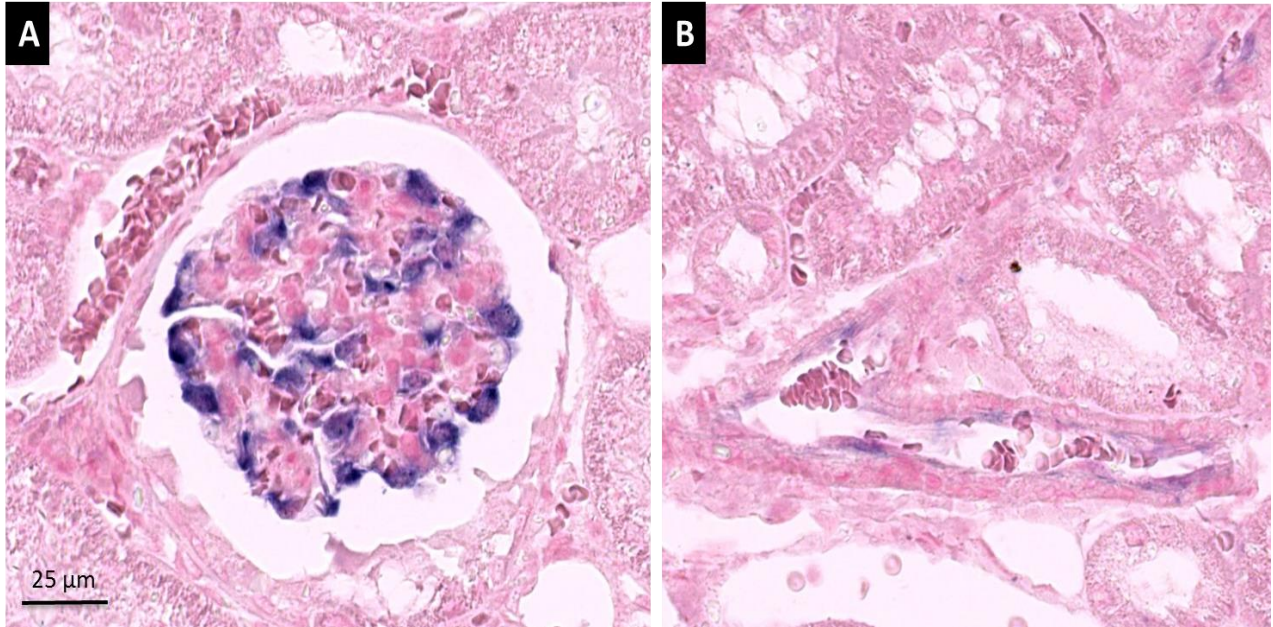


Figure 9: Expression of Sema3G by ISH in the podocytes of the glomerulus from rat adult kidney (A) and in the endothelial cells of arteries (B) (Magnification x40; Blue: NBT substrate for ISH; Red: counterstaining)

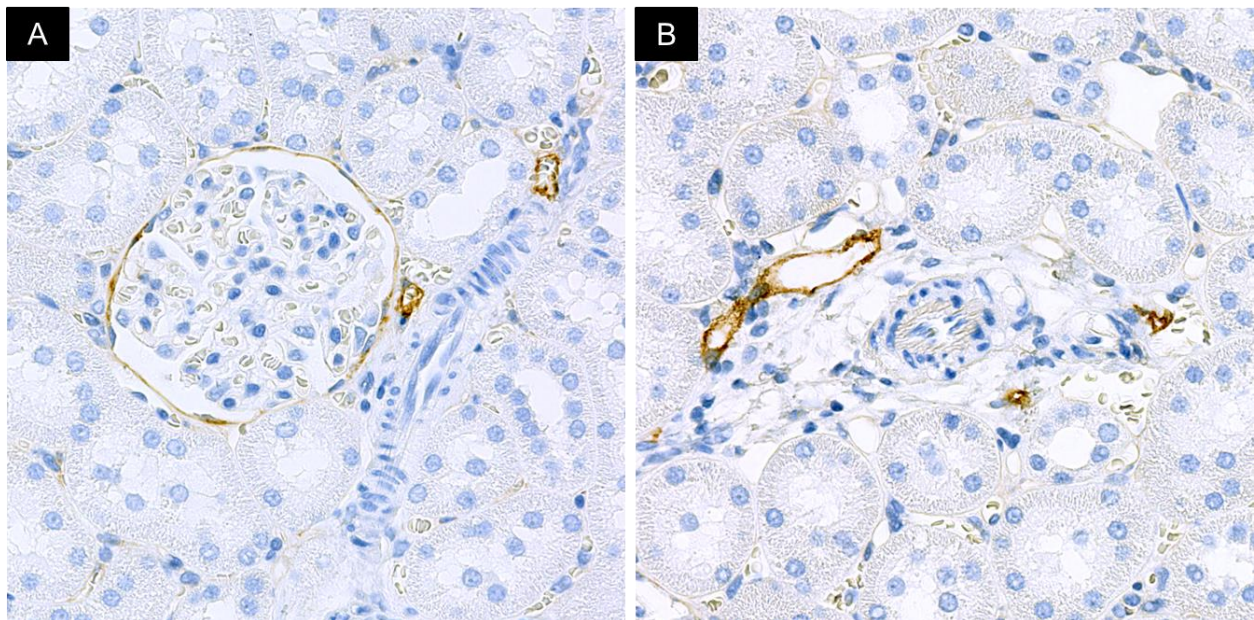


Figure 10: Expression of NRP2 by IHC in the parietal epithelial cells of the Bowmann's capsule in the glomerulus of a rat adult kidney (A) and in endothelial cells of the vascular bed (B) (Magnification x40; Brown: DAB substrate for IHC; Blue: counterstaining)

4.16.3 Expression of CYTC in rat adult normal kidney

Similarly to Sema3G, the staining results at the mRNA level for CYTC showed a strong expression in the podocytes (Figure 11). Mesangial cells and endothelial cells of the glomerulus remained negative.

In the cortex region, few isolated cells in the interstitial tissues between the tubules were stained positively for CYTC (arrow in Figure 11). Additional positive cells in interstitial tissue could be seen in medullary and collecting duct region. These cells seem most likely to be circulating cells, located sometimes close to the vessels and distributed in an irregular manner. Their frequency was varying from one animal to the other. This seems to correlate with previous published data showing that CYTC is produced by macrophages and dendritic cells (Xu, Lindemann et al. 2014) . Epithelial cells of the proximal as well as distal tubules, loop of Henle and collecting ducts were all negative.

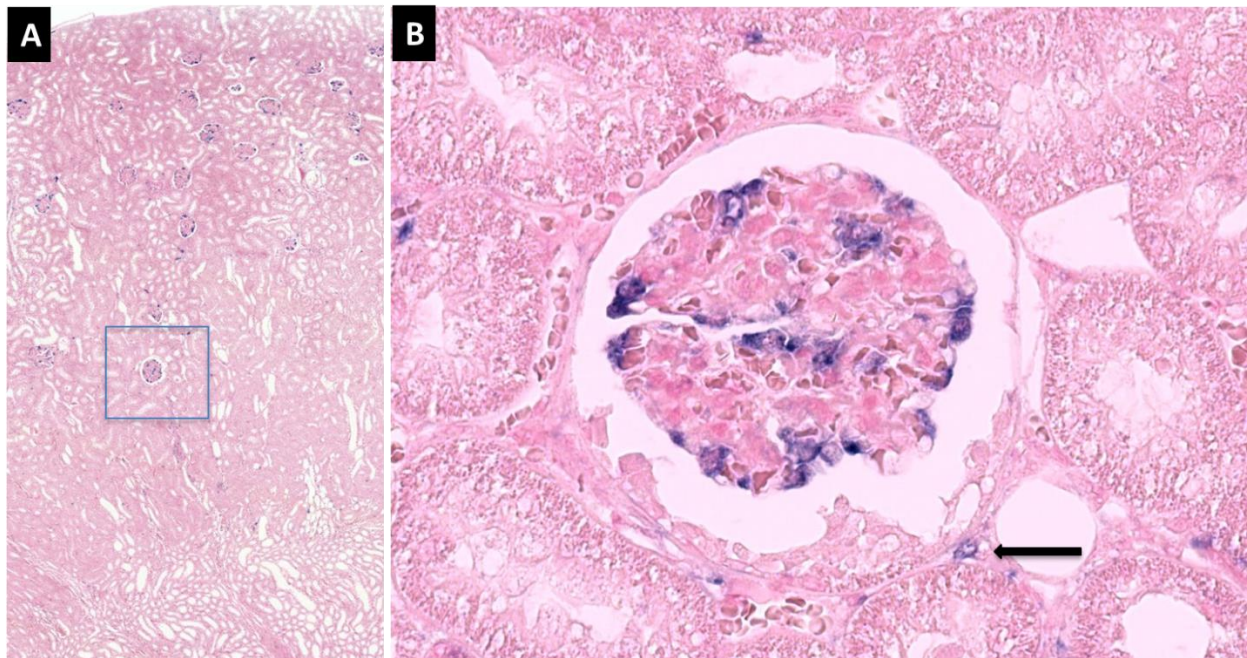


Figure 11: Expression of CYTC by ISH in the podocytes of the glomerulus from rat adult kidney: (A) overview of the cortex region at magnification x1.25 showing the glomerulus specific expression; (B) high magnification of one glomerulus (x40) (Blue: NBT substrate for ISH; Red: counterstaining)

Now, when comparing the protein expression assessed by immunohistochemistry to the mRNA results, immunohistochemistry showed a pretty different pattern of CYTC localization (Figure 12). The protein detection showed a cytoplasmic signal in podocytes (Figure 12) similarly to the *in situ* hybridization, but signal was mainly found in the cytoplasm of the epithelial cells of the proximal convoluted tubules. Previously, no mRNA for CYTC was detected by *in-situ* hybridization in these cells and this means that CYTC is exclusively reabsorb from the lumen of the tubules. The IHC results illustrate the fact that CYTC is metabolized in the proximal tubular cells after a reabsorption by the endocytic receptor megalin (Kaseda, Iino et al. 2007).

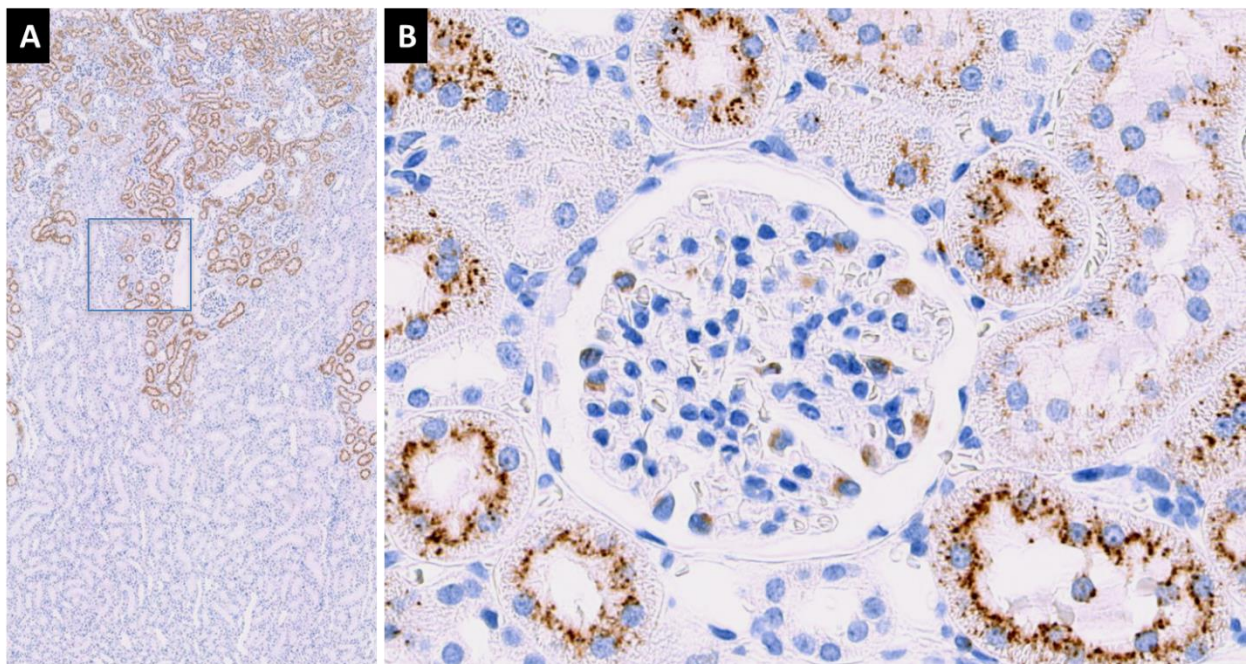


Figure 12: Expression of CYTC by IHC in the podocytes of the glomerulus from rat adult kidney: (A) overview of the cortex region at magnification x1.25 showing presence of CYTC in the proximal convoluted tubule in the cortex region; (B) high magnification of the glomerulus (x40)(Brown: DAB substrate for IHC; Blue: counterstaining)

Summary of Sema3G/CYTC expression in adult rat kidney

The podocytes of the glomerulus are able to synthesize both Sema3G and CYTC.

The two markers co-localize in the glomerulus and are the only cell type of the glomerulus producing these molecules.

At the protein level, CYTC is also produced in the podocytes but the staining results reflect also the reabsorption of the CYTC produced by the proximal convoluted tubules.

4.16.4 Expression of KIM-1 in rat adult normal kidney

Normal rat kidney do not expressed any KIM-1 molecule as demonstrated by the fact generally no signal is observed when conducting *in-situ* hybridization with a rat specific probe for KIM-1 on a normal rat kidney section (Figure 13A).

It remains possible to detect few isolated positive cells expressing KIM-1 in the epithelial cells of the descending portion of the proximal tubule at the cortico-medullary junction in the area corresponding to the segment S3 (see Figure 13B). These scattered positive cells are located in healthy tubules without any sign of pathology. The location remains restricted to this portion of the proximal tubule. Considering that KIM-1 is supposed to reflect any cell injury or cellular stress, this specific pattern illustrates the high susceptibility of this segment to hypoxia due to the paucity of peritubular capillaries in the outer stripe of rodents.

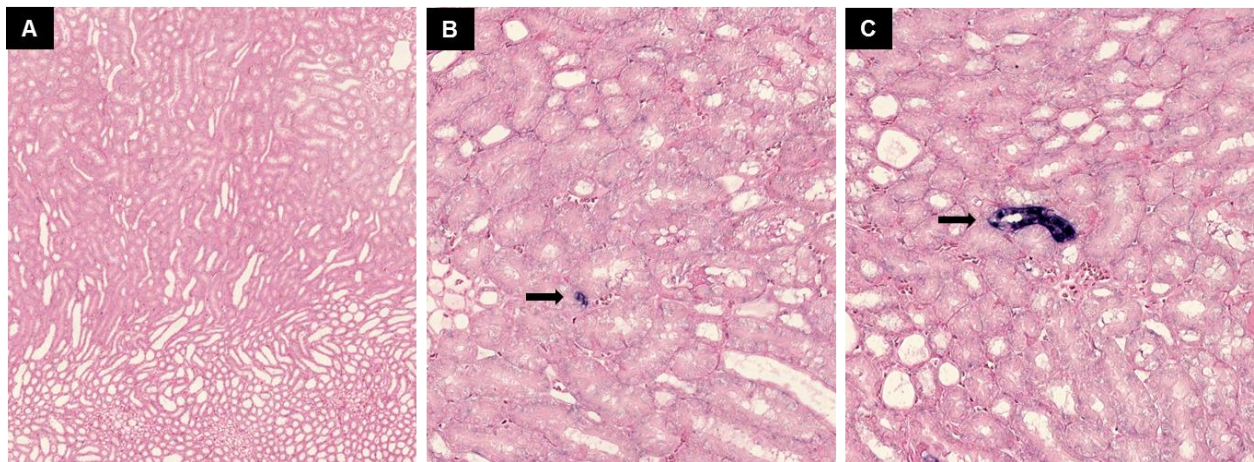


Figure 13: Expression of KIM-1 by ISH in normal rat kidney: (A) KIM-1 is usually not expressed in kidney (magnification x5); Few isolated positive cells (B) and rarely tubules (C) may sometime express KIM-1 in the descending portion of the proximal tubule (Magnification x20) (Blue: NBT substrate for ISH; Red: counterstaining)

4.17 Cross-species expression of Sema3G and CYTC

In order to assess the translational relevance of Sema3G and CYTC podocyte expression, we extend the localization analysis to kidney of other species, including human.

4.17.1 Localization of Sema3G in kidney of mouse / dog / monkey / human

The localization results were obtained using an ISH probe specific for each species (mouse and dog). For monkey and human, the sequence homology is such that the same probe could be used.

The localization data showed that Sema3G is expressed in the podocytes of the glomerulus for all the tested species similarly to the observation in rat. The intensity of the signal varies between the species, being strong in mouse and dog but low in monkey. The difference of expression may not only relate to the quantity of mRNA present but also to the quality/specificity of the probe, therefore no real comparison can be made from a quantitative point of view.

In the vascular bed, some expression could be found time to time in the endothelial cells of the blood vessels but remains a rare event. A representative picture of each species is shown in Figure 14.

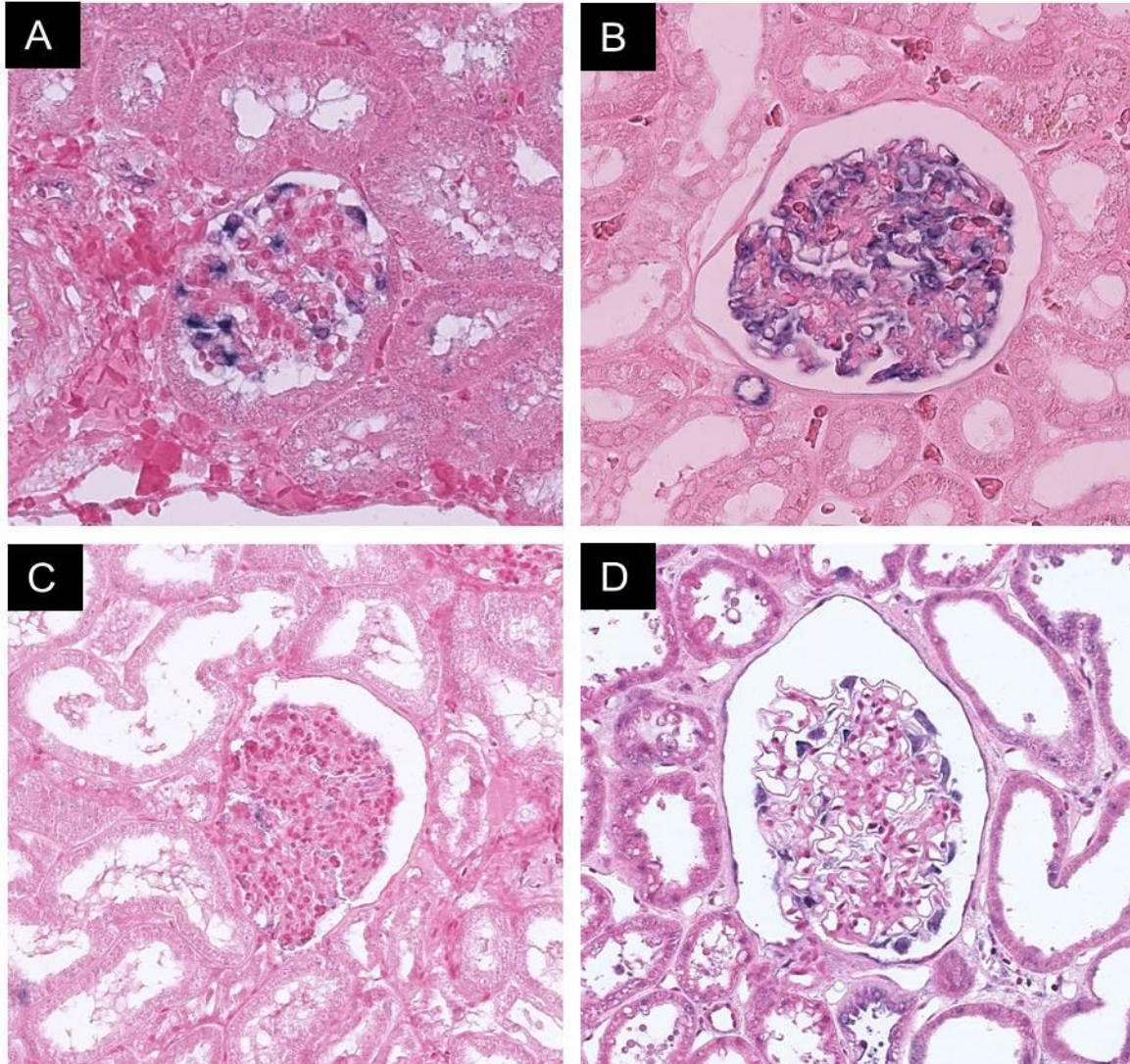


Figure 14: Expression of Sema3G by ISH in the glomerulus of (A) mouse, (B) dog, (C) monkey and (D) human kidney (Magnification at x40 for mouse and dog and at x20 for monkey and human) (Blue: NBT substrate for ISH; Red: counterstaining)

4.17.2 Localization of CYTC in kidney of mouse / dog / monkey / human

The expression results for CYTC at the mRNA level have been generated using a specific probe for each species (except for monkey and human where the same probe was used). No expression of CYTC was found in the podocytes from these species and therefore it seems that CYTC expression is characteristic of rat podocytes.

Failure during the staining protocol giving raise to false negative results or any other technical issue could be excluded as some remaining expression for CYTC could be seen in isolated cells intercalated between the tubule. As described in the rat, these cells certainly correspond to circulating macrophage cells. The total absence of CYTC in the podocytes of the mouse kidney appears is somewhat unexpected as many genes in both species show a similar expression. A representative picture of the glomerulus of each species is shown on Figure 15.

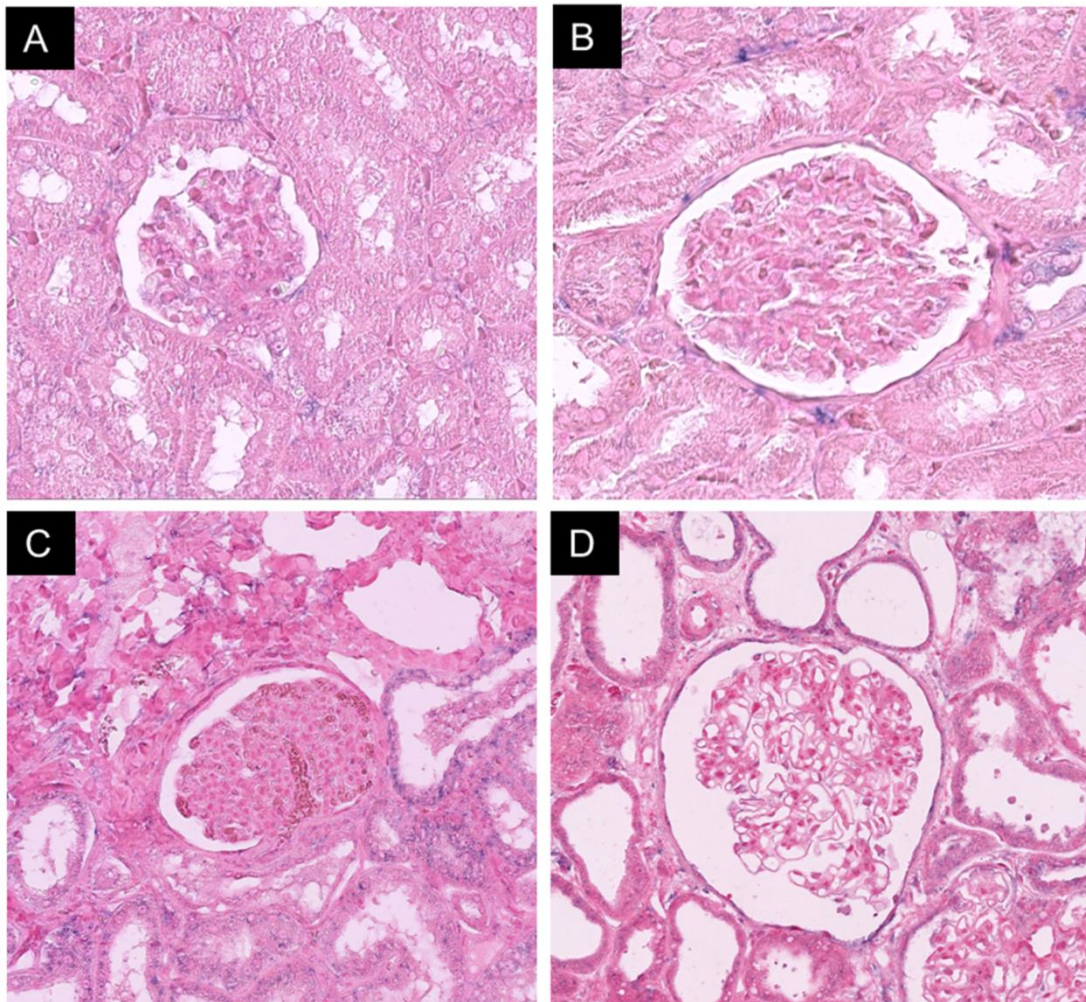


Figure 15: Absence of expression of CYTC by ISH in the glomerulus of (A) mouse, (B) dog, (C) monkey and (D) human kidney. Magnification x40 (mouse and dog); x20 (monkey and human) (Blue: NBT substrate for ISH; Red: counterstaining)

The results of the protein detection were consistent with the mRNA. The same cross-reacting anti-CYTC antibody was used for all species and no staining was found in glomeruli with the exception of rat. Instead, the proximal convoluted tubule cells of the different species were showing a similar pattern to the rat with the reabsorbed cystatin C accumulating in the cytoplasm of the cells at the apical pole (Figure 16).

These results suggest that CYTC may play a unique role in the rat glomeruli compared to other species where the corresponding function could be supported by another molecule or mechanism. But we can also not exclude large variation of expression level in the podocytes between the species and CYTC may remain express but at some undetectable level by immunohistochemistry

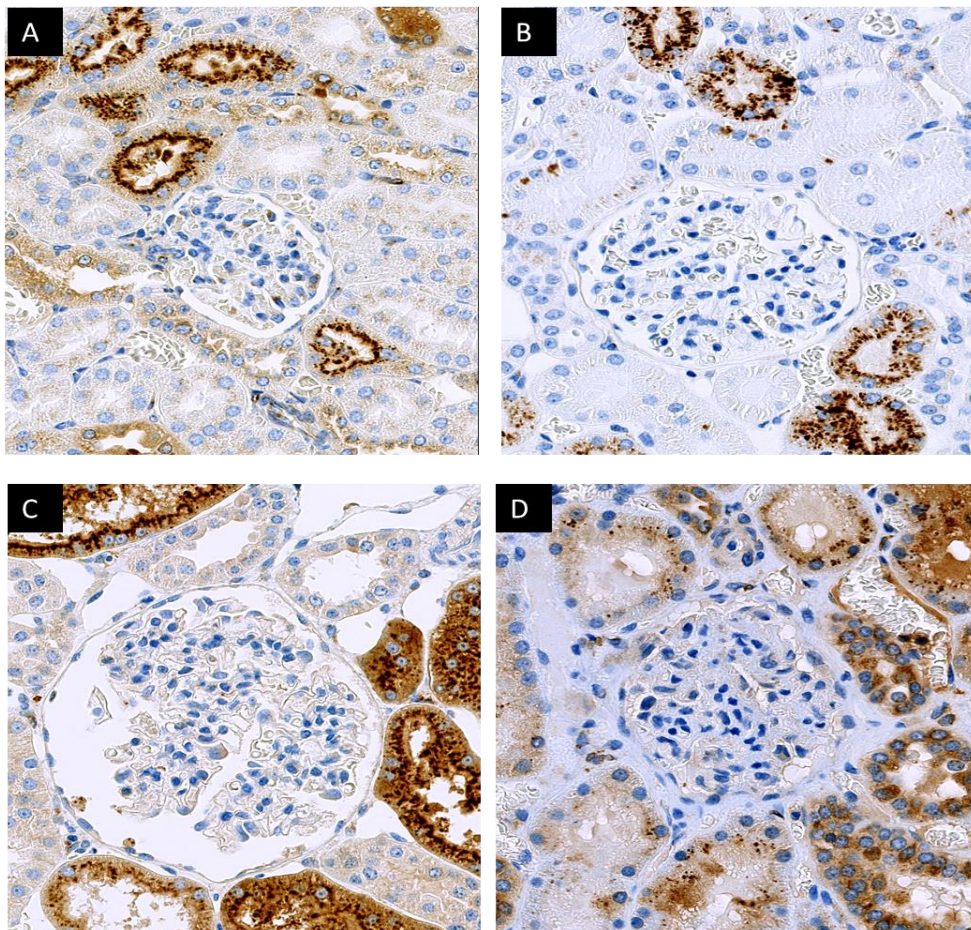


Figure 16: Expression of CYTC protein by IHC in the kidney: glomerulus of (A) mouse, (B) dog, (C) monkey and (D) human kidney are lacking of CYTC expression. Reabsorbed CYTC is visible in proximal tubule. Magnification x40 (mouse and dog); x20(monkey and human) Brown: DAB substrate for IHC; Blue: counterstaining

Summary of Sema3G/CYTC expression cross-species

The expression of Sema3G is similarly located in the podocytes of all the tested species and translates to human.

In the opposite, expression of CYTC in the podocytes seems to be a rat specific location and can't be detected in any other species. This observation indicates that the presence of CYTC is either species specific or is expressed at a lower level in the other species

4.18 Expression of Sema3G and CYTC in rat models of podocytes injuries

Next we investigated the expression of Sema3G and CYTC in different rat models of podocyte injury. These experiments were intended to verify how and if Sema3G and CYTC expression changed in the different models and assess their potential as marker of podocyte injury at a reversible stage versus irreversible stage or if these markers of podocyte injury are in relation with a specific type of injury.

4.18.1 Results of the Albumin overload model

The model of albumin overload according to the method of Yoshida et al, (Yoshida, Nagase et al. 2008) is intended to create a functional impairment of the podocytes due to the excess of albumin injected. The quantity of albumin used is exceeding the filtering capacity of the glomerulus and therefore create some proteinuria. With short treatment duration, the podocyte is not damaged but the filtration is impaired and the flow of protein reaching the proximal tubule is important.

By histopathology, the kidneys of animals receiving albumin showed excessive proteinaceous material in the urinary chamber of the glomeruli and in the tubules. A mild degree of tubular dilation was seen in the cortex.

As the primary goal of this model is to create proteinuria, the first parameter to measure is the quantity of albumin present in the urine samples of the treated animals in order to verify that the model worked properly.

The urines samples of all animals were collected at day 4 and analyzed as described in the material and method section. The results are shown in Figure 17.

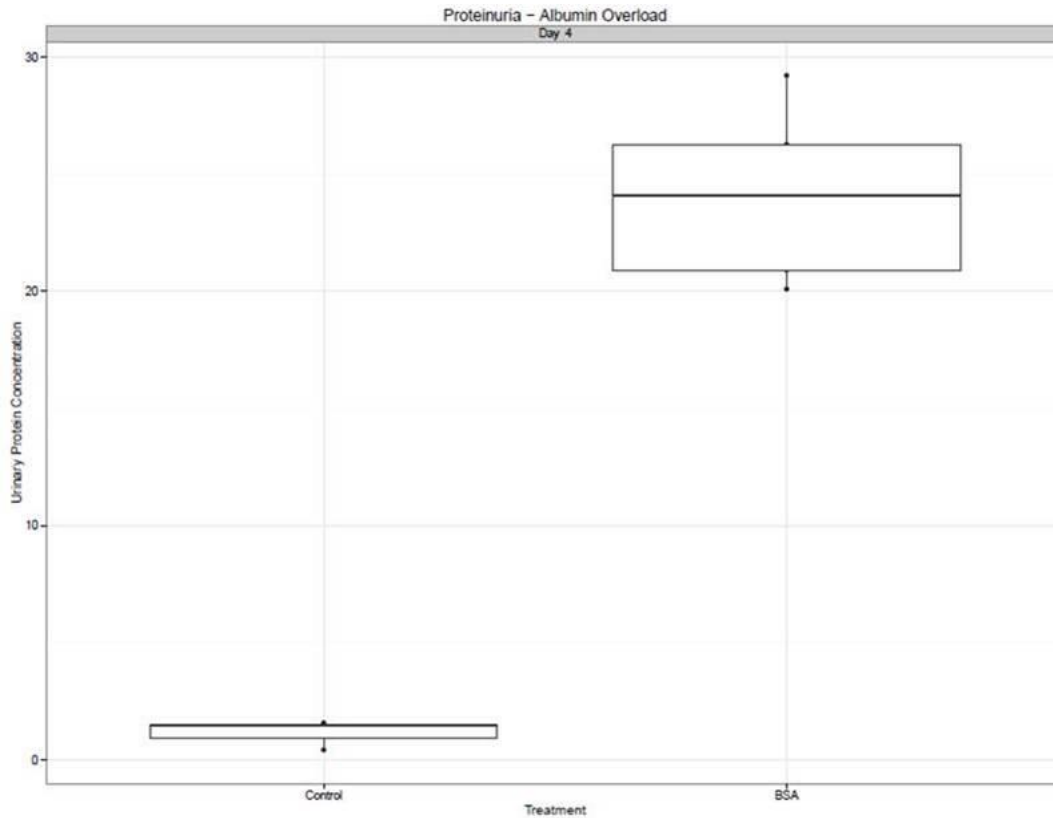


Figure 17: Dosage of albumin in urine samples of PBS or BSA treated animals. The results of the control animals were normalized to 100% and the treatment samples expressed in % of controls. The median is shown by the black line in the box.

These data confirmed that the administration of high dose of albumin during 4 consecutive days resulted into abnormal release of albumin in the urine and showed that the glomerulus was not able anymore to play his role of filtration barrier regarding high molecular weight molecules.

The next step is to look how the two podocytes markers Sema3G and CYTC reacted to this condition of functional impairment and when the filtration barrier capacity is saturated. This question was assessed by *in situ* hybridization using kidney tissue section of PBS and BSA treated animals. The anti-sense probe for Sema3G and CYTC were always tested at the same time with their corresponding sense probe using similar conditions and the staining

results were given after verification of the negativity with the sense probe. The visual evaluation is described after observation of all stained slides.

The expression of Sema3G and CYTC measured by ISH did not showed any visible difference in the staining among the PBS and BSA treated animals. An example of the results obtained with the CYTC probe is shown Figure 18.

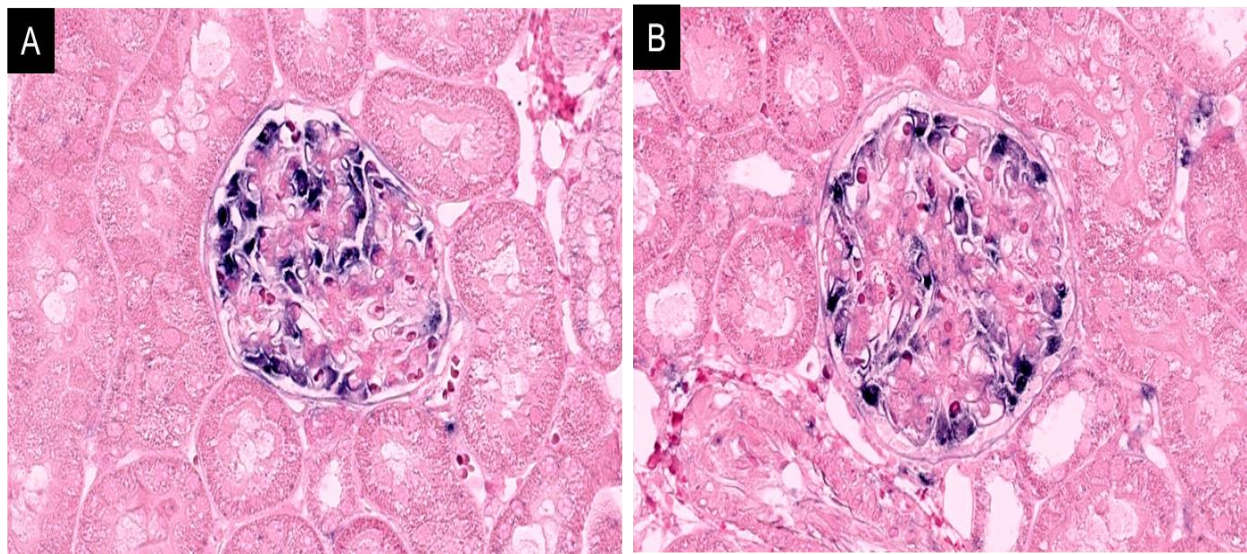


Figure 18: Expression of CYTC by ISH in the podocytes of PBS treated rats (A) versus BSA treated rat (B): no difference of expression is visible. Magnification x40; Blue: NBT substrate for ISH; Red: counterstaining

To make a precise evaluation of the expression of these markers, a quantification of the mRNA signal using image analysis was performed to confirm this result.

The specific optimal density was measured in the glomeruli of the tissue section using the method described previously in the material and method section. The glomeruli were randomly selected and manually drawn (n=40 per slide). Considering that the total number of glomeruli in a transversal section is between 200-250 pieces, the selected number of 40 represents approximately 20% of the total number of elements. The image analysis results are shown in Figure 19 for Sema3G and CYTC.

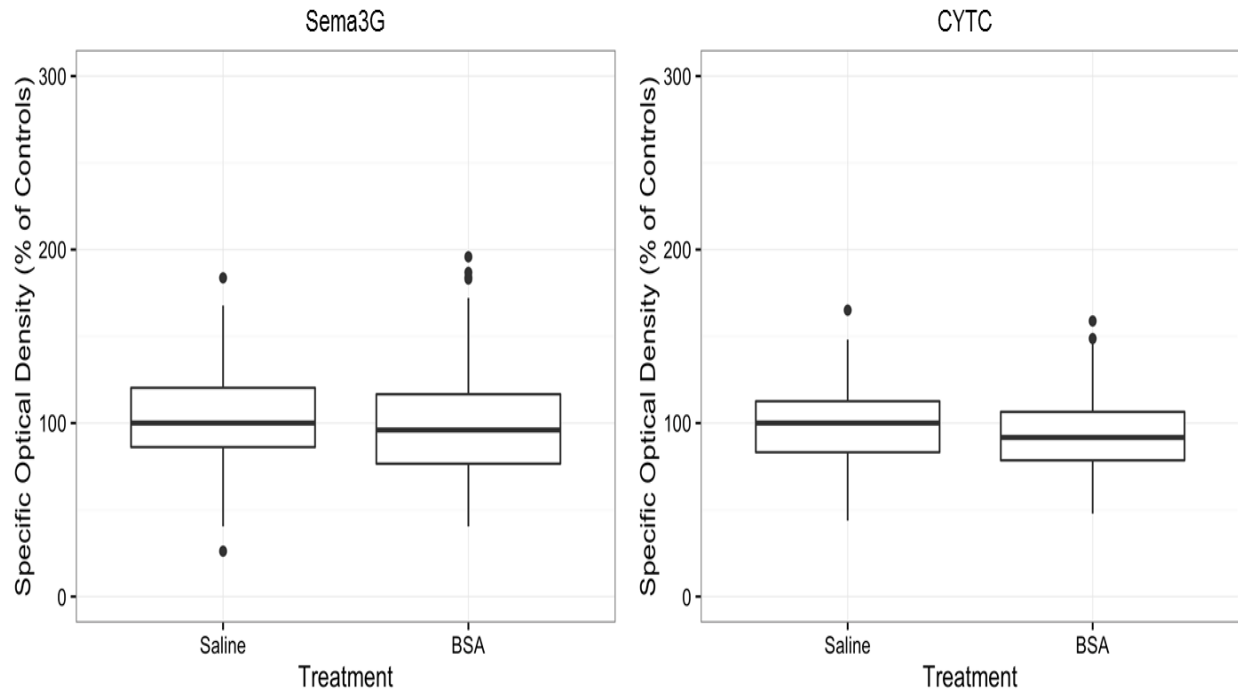


Figure 19: Specific optical density measurement in the glomerulus of PBS or BSA treated rats expressed in % of the median of the control.

The quantitative results of the analysis for both markers confirmed the visual observation and showed that no modification of the Sema3G and CYTC expression is occurring after treatment with high dose of albumin, indicating that the situation of functional impairment do not affect the expression of these two markers.

In parallel to the *in situ* hybridization staining, a second tissue section was used to measure the CYTC protein pattern. The staining results with the anti-CYTC antibody showed that similarly as the mRNA, the protein detected in the podocytes remains unchanged with or without BSA.

Instead, the evaluation of the reabsorbed CYTC by the proximal tubules cells showed a signal that was often diminished in term of intensity and more diffused in the epithelial cells (annotation with * in the Figure 20B) instead of the crispy signal in the apical pole of the cells usually observed. The lumen of many tubule was also found to be filled with

accumulated protein (annotation ** in the Figure 20B). Obviously the reabsorption of CYTC by the epithelial cells was impaired or saturated considering the unusual quantity of albumin present in the portion of the kidney. This impaired CYTC reabsorption in a competitive situation with albumin was described by Nejat et al. (Nejat, Hill et al. 2012) and was related to a saturation of their commonly used megalin receptor. A large quantity of CYTC was probably released in the urine.

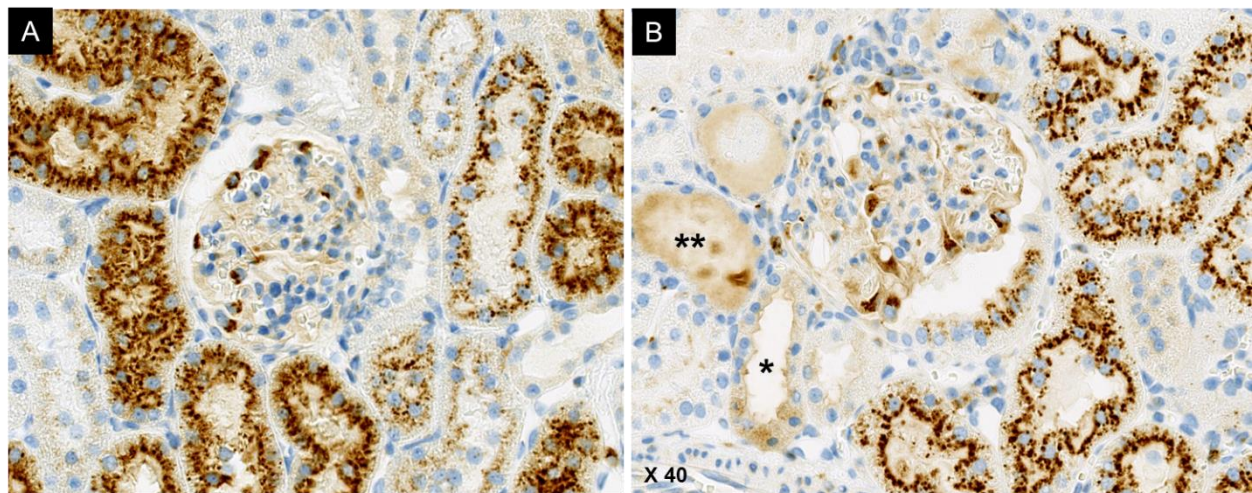


Figure 20: CYTC protein expression by IHC in the kidney of (A) PBS treated animal and (B) BSA treatment animal: No changes in the podocytes can be noticed but impaired reabsorption in certain proximal tubule cells (and **) is visible. Magnification x40; Brown: DAB substrate for IHC; Blue: counterstaining.*

Considering that the presence of high quantity of albumin in the tubule is “unusual” and affecting the reabsorption of CYTC, a “secondary” or “indirect” toxicity of the tubular cells can be expected. Therefore, investigations using the injury marker KIM-1 were performed by *in situ* hybridization.

The staining results with the KIM-1 probe in the PBS treated animals group showed that the presence of KIM-1 was rare or restricted to few isolated positive cells in the descending portion of the proximal tubule at the cortico-medullary junction. It has to be mentioned that one outlier animal was found and this animal showed a damaged nephron expressing KIM-1. This animal was not considered for the analysis and discussion.

In the BSA treated animal group instead, KIM-1 expression became visible in all animals and was broadly distributed in the kidney (cortex and outer medulla). A positive staining was found as well in the proximal part of the tubule as in the descending part. In some cases, signal could be observed along the entire proximal tubule.

The cells expressing KIM-1 were either strongly positive or remain completely negative without gradient of intensity. The distribution of positive cells/tubules in the cortex was relatively randomized. At the junction with the medulla, the presence of positive tubules was frequent and was often in dilated tubules. The overall staining gave an impression of “patchy distribution”. Some pictures of BSA treated animals are shown Figure 21.

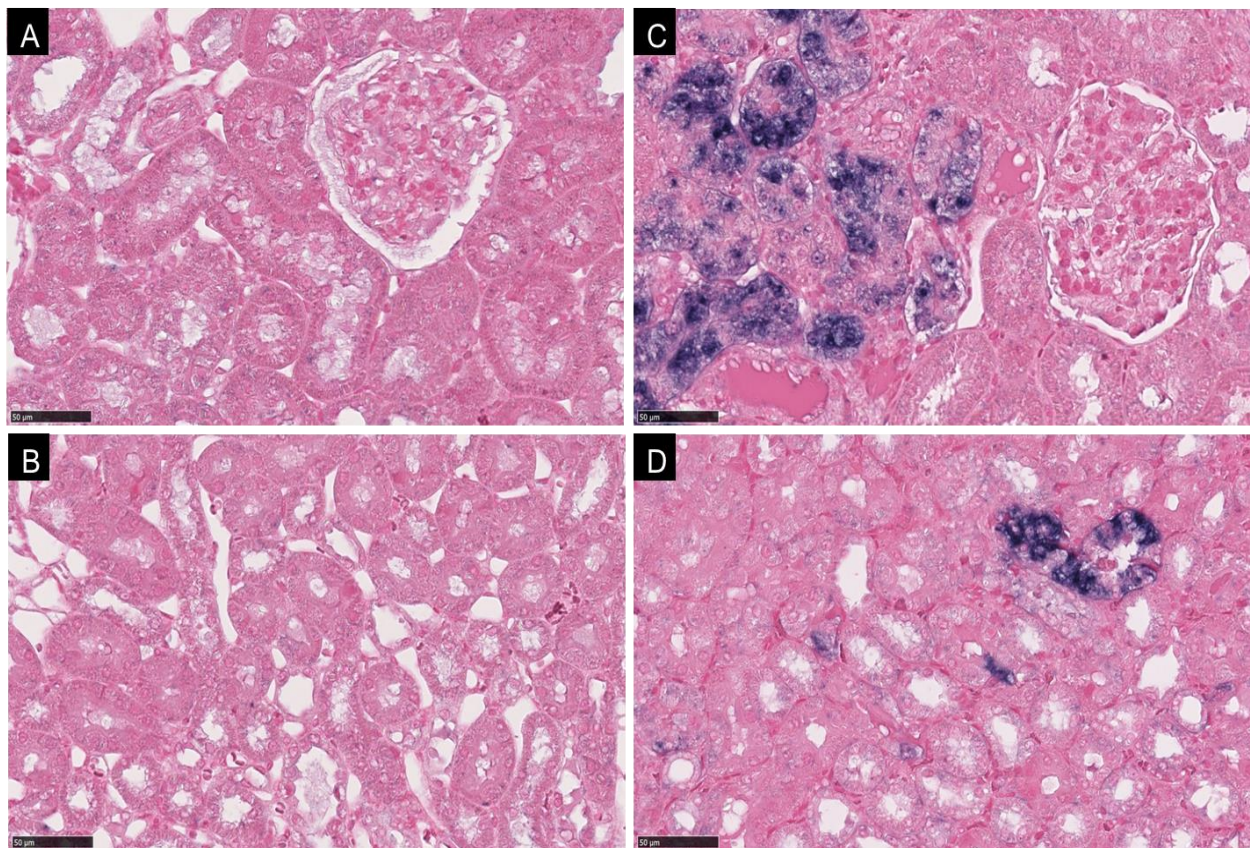


Figure 21: KIM-1 expression by ISH in rat kidney after PBS treatment (A: cortex)(B: outer medulla): No KIM-1 expression could be detected. After BSA treatment (C: cortex)(D: outer medulla): KIM-1 is expressed in damaged tubule. Magnification x40. Blue: NBT substrate for ISH; Blue: counterstaining.

We attempt to define a global pattern of KIM-1 expression in the different part of the kidney. Therefore, the fingerprint described in the material-method part was generated for KIM-1. The first step consists in a segmentation that identifies the regions of the kidney: cortex, outer-medulla, inner-medulla/pelvis. A none-tissue region was created and excluded from the analysis. The second step consists of a sensitive detection of the KIM-1 signal based on the staining intensity. Segmentation and analysis results are shown in Figure 22.

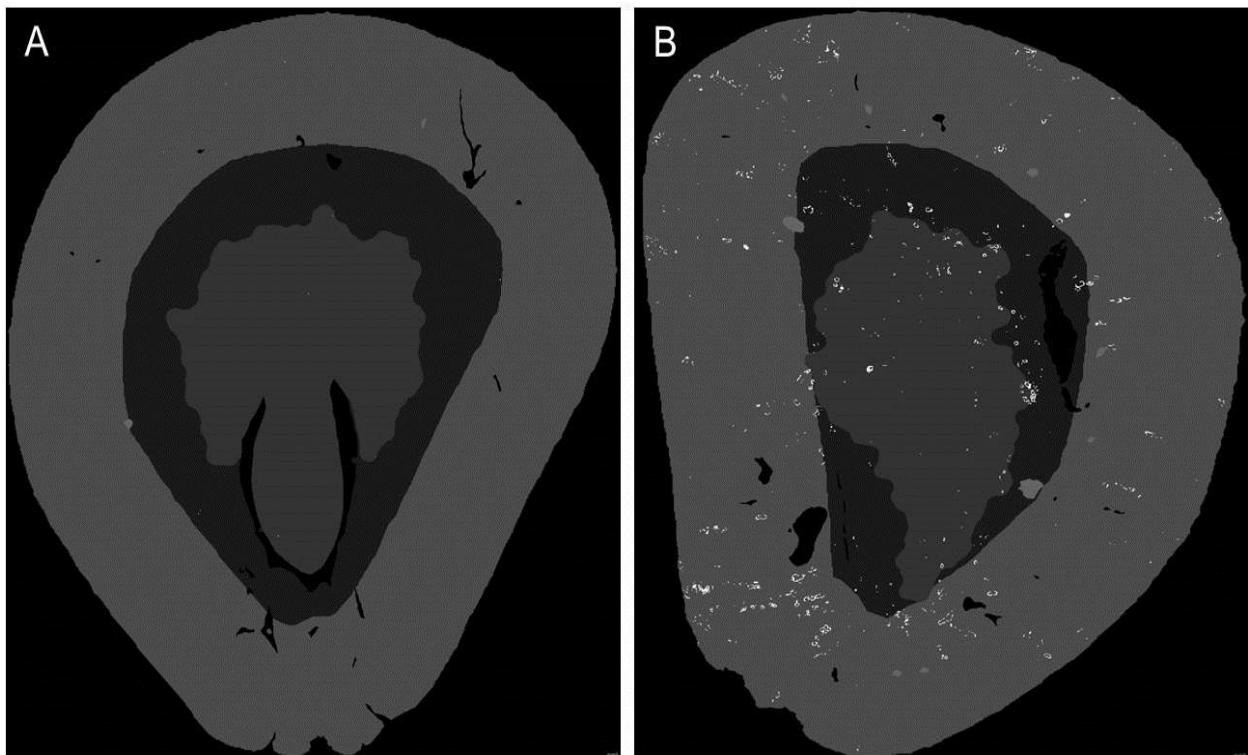


Figure 22: Fingerprint results for the KIM-1 expression pattern by ISH using the Definiens software: (A) PBS treated animal, (B) BSA treated animal. The cortex is represented in light grey; outer medulla in dark grey; inner medulla/pelvis in grey. The KIM-1 expression is represented in white color and appears as patchy signal in the cortex only of BSA treated animals.

From this global pattern visualization and segmentation, it results that the animal treated with BSA showed a patchy distribution profile, equally distributed between the different segments of the kidney. When specifically assessing the signal intensity data for the KIM-1 signal in the 3 segments, the intensity of KIM-1 is distributed between the different segments but with higher quantity in cortex compare to medulla (Figure 23).

This demonstrates that after a functional impairment of the podocytes related to an overload of albumin, KIM-1 expression is induced in the proximal tubule cells that are receiving a flow of large protein. The injury is distributed all along the proximal tubule in cortex until the medulla.

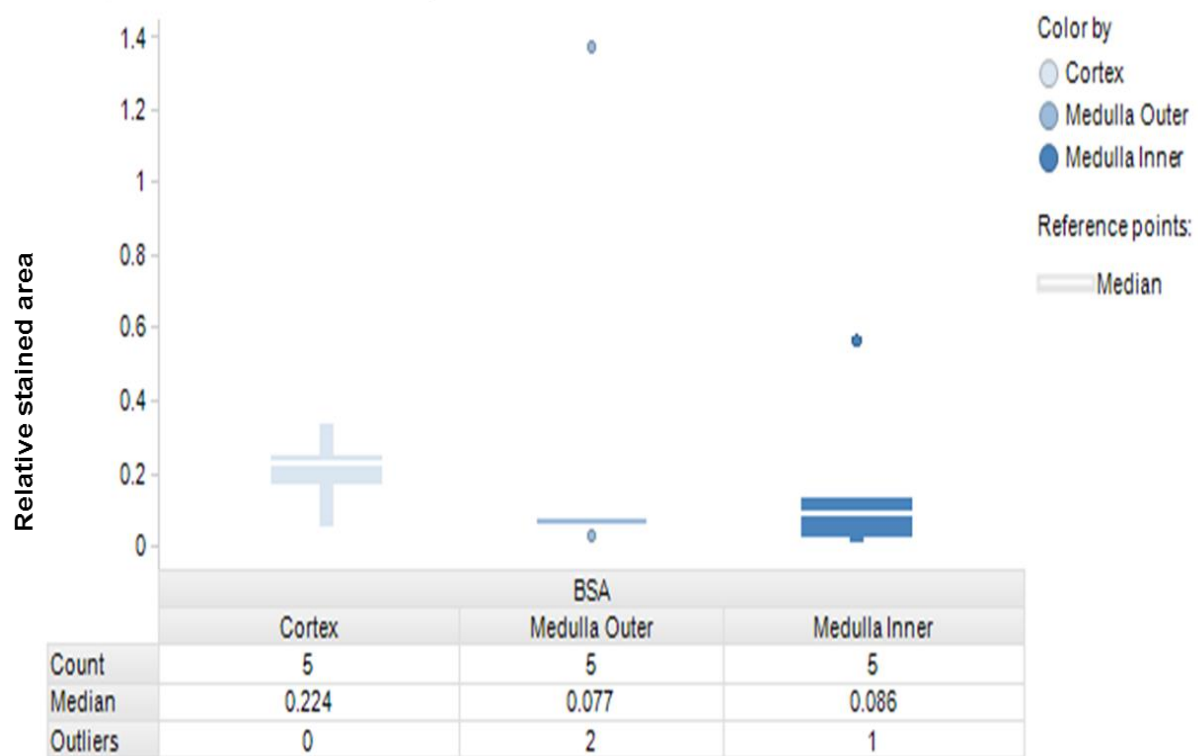


Figure 23: KIM-1 quantification in the different segments of the kidney in a situation of albumin overload. Analysis was performed by Definiens and results are expressed in relative area stained.

Summary of the albumin overload model results

With a functional alteration of the glomerulus, the expression of Sema3G and CYTC remains normal in the podocytes although the filtration barrier affected.

This abnormal presence of albumin is disturbing the reabsorption of CYTC by the proximal tubular cells and is inducing some toxicity as indicated by the tubular injury marker KIM-1 all over the proximal tubule.

4.18.2 Results of the Passive Heymann nephritis model

The model of Passive Heymann nephritis is used to reproduce the pathogenesis of human membranous nephropathy. This model is characterized by proteinuria, a sub-epithelial immune deposition that obscures the slit diaphragm. Complement activation and deposition occurs in the glomerular basement membrane and affects the podocytes, causing damage and intracellular signaling activation. In this situation, there is a structural impairment that leads to podocyte stress and adaptation reaction. The only histological changes are the thickening of glomerular basement membrane and foot effacement process that can usually be observed only by electron microscopy.

The histopathological evaluation of the kidney samples taken from rats treated with anti-FxA1 antibody was difficult because of the freezing technique chosen for this model. The nature and intensity of glomerular changes was difficult to appreciate. Some glomerular sections clearly showed hypertrophy or desquamation of podocytes. In the majority of animals, foci of minimal tubule-interstitial inflammation were noted.

With the help of immunofluorescence, the deposition can be visualized by using an anti-c3 complement FITC-conjugated antibody on frozen tissue section and can be observed by fluorescent microscopy (Figure 24). At this time point of day 14 post anti-FxA1 injection, the presence of complement deposition became clearly visible with this method (green signal in Figure 24) and the deposit is classically described as a “string of pearls” pattern in the glomerular capillary.

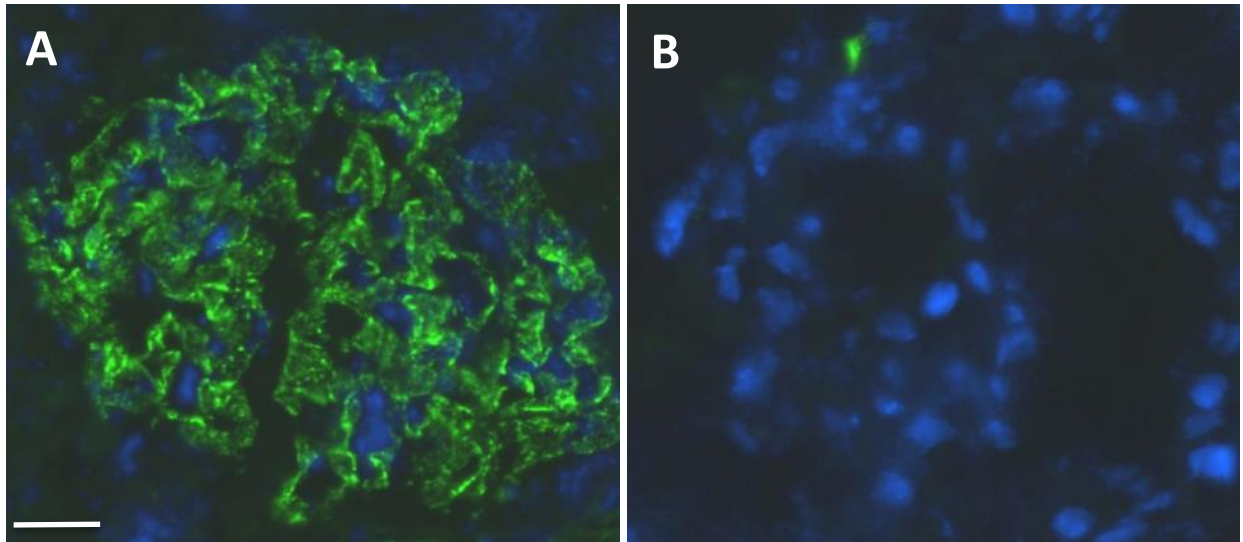


Figure 24: Rat glomerulus of anti-FxA1 treated animal (A) and sheep IgG treated animal (B) stained with an anti-C3 antibody to verify the deposition complement in the GBM: Presence of complement deposition is visible only after anti-FxA1 treatment. (Magnification x40) (Green: anti-c3 detection with Alexa488, Blue: DAPI counterstaining).

The presence of signal in the glomeruli of anti-FxA1 treated animals confirms the complement deposition by this “string of pearls” pattern when compared to animal treated with the anti-sheep Ig only. In the IgG treated group not any signal could be observed. This result confirmed the validity of the model.

The analysis of the urine samples also confirms the development of the disease model. Urine was collected at day 6 and 13 and the measurement of the excreted albumin at these two time points showed a time related increase of the proteinuria (Figure 25). At day 6, the increase of albumin released is still moderate (except one animal which is already quite high) but a stronger albuminuria is happening after 13 days. The time point of day 5 is usually described as the starting point for proteinuria development during the heterologous phase of the disease, followed by the autologous phase of the disease with establishment of a stronger proteinuria. Looking at the urinary data, the proteinuria may not be very strong but remains enough to conclude of a pathological situation.

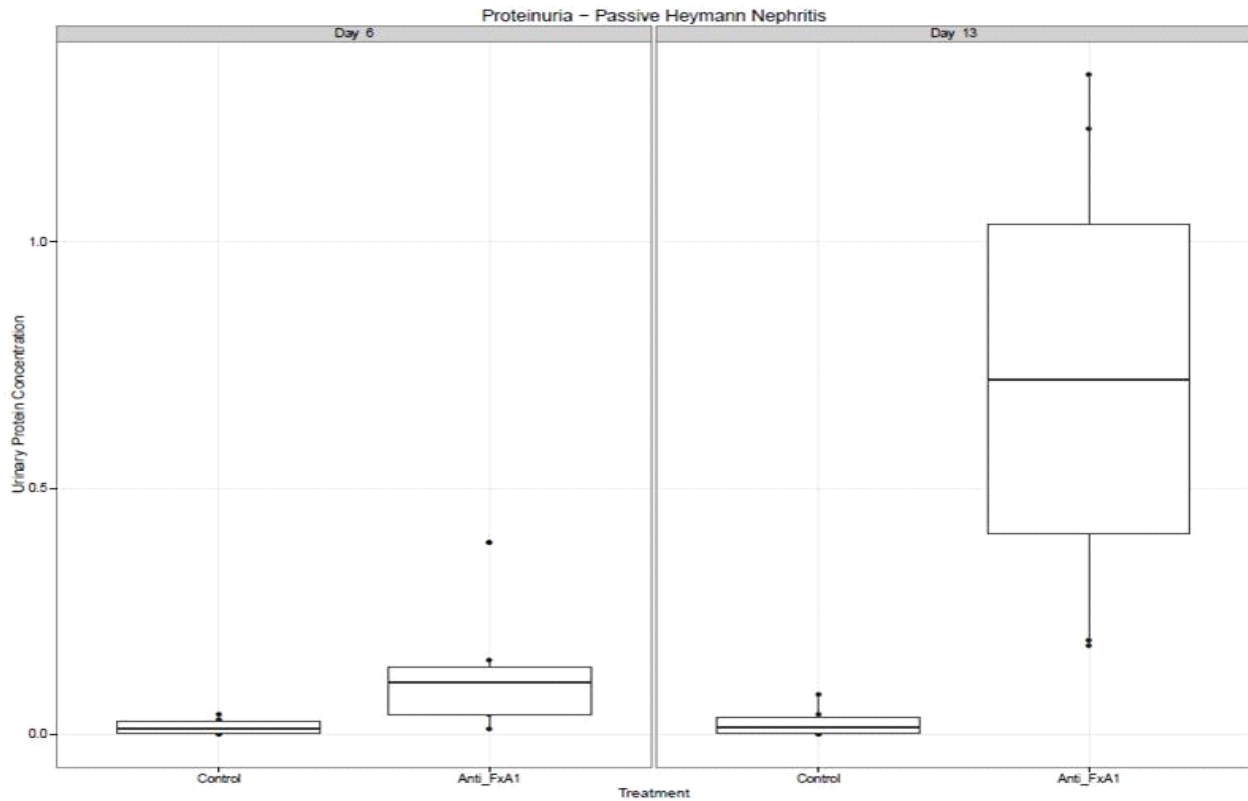


Figure 25: Dosage of albumin in the urine of anti-sheep IG or anti-FxA1 treated animals. The results of the control animals were normalized to 100% and the treatment samples expressed in % of controls. The median is shown by the black line in the box.

In this context of proteinuria, the expression of the two podocyte markers has been assessed on the frozen tissue sections by *in situ* hybridization using the same probe and a slightly modified protocol for frozen tissue.

The staining results were more difficult to assess due to the histological quality of the samples compared to FFPE but was nevertheless possible to perform the analysis.

Sema3G staining using ISH tends to show a decrease of the intensity in the podocytes of the glomeruli but in some others, the differences are not obvious. It indicates that there are some variations and potential intensities of reaction within the same animal. A picture from an affected glomerulus is shown in Figure 26.

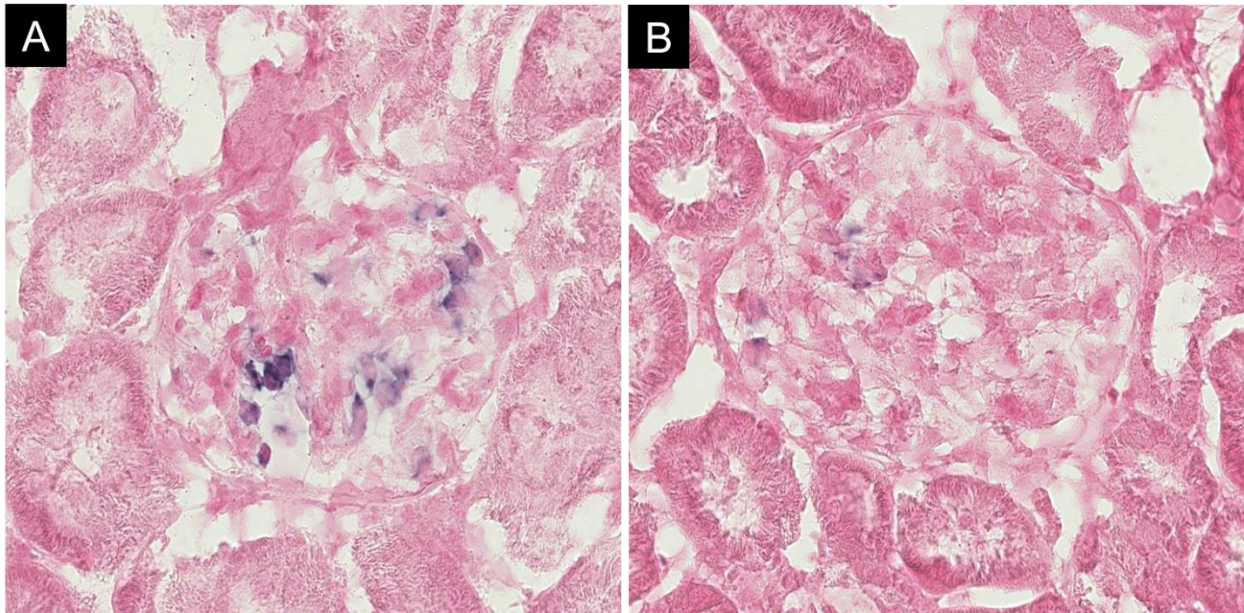


Figure 26: Expression of Sema3G by ISH in the podocytes of sheep IgG (A) and anti-FxA1 (B) treated rat (frozen sections). The Sema3G signal is downregulated with anti-FxA1 injection. Magnification x40; Blue: NBT substrate for ISH, Blue: counterstaining)

In the opposite, the staining for cystatin C at the mRNA level didn't show any difference between the anti-FxA1 and the sheep serum injected animals (data not shown). Consistently with the mRNA results, the staining at the protein level did not revealed any modification of the expression in podocytes (Figure 27). Also the reabsorption of the protein by the epithelial cells of the tubules was not affected. No released of protein in the lumen could be detected at any place. No further interpretation of the staining results could be done with these samples considering the poor quality of the sections.

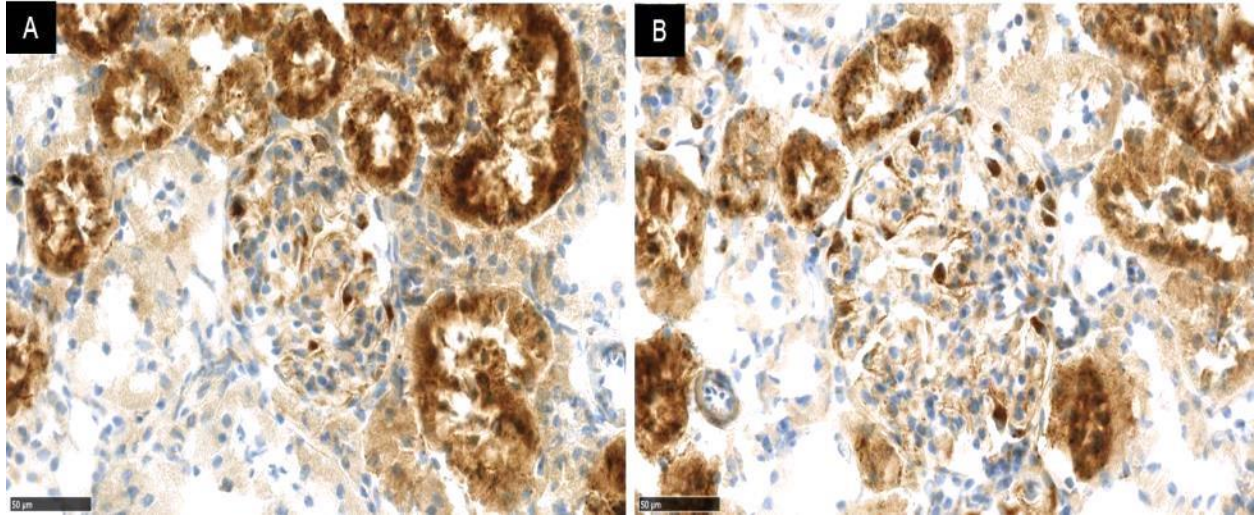


Figure 27: Expression of CYTC by IHC (frozen section) in the glomerulus of sheep IgG treated rats (A) versus anti-FxA1 treated rats (B): No change could be observed. (Magnification x40; Brown: DAB substrate for IHC, Blue: counterstaining).

The quantification of the mRNA results by image analysis was performed for the ISH markers Sema3G and CYTC. In term of method, the same rule used in the analysis of the protein overload model was used and 40 manually drawn glomeruli per section were analyzed.

The quantitative image analysis results confirmed the slight decrease of Sema3G expression in the glomeruli in the anti-FxA1 treated animals and the changes were statistically significant with $p < 0.05$. Instead, no statistically significant change could be measured for the expression of CYTC as already observed visually (Figure 28).

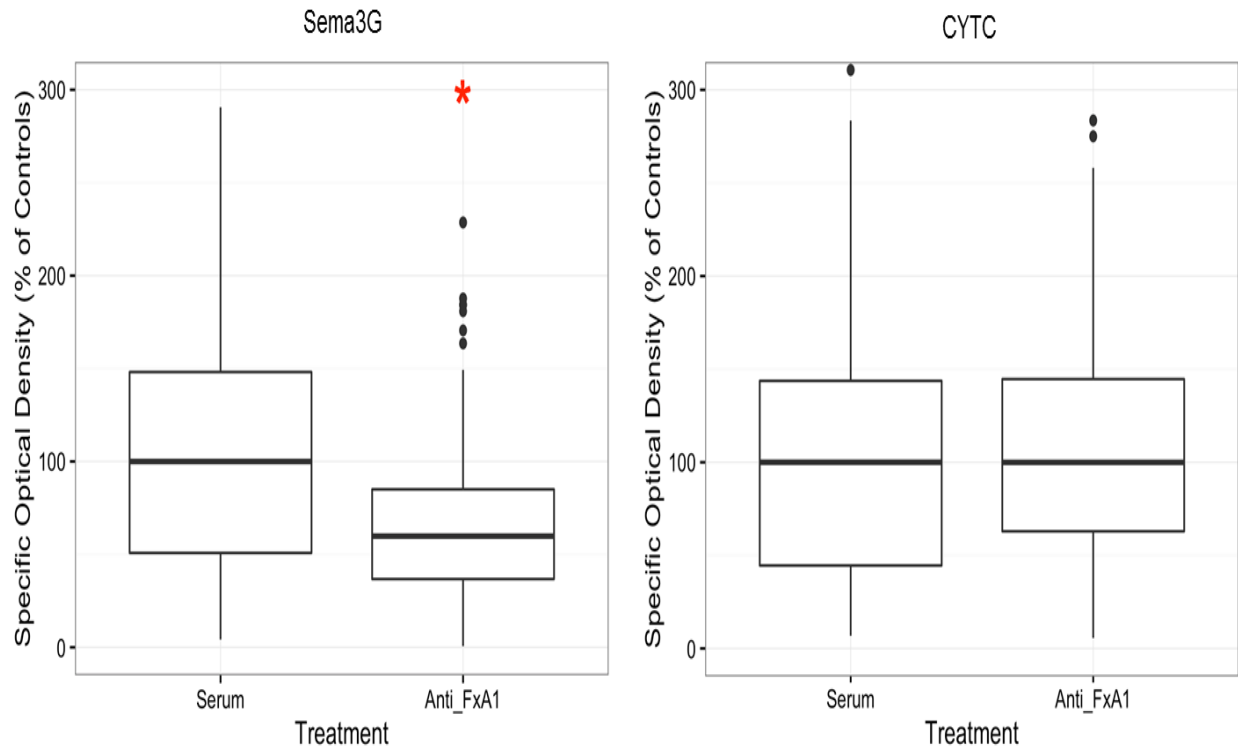


Figure 28: Specific optical density measurement in the glomerulus of sheep serum or anti-FxA1 treated rats. Results are expressed in % of the median of the control group.

KIM-1 staining on the anti-sheep IgG injected animal tissue samples (control group) was globally negative for all animals. In the anti-FxA1 group, KIM-1 expression was clearly visible but limited to few enlarged tubules located in the area of the descending portion of the proximal tubule. Only one animal was found with some tubules stained in the outer cortex. A representative picture is shown in Figure 29.

The availability of frozen materials only made the fingerprint quantification not feasible and only the descriptive expression of KIM-1 expression was possible.

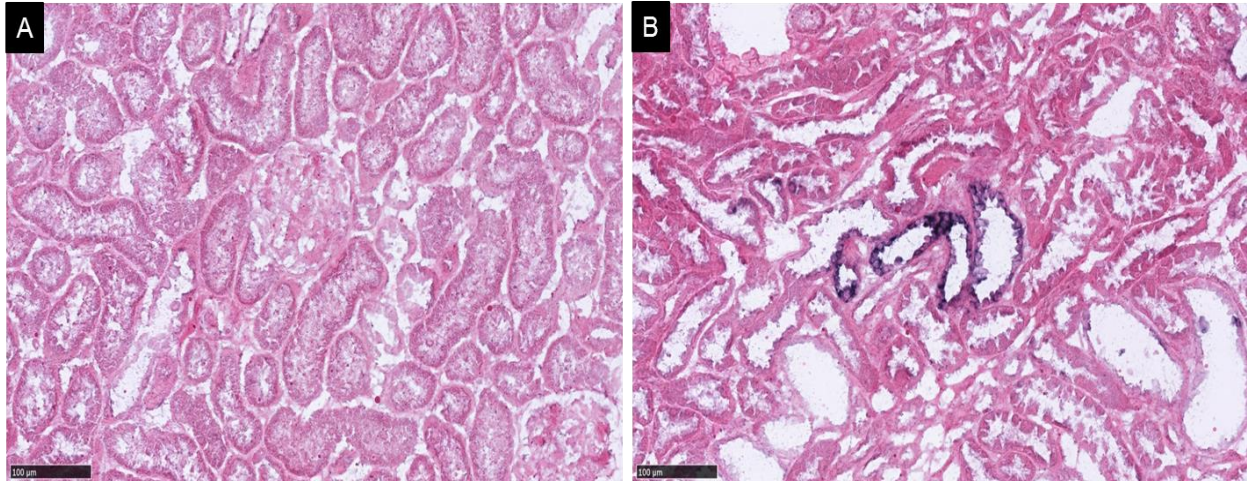


Figure 29: Expression of KIM-1 by ISH in the kidney of anti-FxA1 treated animal. (A) The cortex region was devoiding of signal when some tubules at the junction between cortex and medulla (B) appears positive for KIM-1. (Magnification x20; Blue: NBT substrate for ISH, Red: counterstaining)

Summary of the PHN model results

The structural model of podocyte injury with complement deposition in the slit diaphragm and proteinuria showed a difference of behavior between the two markers Sema3G and CYTC.

In the podocytes, Sema3G expression was decreased when CYTC remains unchanged.

With this result, Sema3G demonstrate an interesting profile and shows that its expression can be modulated in a situation of podocytes adaption related to stress.

The tubular injury as measured by KIM-1 showed a limited toxicity.

4.18.3 Results of the nephrotoxicity models

4.18.3.1 Podocyte markers in *in vivo* rat studies

The podocyte is the primary target of the puromycin aminonucleoside (PAN), therefore the PAN rat model became a powerful tool for investigating podocytes pathophysiology. There is a progression of the glomerular lesions from podocytes effacement to glomerular scarring. The podocytes foot processes disorganize into broad expanses of epithelial cytoplasm and show typical flattening and loss of foot process, until podocytes detachment. In this situation, this model should allow us to study the reaction of the two markers in a clear drug-induced toxicological context. As a comparator model, cisplatin-induced nephrotoxicity primarily occurs in kidney proximal tubule epithelial cells. Cisplatin is cleared by the kidney through glomerular filtration without damaging the podocytes but then the uptake of cisplatin in renal tubular cells is high, leading to cisplatin accumulation and tubular cell injury and death.

By histopathological examination of the kidneys of PAN treated animals, the main lesions were seen in the glomeruli, and consisted in minimal or moderate vacuolation and mesangial proliferation, but also a slight fibrous thickening of the Bowman's capsule. Minimal tubular changes were observed, mostly tubular basophilia. The glomerular changes appeared in few animals on day 7 whereas all animals were affected on day 14. The histological lesions observed in rats treated with cisplatin were moderate to severe tubular basophilia, sloughing or necrosis alternating with cellular hypertrophy and regeneration in both the pars convolute and the pars recta of the proximal tubules.

The analysis of the total protein in the urine samples was measured at day 3, 7 and 14 in the vehicle, PAN and cisplatin treated animals. Under PAN treatment, the level of proteins released is increasing only after 14 days of treatment and reveal the loss of function of the podocytes. This loss of barrier function is often described to occur earlier (e.g. day 8) but was not observed in our case.

In comparison, the cisplatin treatment does not modify the level of proteins released by the kidney at day 7 and day 14 time points. Instead, there is a transient release of protein at day 3 that illustrate the single dose treatment effect and its toxicity effect on the tubular cells. This proteinuria is a tubular type proteinuria composed of low molecular proteins such as beta-2 microglobulin, which in normal conditions are completely reabsorbed by proximal tubules (and not high molecular weight protein as in the glomerular proteinuria). It means that at day 3, the tubular function is affected but not the glomerulus and at later time point the tubular cells are kind of restoring their capacity of reabsorption (Figure 30).

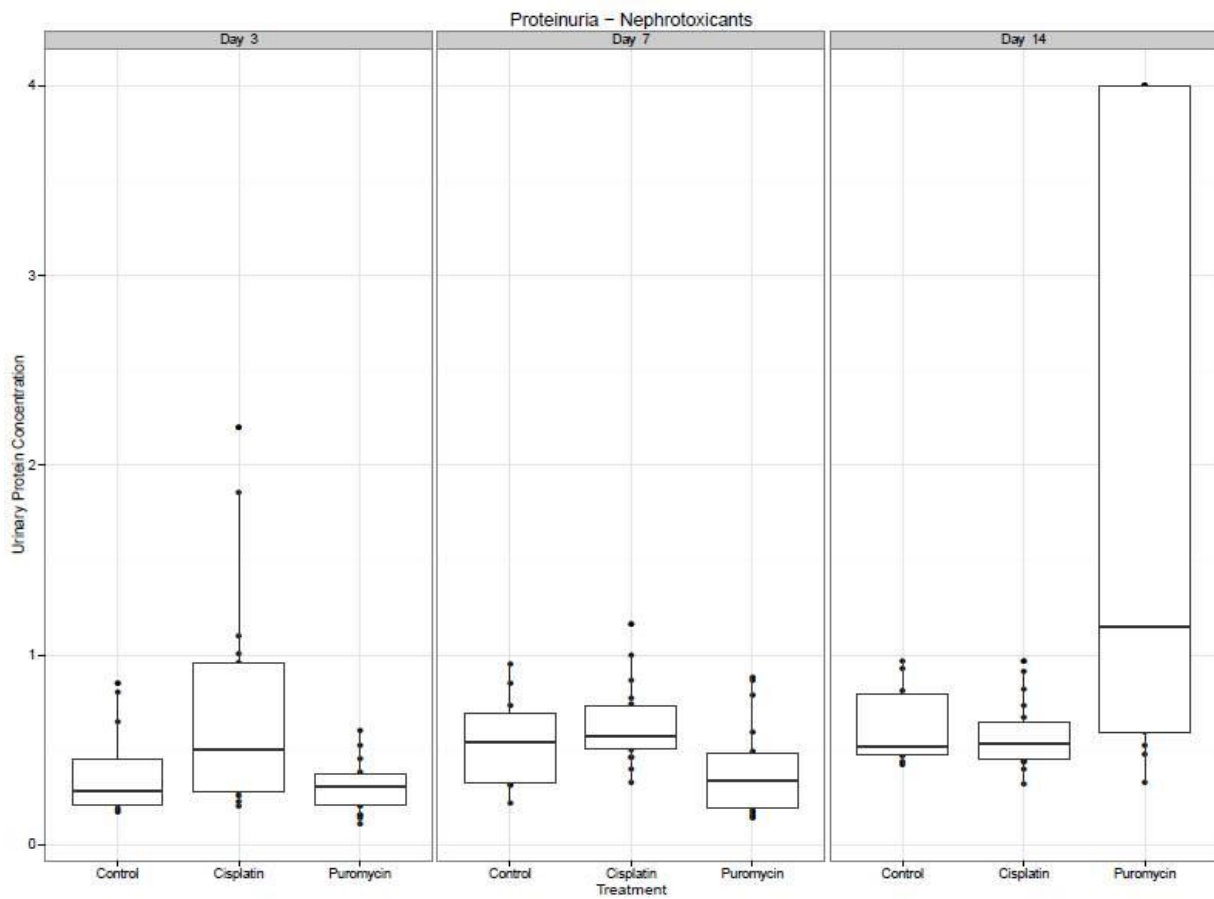


Figure 30: Proteinuria levels in the urine of PAN and Cisplatin treated animals. The results of the control animals were normalized to 100% and the treatment samples expressed in % of controls. The median is shown by the black line in the box.

Assessment of Sema3G and CYTC in these two toxicity models was conducted.

In the PAN treatment study, Sema3G was tested by *in situ* hybridization at all time points and compared to the vehicle group. Representative pictures from the different time points in animal treated with PAN are show in Figure 31.

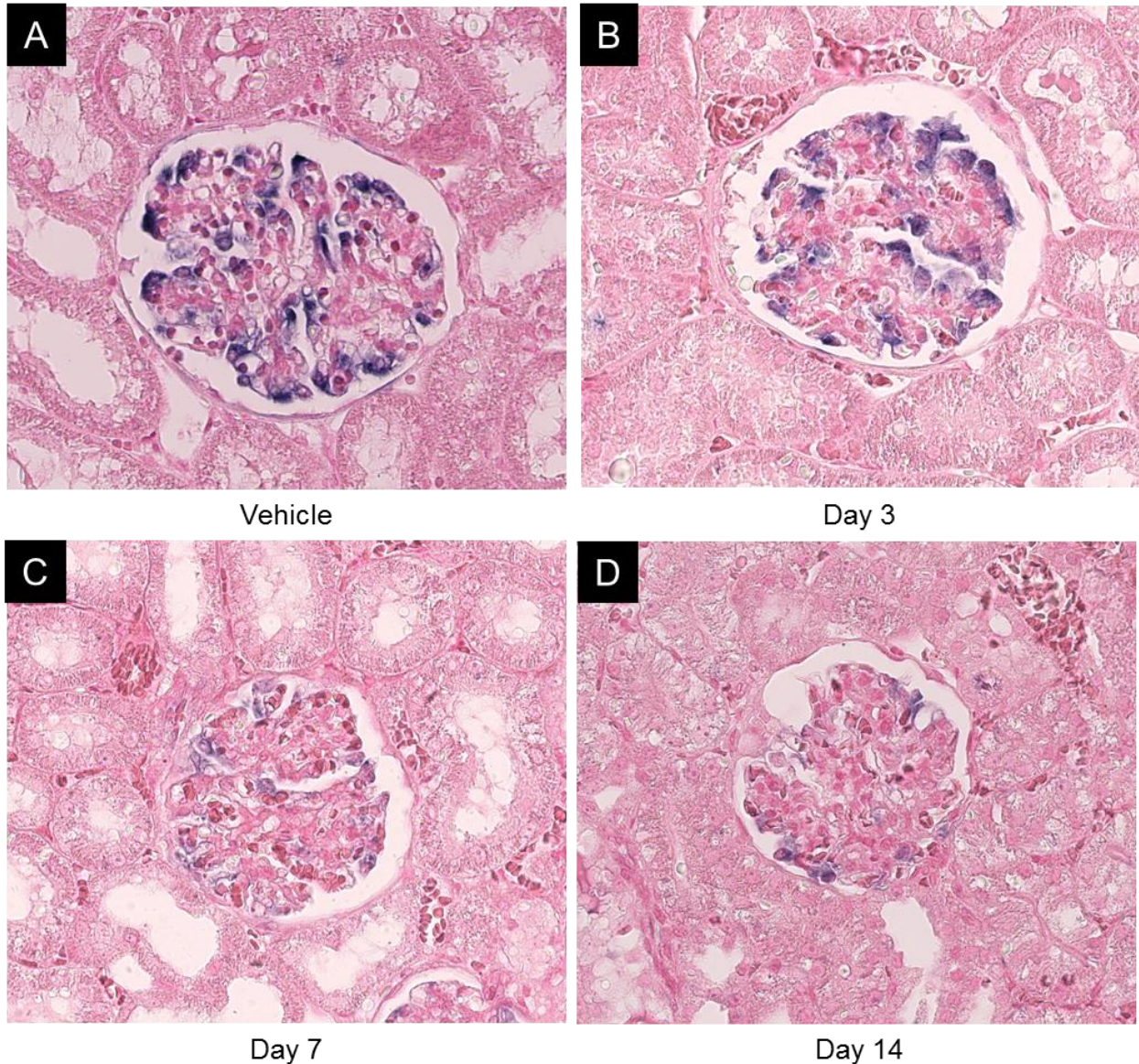


Figure 31: Time course of Sema3G expression by ISH in glomerulus after treatment with PAN: Podocytes are expressing Sema3G in vehicle group (A). After PAN treatment for 3 days (B), 7 days (C) and 14 days (D), Sema3G expression is decreased. Magnification x40; Blue: NBT substrate for ISH, Red: counterstaining.

After treatment with PAN, the expression of Sema3G is similar to vehicle group during the first three days. From day 7, the number of podocytes expressing Sema3G seems to be reduced and the staining intensity in the cytoplasm of the cells becomes lower. After 14 days of treatment, the signal for Sema3G continues to reduce and became barely detectable in some glomeruli. We can clearly see a time related effect of the treatment on this marker.

Using the same tissues samples, the expression of CYTC by *in situ* was performed. Similarly to Sema3G, no change occurs at day 3 but instead, the signal for CYTC starts to increase in intensity from day 7 until day 14 treatment time point.

Examples of the result for CYTC expression with PAN treatment are shown in Figure 32.

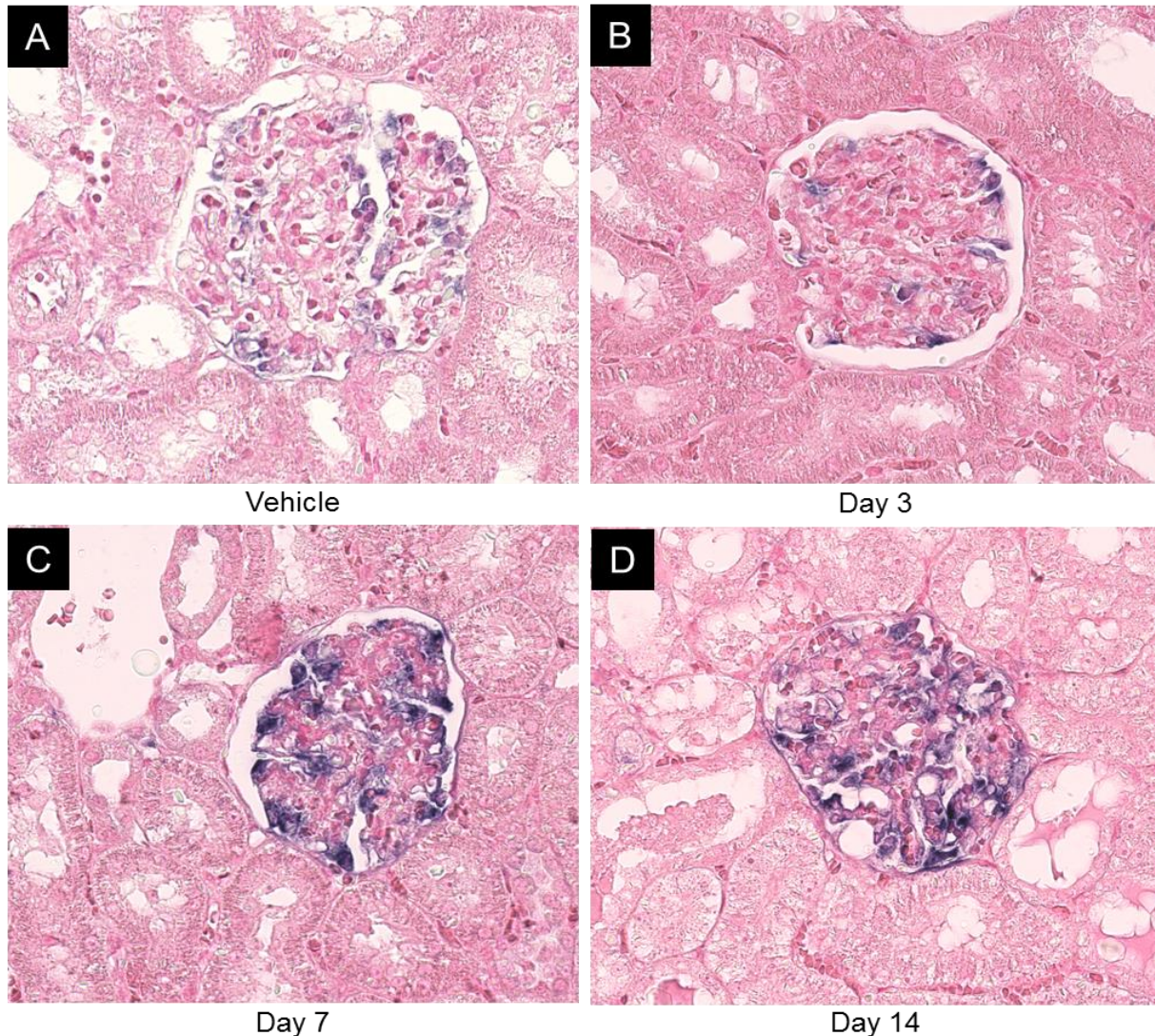


Figure 32: Figure 31: Time course of CYTC expression by ISH in glomerulus after treatment with PAN: Podocytes are expressing CYTC in vehicle group (A). After PAN treatment for 3 days (B), 7 days (C) and 14 days (D), CYTC expression is increased. Magnification x40; Blue: NBT substrate for ISH, Red: counterstaining.

CYTC immunohistochemistry in the same samples demonstrates that CYTC protein expression followed the same dynamic of the mRNA. CYTC antibody gave an increasing staining intensity in podocytes according to the treatment duration (Figure 33). In the tubular compartment, the staining is reduced in epithelial cells of the tubules. Sometimes, accumulation of protein could be detected in the lumen of some tubules (not shown). This shows that the reabsorption of the CYTC is perturbed compared to the normal situation.

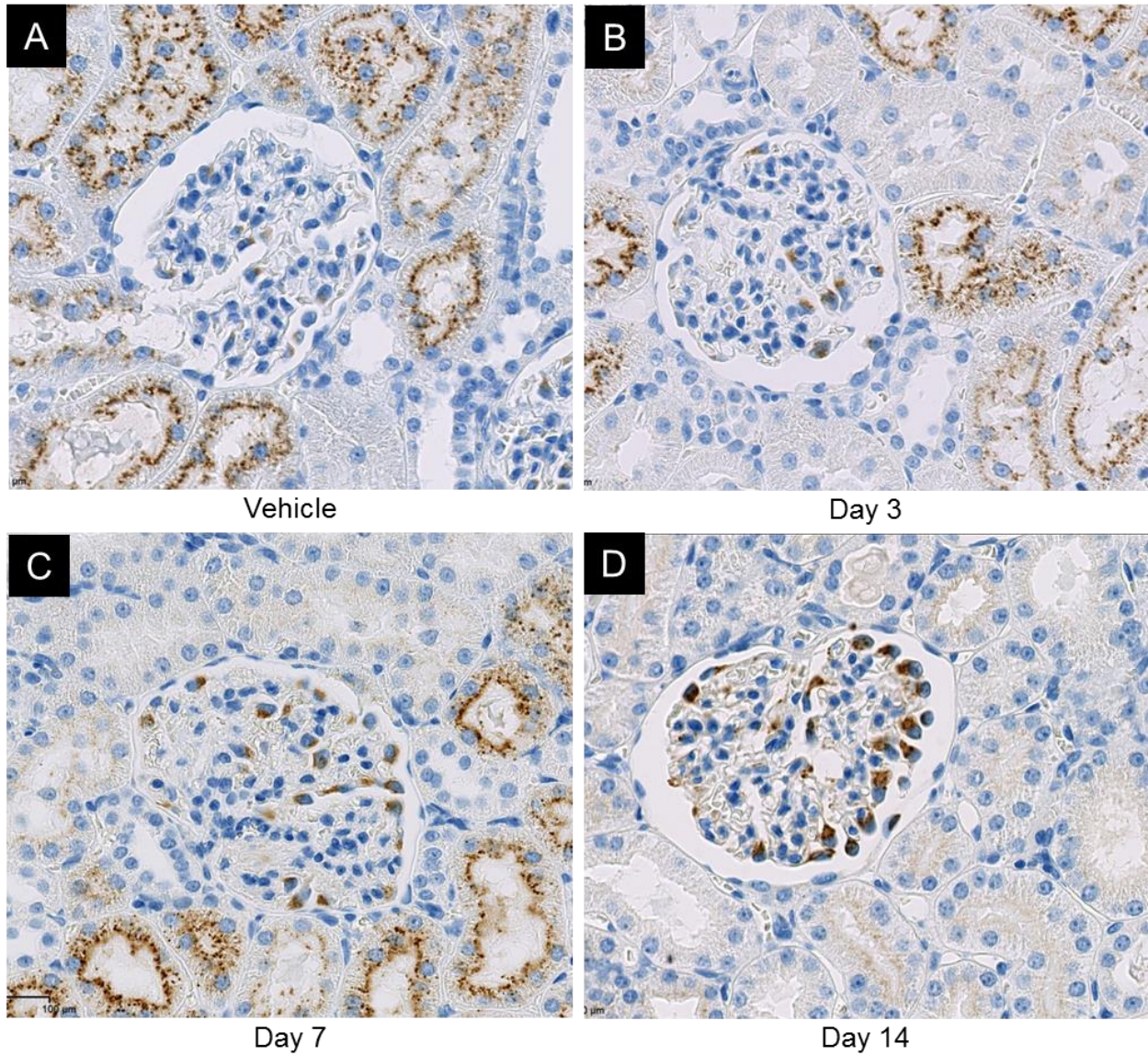


Figure 33: Figure 31: Time course of CYTC expression by IHC in glomerulus after treatment with PAN: Podocytes are expressing CYTC in vehicle group (A). After PAN treatment for 3 days (B), 7 days (C) and 14 days (D), CYTC expression is increased. In the proximal tubule, CYTC reabsorption is diminished upon treatment. Magnification x40; Brown: DAB substrate for IHC, Blue: counterstaining.

In the samples treated with Cisplatin for 3, 7, and 14 days, the results for Sema3G and CYTC were as follow:

The treatment of animals with Cisplatin at 3 mg/kg for the same time points as PAN did not change Sema3G expression in the podocytes. The staining intensity remains similar to controls independently from the treatment time. Also no changes could be noticed in the vascular bed. A picture at day 14 is shown Figure 34.

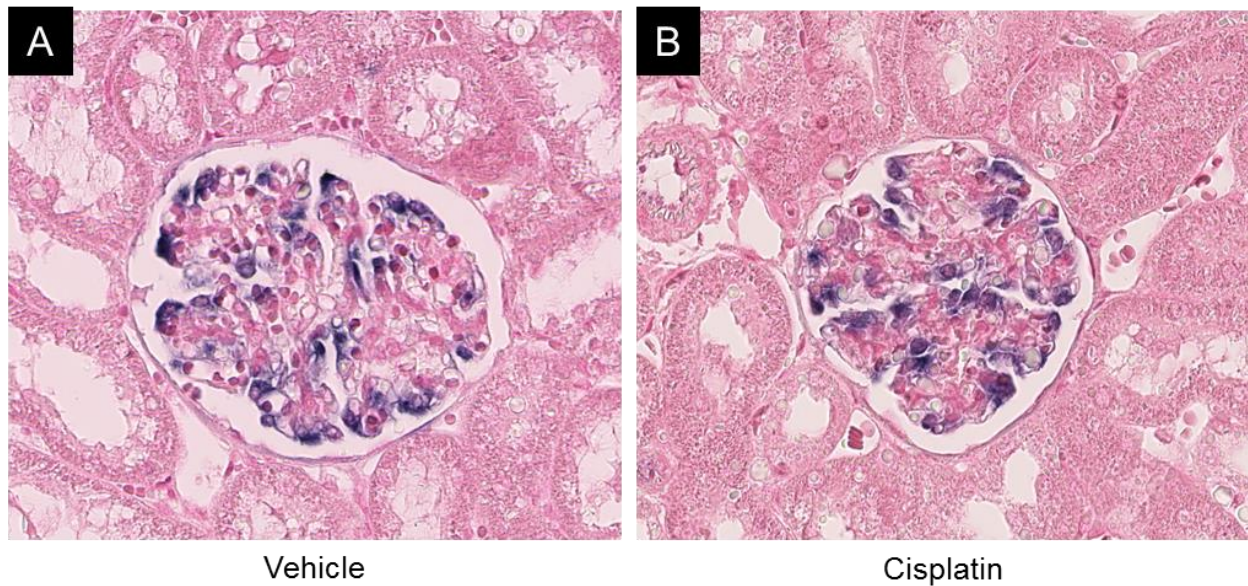


Figure 34: Sema3G expression by ISH in the glomerulus after 14-days treatment with Cisplatin: between (A) vehicle group and (B) Cisplatin (3mg treatment dose), Sema3G expression remains unchanged. Magnification x40 (Blue: NBT substrate for ISH, Red: counterstaining)

For Cystatin C, the level of mRNA in podocytes was also similar to control animals. The only difference noticed was an increased number of circulating cells positives for CYTC. These cells were located between the tubules, distributed all around the section but mainly in the cortex region and certainly correspond to inflammatory infiltrating cells already described. Their quantity varied from animals to animals.

Similarly, the level of the protein CYTC in podocytes was not affected by cisplatin

treatment. Instead, the tubular reabsorption was perturbed. The staining in the epithelial cells of the tubule was irregular, quite faint and not following the apical border of the cell. The Figure 35 is showing a comparison of CYTC expression in the tubule of normal kidney and cisplatin treated kidney.

It is interesting to notice that the treatment effect on CYTC reabsorption seems to be more prominent with PAN than with Cisplatin but it has to be taken in consideration that in this model, Cisplatin was given only once at the beginning of the study, as multiple doses would have been too toxic for the animals.

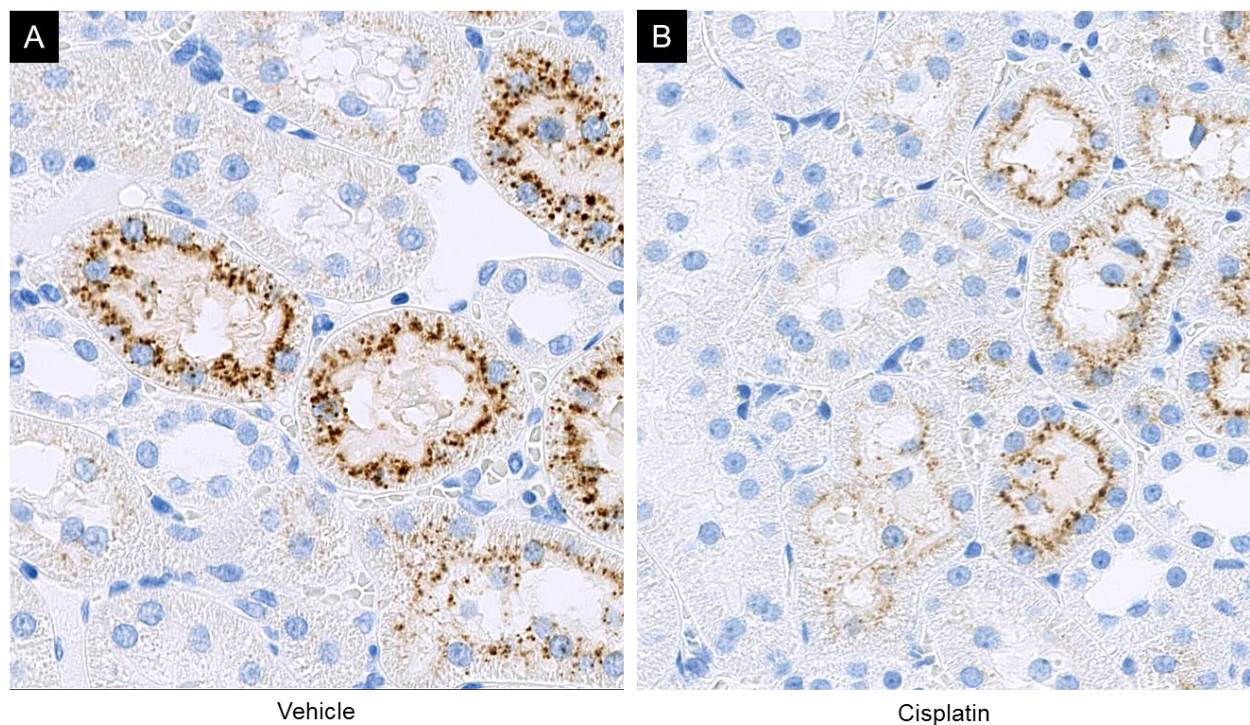


Figure 35: CYTC protein expression by IHC in the tubular epithelial cells 14-days after treatment with Cisplatin: Normal CYTC reabsorption in vehicle group (A) and impaired CYTC reabsorption (B) after Cisplatin (3mg treatment dose). Magnification x40 (Brown: DAB substrate for IHC; Blue: counterstaining)

All the staining intensities of Sema3G and CYTC mRNA in the glomerulus were measured by image analysis using 40 glomeruli. Results for Sema3G are shown in Figure 36 and for CYTC in Figure 37. In both graphs, the results are expressed in % of the median of the control group.

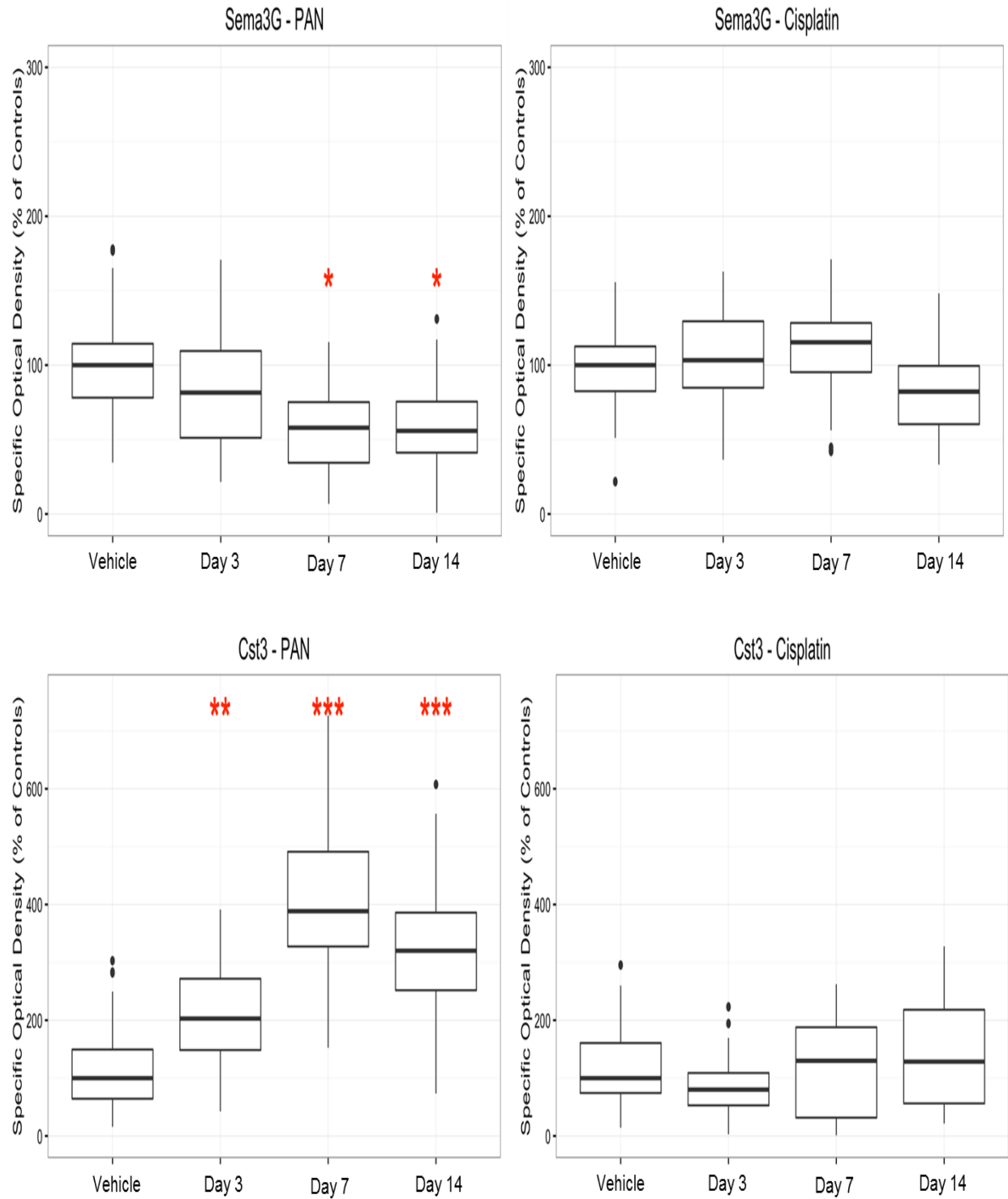


Figure 36 and 37: Quantification of Sema3G and CYTC expression in the podocytes of PAN and Cisplatin treated animals for different time point (day 3, 7 and 14)

The image analysis data confirmed the visual assessment and confirmed that Sema3G is down regulated in a time dependent manner after treatment with the glomerulus-specific toxicant PAN. At day 3, the decrease is minimal and remains not statically significant. From day 7, the decrease of Sema3G mRNA level is statically significant with a value $p < 0.05$. The overall level of Sema3G at day 14 is still decreasing but is not more significant (remain at $p < 0.05$) for the reason that the variations between the glomerulus and the animals are increasing. Upon treatment with cisplatin, Sema3G expression remains more or less similar to the control group at all time points.

In the CYTC image analysis results, we confirmed that the induction of these two markers is anti-correlated but with the difference that the upregulation of CYTC is here already visible and statistically significant at day 3 ($p < 0.01$) and became strongly significant ($p < 0.001$) at day 7 and day 14. CYTC expression after Cisplatin treatment remains unchanged at any time point.

For both markers, it is important to notice that their modulation induced by the treatment is anterior at the proteinuria in urine which was present only at the day 14.

Summary of the nephrotoxicant model results: in vivo data

***In two models of drug-induced toxicity,
The podocyte expression of Sema3G and CYTC is affected only with the
glomerular specific toxicant PAN.
Both markers are differentially regulated in a time dependent manner and their
induction is anticipating the proteinuria in the urine.***

***With the tubular toxicant Cisplatin, both markers remained unchanged in the
podocytes. The reabsorption of CYTC protein by the proximal convoluted tubules is
instead affected.***

4.1.1.1 Tubular injury marker in in vivo rat studies

The last assessment performed on the kidney samples in situation of drug-induced toxicity was an evaluation of the tubular damages using KIM-1.

In the PAN treated animals at day 3, no noticeable changes could be observed compared to control in the KIM-1 expression. Except few isolated positive cells at the cortico-medullary junction, no expression was detected in the cortex. Only one single animal had some positivity in a small part of the cortex region.

At day 7, some positive cells were sometime detectable in the cortex, in the convoluted proximal tubule attached to the glomerulus. The expression of KIM-1 in the descending portion of the proximal tubule at the cortico-medullary junction remains rare. The observation of positivity in convoluted proximal tubule became quite frequent by looking at day 14 treated samples. The staining was sometimes positive in the cells of the Bowman's capsule, in the entire proximal convoluted tubule and affecting a deeper part of the cortex. The presence of positive tubules at the junction of the cortex and the medulla was frequent. Some representative pictures are shown in Figure 38.

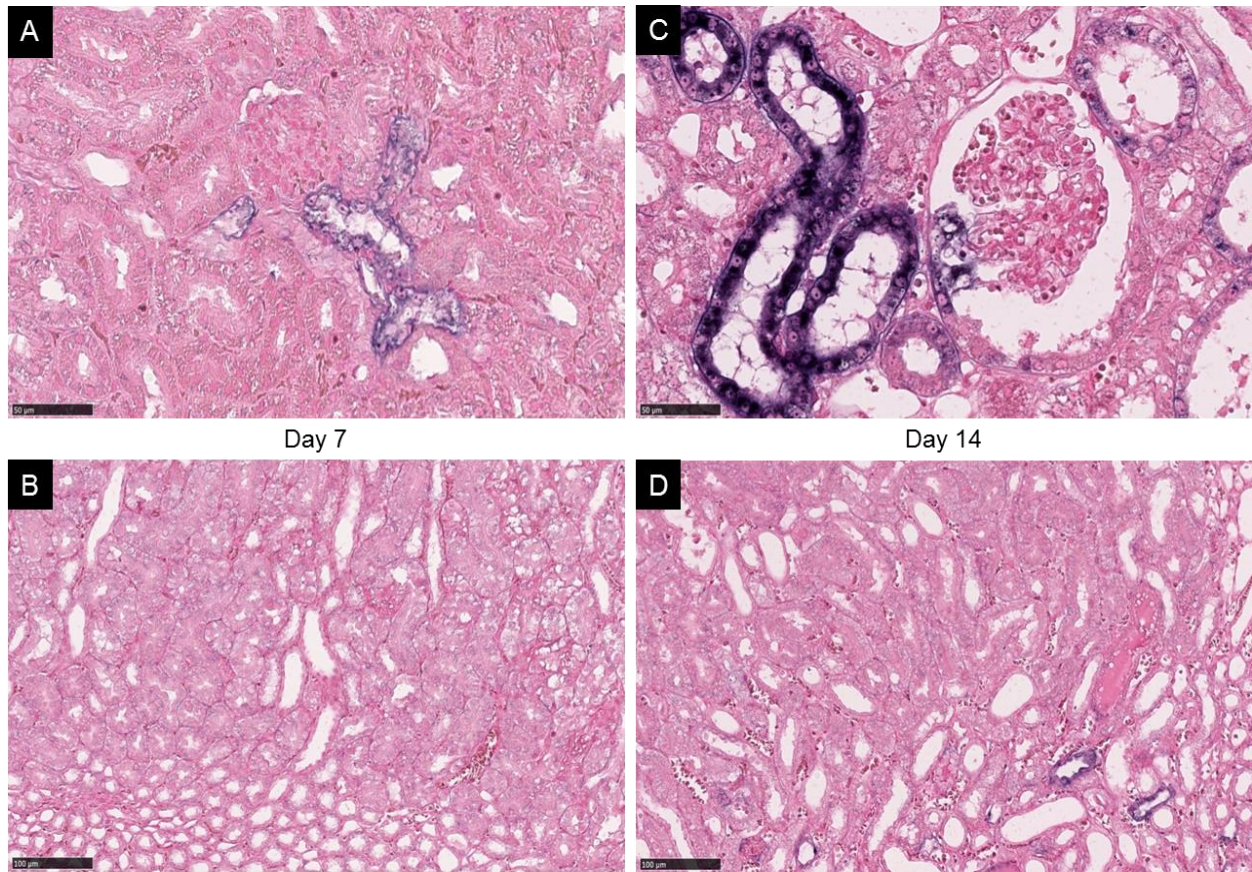


Figure 38: Expression of KIM-1 by ISH in the kidney of PAN treated animals. In cortex (A) and (C), KIM-1 is increasing with treatment time in the damaged proximal convoluted tubule and also sometime in the parietal cells of the Bowmann's capsule (day 14 only). At the cortico-medullary junction (B) and (D), KIM-1 expression is rare. Magnification x40 (A) (C) and x20 (B)(D). Blue: NBT substrate for ISH; Red: counterstaining.

The KIM-1 positivity as observed in these samples are showing a time dependent progression but also a spatial progression. As already mentioned, the first place where positive cells for KIM-1 are usually observed is in the descending portion of the proximal tubule and this location was interpreted as the most sensitive of the kidney.

These time course results showed that there is an indirect tubular injury induced by PAN. Considering that PAN is a toxicant for the glomerulus, we can visualize with KIM-1 the downstream damages of the drug in the convoluted proximal tubule (segment S1) and the progression of the lesions that expand to the inner cortex until the segment S3 at the junction with the medulla.

Looking now at the cisplatin study samples, the KIM-1 expression was studied the same way, focusing on the location of KIM-1 positivity and looking how it relates to the treatment duration.

The injury (assessed by KIM-1 positivity) is already started at day 3 with strong positivity observed in the descending portion of the proximal tubule at the cortico-medullary junction. Positivity in the cortex was rare except few isolated positive cells noticed until the lower part of the cortex.

At day 7, there is a progression of the injury and positivity is found not only at the junction of cortex and medulla but became frequent until the outer cortex in many tubules. From day 14, the KIM-1 staining is generalized in all the cortex regions of the kidney. Most of the tubes expressing KIM-1 were strongly dilated. It gives the impression at this time point that the staining is regressing in some cells that seems to be degenerating cells.

With this treatment, the KIM-1 expression is following a progression that starts in the cells of the descending convoluted tubule and then spread rapidly toward the outer cortex region. Compared to PAN treatment, the evolution of the positivity of KIM-1 is completely inverted, with an axis of progression from segment S3 until S1.

The Figure 39 shows some representative animals that illustrate the observation.

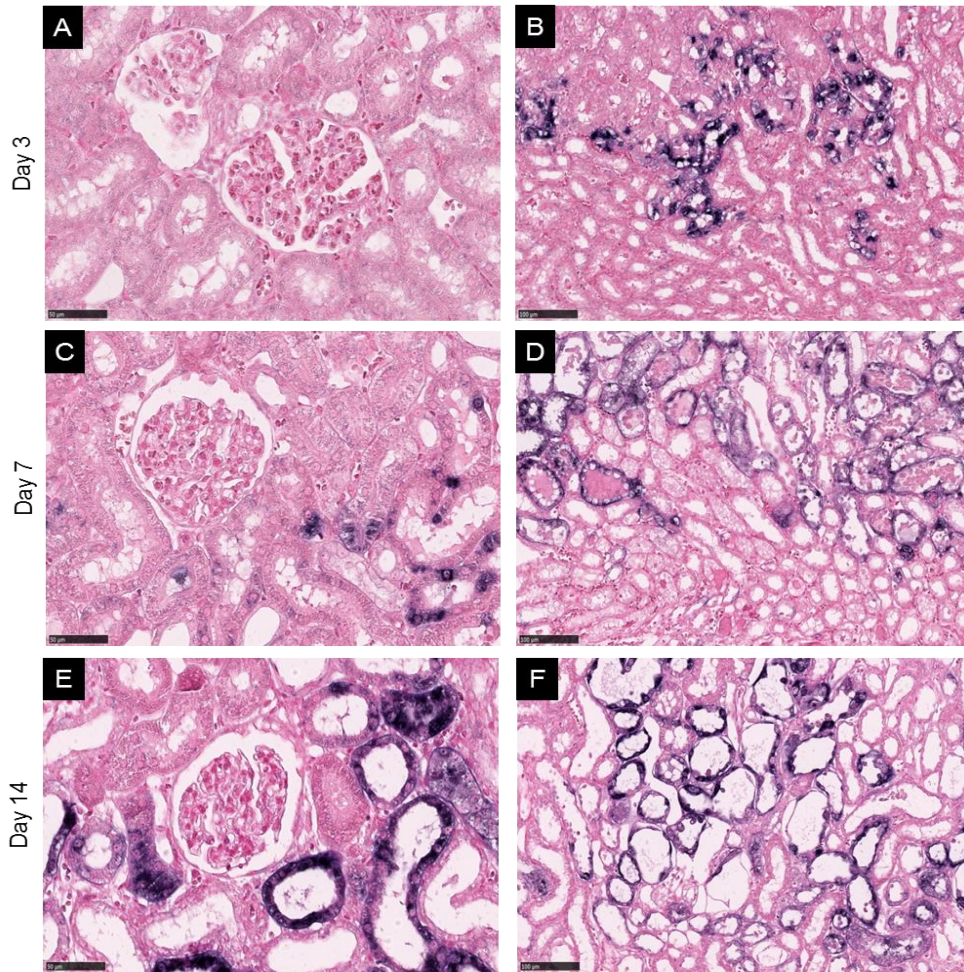


Figure 39: Expression of KIM-1 by ISH in the kidney of Cisplatin treated animals. In cortex, (A) (C) (E) KIM-1 is increasing with treatment time in the damaged proximal convoluted tubule. At the cortico-medullary junction (B)(D)(F), KIM-1 expression is strong already at day 3. Magnification x40 (A)(C)(E) and x20 (B)(D)(F) (Blue: NBT substrate for ISH; Red: counterstaining).

As the KIM-1 expression sounds to have a real differential spatial and temporal expression according to the treatment, the fingerprint approach was applied to this series of samples in order to standardize the dynamics.

The overall pattern results are shown in Figure 40 for the PAN treatment and in Figure 41 for treatment with cisplatin. It confirms that the staining is progressing in different area of the kidney in a time dependent manner. The axis of progression differs from one drug to the other and therefore indicates precisely the currently location of toxicity.

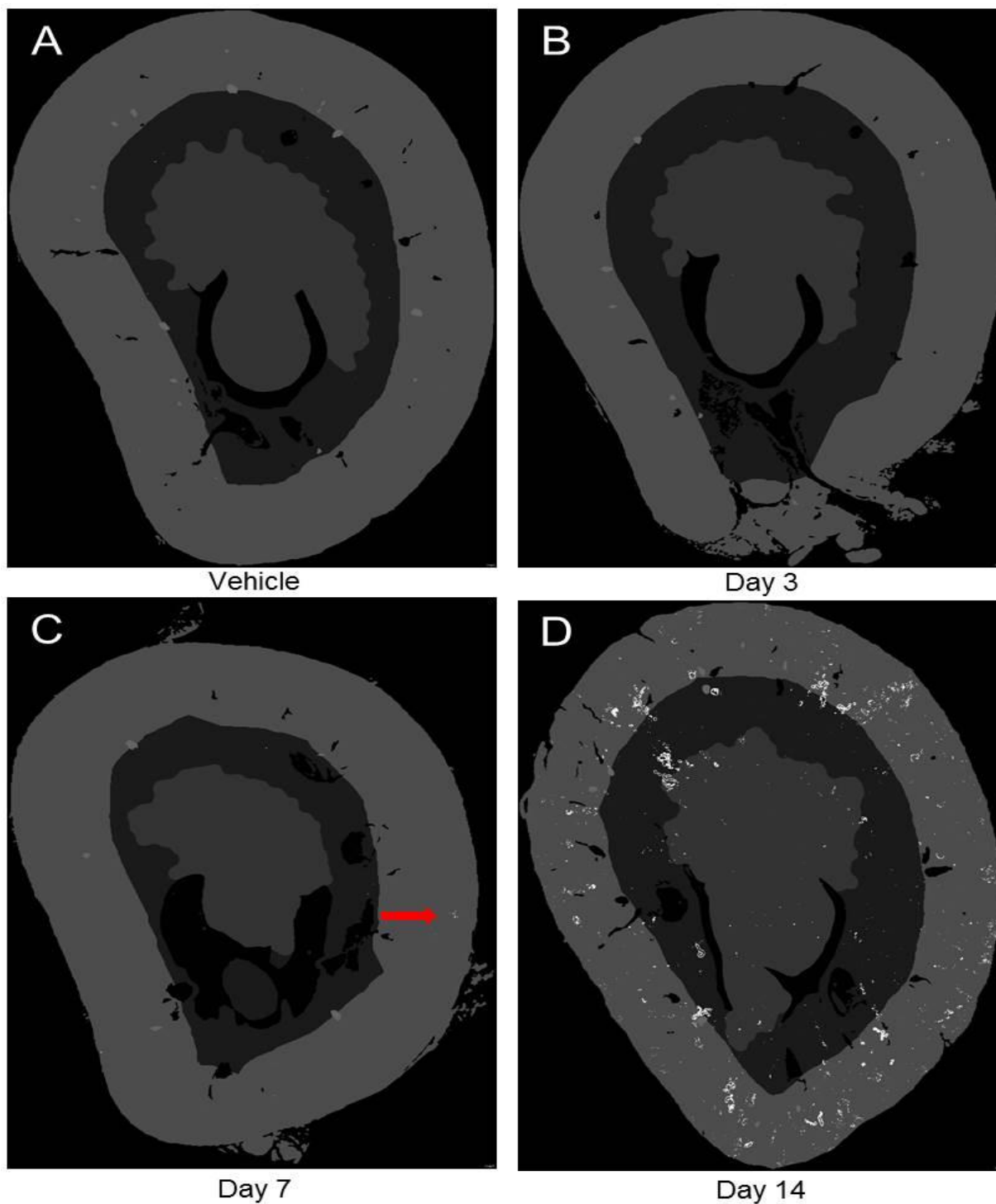


Figure 40: Fingerprint of KIM-1 expression after PAN treatment. Created with Definiens. The cortex is represented in light grey; outer medulla in dark grey; inner medulla/pelvis in grey. The KIM-1 expression is represented in white color and appears as patchy signal increasing with time of treatment in the cortex mainly.

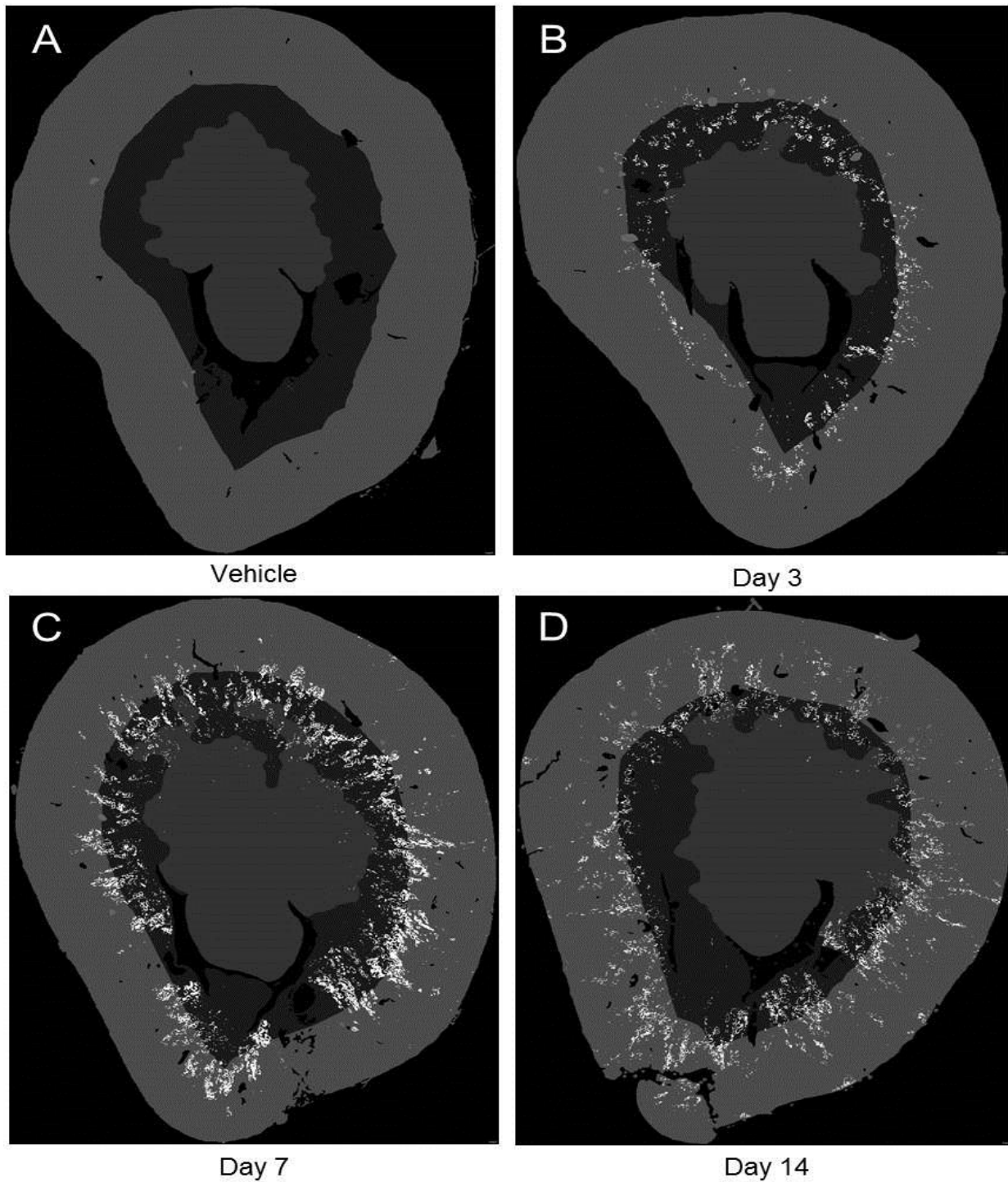


Figure 41: Fingerprint of KIM-1 expression after Cisplatin treatment. Created with Definiens. The cortex is represented in light grey; outer medulla in dark grey; inner medulla/pelvis in grey. The KIM-1 expression is represented in white color and appears as “ray” of signal

increasing with time of treatment.

The quantification of the signal intensity in the different part of the kidney after PAN treatment (Figure 42), shows an absence of KIM-1 expression in any part of the organ at day 3 and until day 7. The signal intensity was very low and without any anatomic distinction between cortex and medulla. Instead at day 14, the signal for KIM-1 became strong particularly in the cortex region and the intensity of the signal is decreasing toward the medulla part. The treatment point of day 14 is clearly showing a differential expression pattern between the three segments.

After treatment with Cisplatin, the spatial profile of KIM-1 is very interesting and strongly time dependent. In the segmented kidney (see Figure 43), the signal for KIM-1 in the inner medulla/pelvis segment is expressing very few KIM-1 after treatment and stays stable at any time point. In the opposite, the levels of KIM-1 in the outer-medulla are the first to be upregulated already at day 3 and dramatically increased at day 7. The Figure at day 14 announces a reduction in the progression certainly associated to a degeneration of the cells and/or necrosis. In the cortex, the data shows a certain delay in this compartment compare to the others and this part is affected only in a second moment, progressing at day 7 and remaining more or less stable at day 14.

We could illustrate that the expression of KIM-1 follows a clear dynamic and that PAN versus Cisplatin toxicity in the renal tubular cells can be discriminated by monitoring the location of KIM-1 expression.

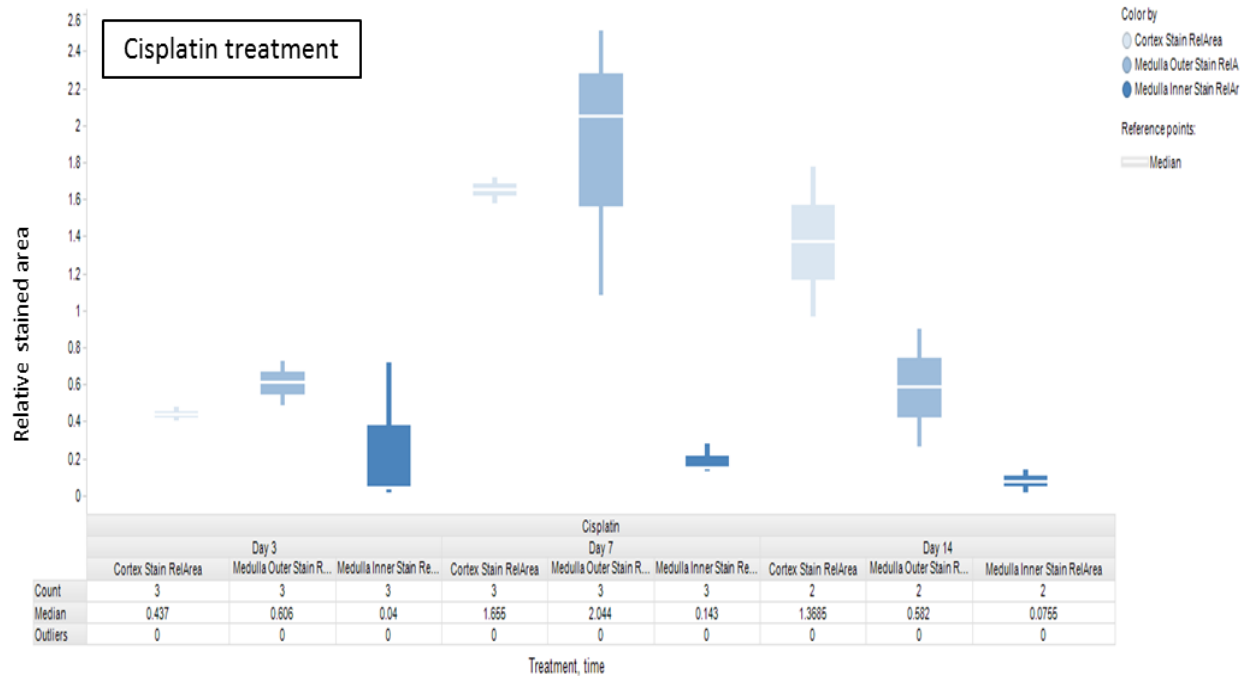
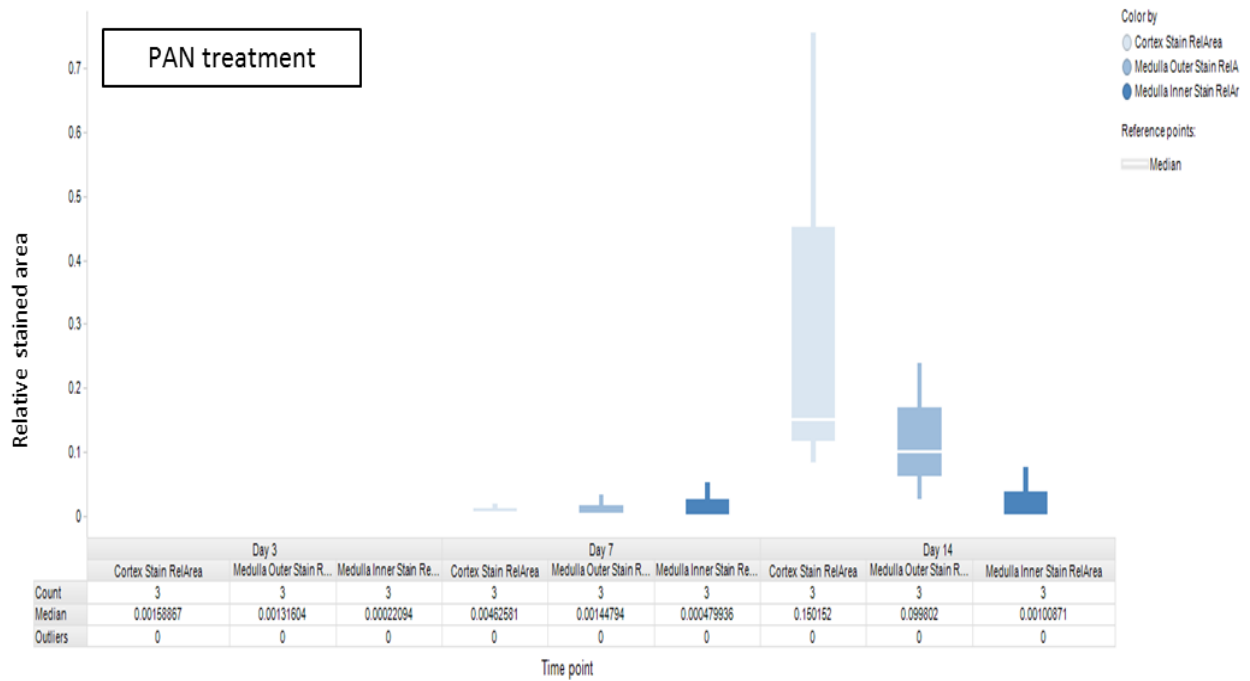


Figure 42 and 43: Expression of KIM-1 in the segmented kidney (cortex, outer medulla, inner medulla) after treatment with PAN (top) and Cisplatin (bottom) for 3, 7 or 14 days.

Summary of the nephrotoxicant model results: tubular damage data

The time course with the toxicants PAN or Cisplatin revealed a differential pattern of KIM-1 expression

The topography of KIM-1 with PAN toxicity is starting from the convoluted portion of proximal tubule and progress toward the descending part.

The induction of KIM-1 with the tubular toxicant Cisplatin is going in the opposite direction

The pattern and spatial distribution of KIM-1 can be used to discriminate between primary and secondary tubular toxicity

4.19 *In vitro* studies using toxicant

We were now interested to see if this differential expression is something that could be reproduced *in vitro* using a rat podocytes culture treated with the same toxicants.

We decided to use and implement a rat primary isolated podocytes culture considering that no good quality cell line is available for this cell type and for this species.

Isolation and primary culture of the rat podocytes was done accordingly to the improved method described by Katsuya K et al. in 2006 (Katsuya, Yaoita et al. 2006) and the details of the isolation and culture are given in the material method part.

Before performing any experiment with the cells, the culture yield and performance had to be evaluated. According to the paper of Katsuya K et al., the number of isolated glomeruli expected from the perfusion of one rat should be around 20'000 glomeruli. This number was reached by us on several isolation tests and in some cases of optimal perfusion a maximum of 50'000 glomeruli could be obtained. From the cellular outgrowth, the expectations are around 600'000 purified podocytes according to the authors. From the in house results, this number was also found with some pick of 1'400'00 cells from one perfused rat. Also if these numbers are indicating a good implementation of the published method, this stays a culture method which is long and difficult. Running a treatment based experiment with different time point remains difficult and procurement of enough cells is a limitation to the method and number of experimental data. Therefore, our data have been generated from only one donor rat as all other experiments didn't provide enough cells to test the two compound PAN and cisplatin at different time point.

During the process of podocytes isolation, several microscopic examination steps were performed to verify the quality of the culture. The isolation and attachment of the glomeruli can be assessed at the first day after seeding by verifying the absence of tissue fragments or impurities. At day 4, the cellular outgrowth is visible around the glomeruli. After the re-culture, isolated podocytes should be some large cells, branched, often binucleated and arborized. If this phenotype can be observed, some good mature podocytes were obtained. In the opposite, if some small, polygonal, cobblestone-like shape cells are observed, the

podocytes are dedifferentiated. An illustration of the different microscopic observations is shown in Figure 44.

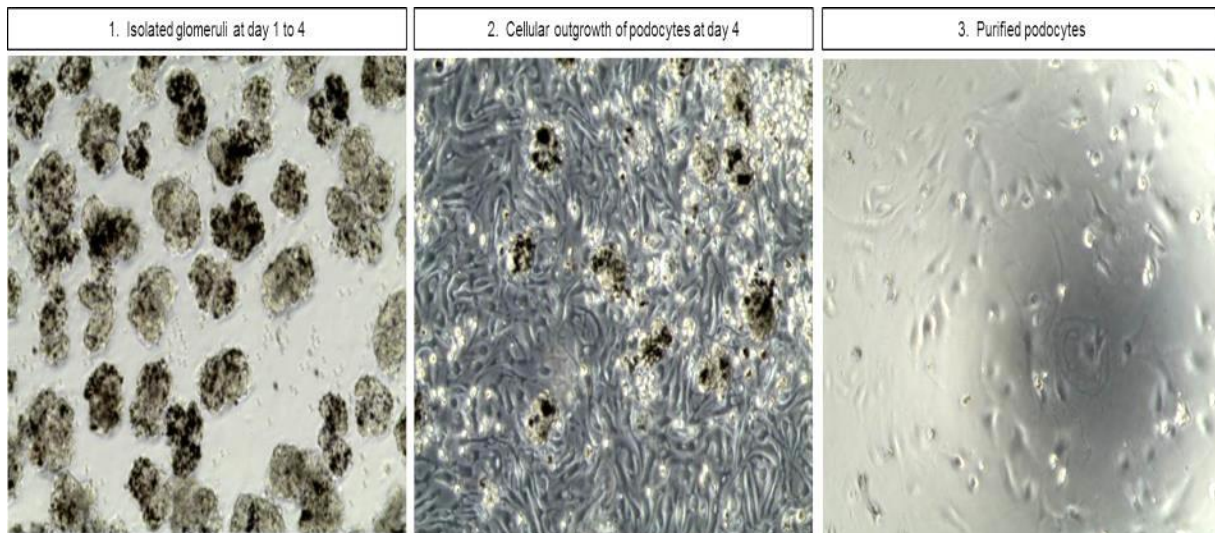


Figure 44: Picture of isolated glomeruli between day 1 and 4 (left), cellular outgrowth at day 4 (middle) and isolated purified podocytes (right)

By immunofluorescence, a specific staining for podocin and synaptopodin on purified podocytes was performed at day 1 after seeding. With the DAPI staining we could observed some binucleated cells as expected and with a very elongated shape. The signal for podocin was cytoplasmic and strong, when the staining for synaptopodin was membranous, less intense and was present on only elongated cells.

Some rounded shape cells were also observed. These cells are not well attached yet and have foot process which is not developed for the moment (see Figure 45). Microscopic observation could not detect any contamination by other cells type like macrophage or mesangial cells.

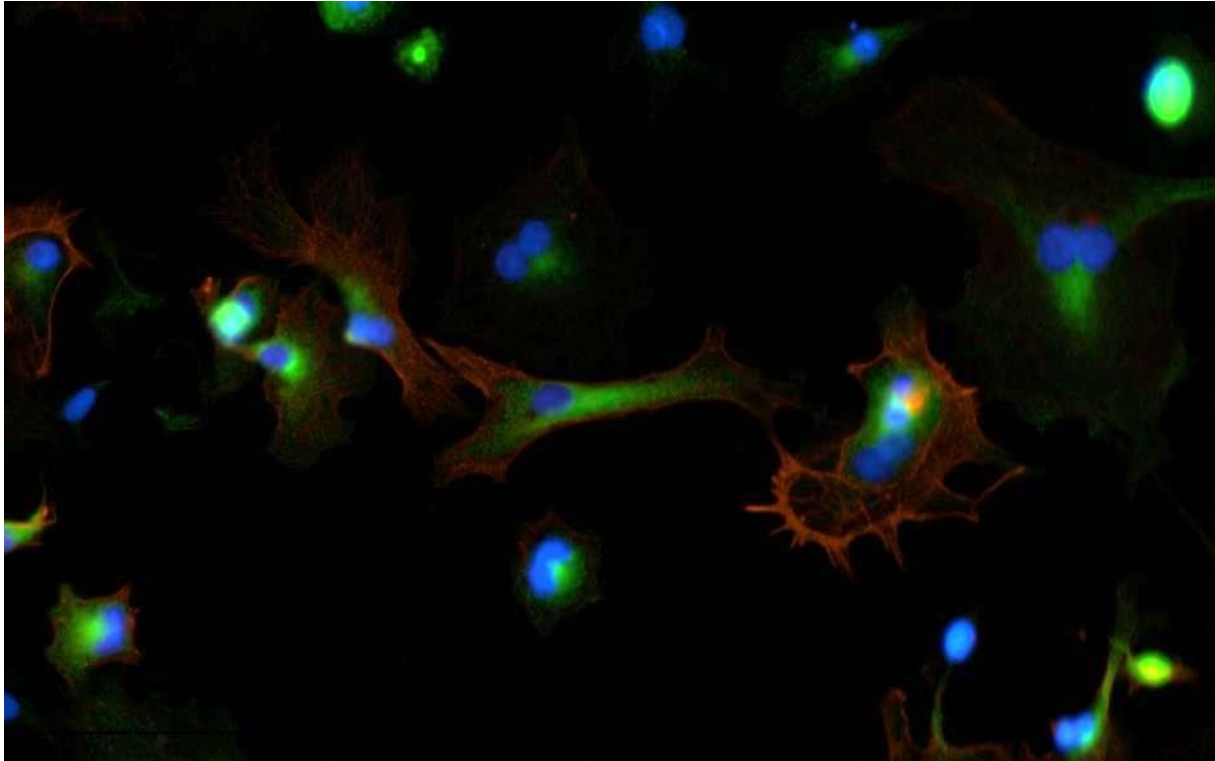


Figure 45: Immunofluorescence on primary podocytes culture at day 1 using anti-podocin (green), anti-synaptopodin (red) and Dapi (blue) as counterstaining.

For a good morphological quality preparation, the cells were distributed in collagen type-I coated wells at a density of around 30'000 cells/well and were treated the next day for 3h, 6h, 24h and 48h either with PAN or with Cisplatin. Most of the time points were done in triplicate. At the end of the experiment, total RNA was extracted for gene expression analysis.

In a first approach, we merged the replicates and time points for each specific treatment (namely vehicle, cisplatin, PAN 0.1 μ g/ml and PAN 1 μ g/ml) in order to get an overall impression of the cells reactivity and behavior. The parameters for the analysis were considering only the annotated probe sets and the transcripts with an absolute expression level over 50 (MAS 5.0). The fold change comparison was set with a minimum upregulation or downregulation fold change of 1.5 and data were fitted onto an ANOVA model with alpha at 0.05.

By applying these parameters, from the 31042 probe sets of the gene chip array, only 13046 remaining probe sets had a correct annotation and/or didn't fail the expression level filtering criteria. Within this selection, 128 probe sets had a fold change expression > 1.5 compared to the vehicle group but many failed at the statistical ANOVA test. At the end, only 27 differentially expressed genes as compared to the vehicle group were considered statistically significant.

From this low number of differentially regulated genes, the largest fraction appeared to be stress-related genes including heat-shock proteins or apoptosis related genes. We can already postulate of relatively weak effect of the drug on the culture. It means that either the drug concentrations applied were too low or the reactivity of the cells was weak and extremely variable. The complete list of regulated genes is available in Supplementary data part (Supplement data Table 4).

Our two candidate genes *Sema3G* and *Cst3* were not within the 27 significantly regulated genes. But looking at their global reaction, *Sema3G* is nevertheless showing a nice trend: there was no difference upon cisplatin treatment but instead PAN treatment is regulating down *Sema3G* in a dose dependent manner. None of the results were significant due to high standard deviation variations. The downregulation of *Sema3G* was not related to general cytotoxicity of the treatment agents as proven by the stability of the housekeeping gene *Actb* on the same samples. A general reactivity of the cell was also proven by looking the stress gene *Hspa1a* that was upregulated by both treatments Cisplatin and PAN.

In the opposite of *Sema3G*, the global reaction of *Cst3* instead was completely unrelated to both, treatment and dose.

The graphical results of the earlier mentioned genes are shown in Figure 46.

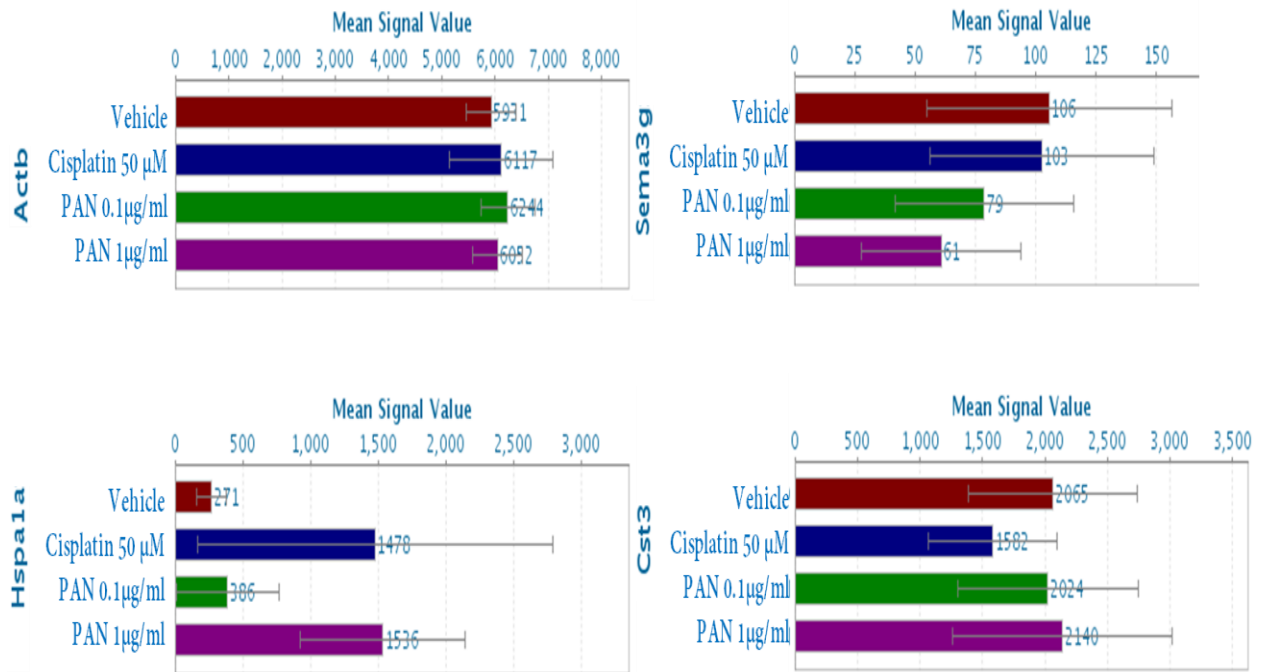


Figure 46: Gene expression results for some selected genes after treatment of the rat podocytes culture with Cisplatin (50 μ M) or PAN (0.1 or 1 μ g/ml).

Independently from the fold change analysis, a supervised analysis was performed. Each signature was built on previous knowledge to verify the specificity of the culture, the potential contamination of the culture, the pathological stage and to follow the reaction of the gene of interest over time.

The selection of podocytes specific gene was chosen from literature (Katsuya, Yaoita et al. 2006, Patrakka and Tryggvason 2010) as well as the selection of pathological activation genes, endothelial cells markers and mesangial cells markers. Average expression levels expressed as a “score” for the different gene signatures were derived for untreated podocytes compared to treated cells at the different time points. In addition, two different comparators were used; (i.) a normal whole kidney sample and (ii.) samples from laser capture micro-dissected glomeruli (the same samples as for the identification of glomeruli specific genes).

The details of the gene list are described below:

Gene list for podocytes specific genes

Probe Set	Gene Symbol	Gene
1395337_at	Tjp1	tight junction protein 1
1388786_at	Synpo	synaptopodin
1369895_s_at	Podxl	podocalyxin-like
1369695_at	Wt1	Wilms tumor 1
1368412_a_at	Ptpro	protein tyrosine phosphatase, receptor type, 0
1370081_a_at	Vegfa	vascular endothelial growth factor A
1369942_at	Actn4	actinin alpha 4
1367681_at	Cd151	CD151 molecule (Raph blood group)
1389282_at	Itga3	integrin, alpha 3
1380537_at	Nckap1l	NCK associated protein 1 like
1388177_at	Ddn	dendrin
1369153_at	Nphs1	nephrosis 1, congenital, Finnish type (nephrin)

Gene list for endothelial cells

Probe Set	Gene Symbol	Gene
1371545_at	Pecam1	platelet/endothelial cell adhesion molecule 1
1389234_at	Vwf	von Willebrand factor

Gene list for mesangial cells contamination

Probe Set	Gene Symbol	Gene
1369652_at	Thy1	Thy-1 cell surface antigen
1375010_at	Cd68	Cd68 molecule
1369651_at	Thy1	Thy-1 cell surface antigen

Gene list for impaired podocytes

Probe Set	Gene Symbol	Gene
1369640_at	Gja1	gap junction protein, alpha 1
1367600_at	Des	desmin
1372002_at	Gja1	gap junction protein, alpha 1

The podocytes specific gene list tells us about the characteristics of the cells during the culture time. All the tested genes were well expressed in the primary podocytes culture at a much higher level than a whole kidney sample, indicating an enrichment of the podocytes specific genes in these samples. This tells us that the isolation method of podocytes performed well and that the culture was of good quality. Nevertheless, two genes from the gene list tested, namely nephrin and dendrin had a very low expression level compared to normal kidney and isolated glomeruli. In fact, this reproduce the observation already done by Katsuya et al. (Katsuya, Yaoita et al. 2006) and can be explain by the fact that nephrin is a marker of the slit diaphragm. The cultured cells didn't reach this maturation step and were not able to develop such specific and elaborate filtration structure in vitro. Excluding these two genes, the podocyte gene list score in cultured cells reached higher levels than observed for the isolated glomerulus sample. The Figure 47 is showing the scoring results

of the podocytes specific genes in the culture compared to kidney and glomeruli with and without the Nphs1/dendrin genes.

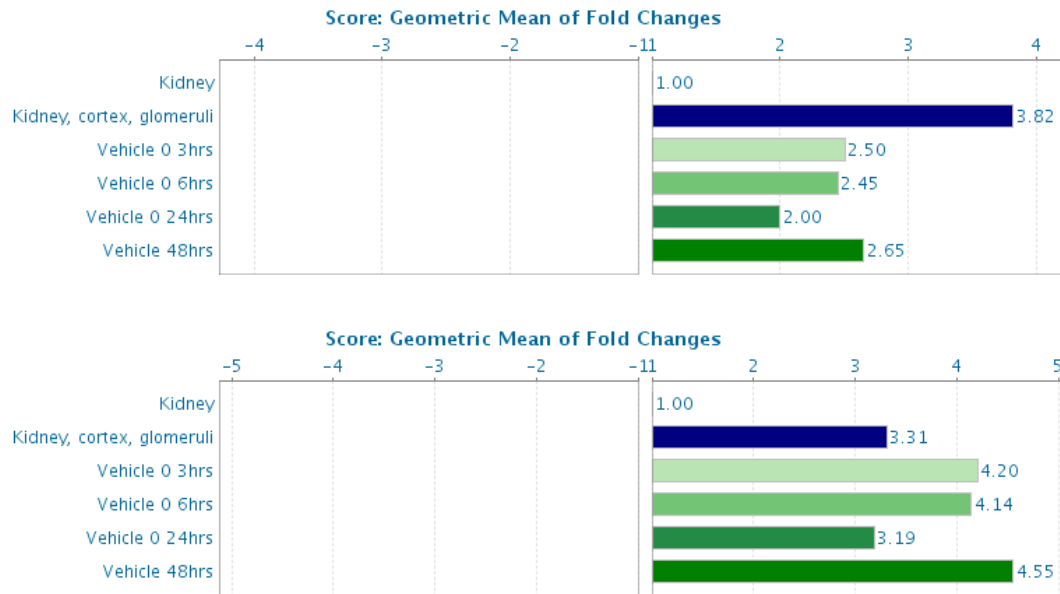


Figure 47: Gene expression results for podocytes specific genes in the untreated culture at different time points. The values represent the geometric mean of the fold change between any treatment group and whole kidney, for all genes in the list. Top: gene list with Nphs1 and dendrin. Bottom: gene list without Nphs1 and dendrin.

The cultured podocytes were also scored for the presence of endothelial cells and mesangial cell contamination: no changes for endothelial cells could be detected in the culture as well for mesangial cells until 24hours. At 48h, the level of mesangial/fibroblast genes has been found to be suddenly increased and could indicate some proliferation of these cells in the culture. The time point of 48 hours has been removed for further analysis (Figure 48 and 49).

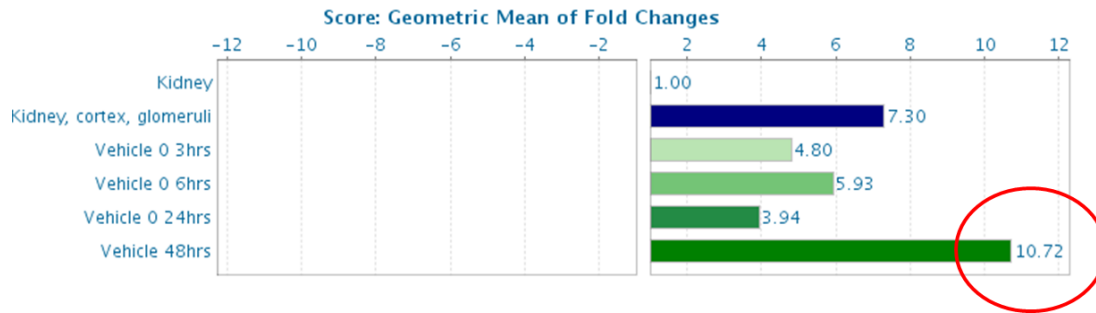


Figure 48: Contamination of the culture by mesangial cells, as indicated by increased expression scores in a gene list specific for this cell type, is appearing after 48 hours of culture.

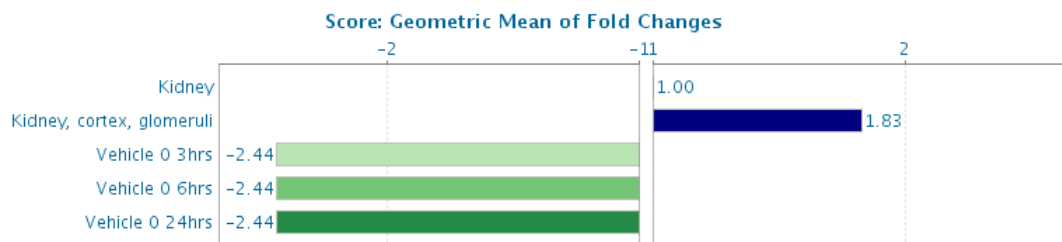


Figure 49: Absence of contamination of the culture by endothelial cells, as indicated by negative expression scores in a gene list specific for this cell type, compared to whole kidney.

The next gene list was built around pathological markers and the results showed an increase of these markers in the cultured cells. These signs of abnormality are related to an in vitro context and are also in agreement with the results of Katsuya et al. method (Figure 50)

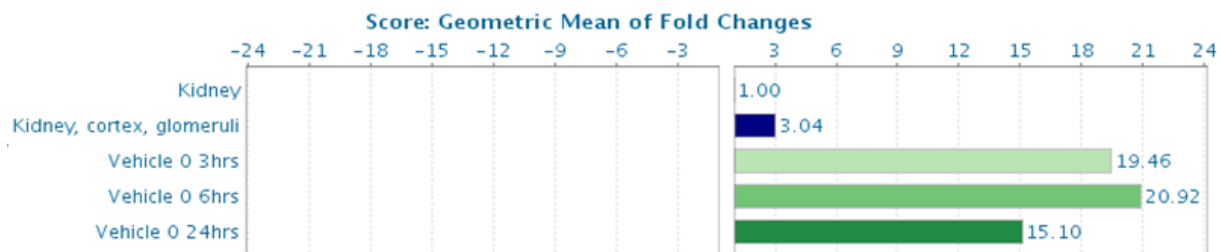


Figure 50: Scoring results for markers of impaired podocytes in culture, compared to whole kidney.

Finally, the analysis of the raw expression levels of Sema3G and CYTC transcripts in the untreated cells revealed a good and relatively stable expression level for CYTC in the culture. Instead, the levels of Sema3G transcripts are very low and tend to decline with the culture duration, indicating that the culture conditions are rapidly affecting the expression of this marker (Figure 51).

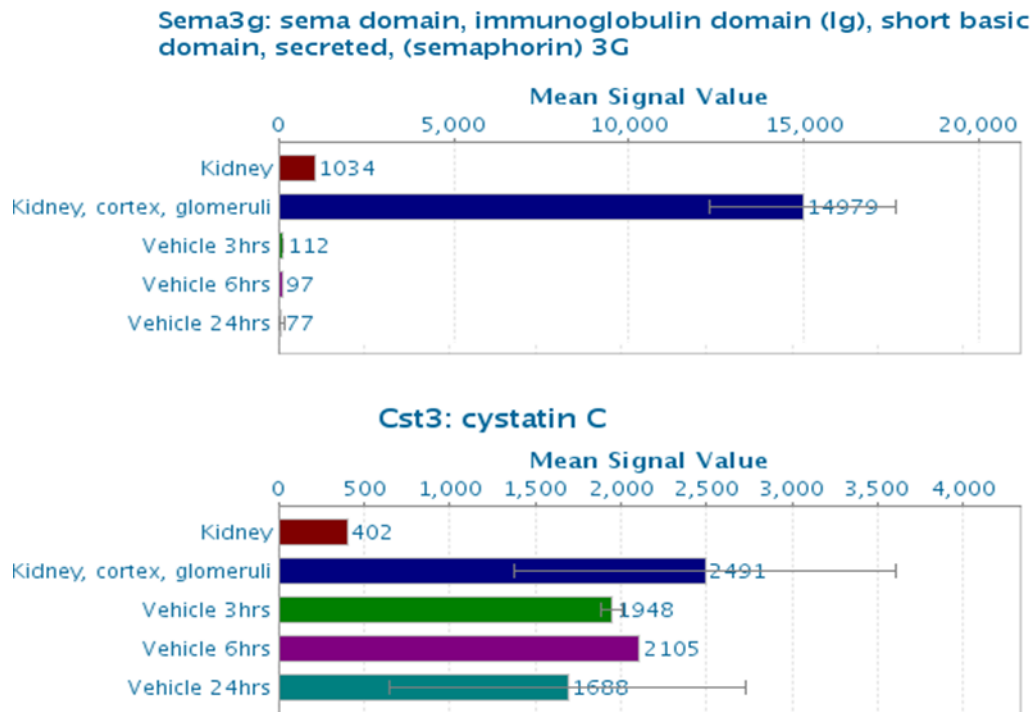


Figure 51: Expression levels of Sema3G and Cst3 in untreated culture of podocytes compared to whole kidney

The scoring results of Sema3G expression in podocytes culture after treatment with Cisplatin revealed that there is no treatment effect on this gene in podocytes. Cisplatin treated samples showed a decreasing expression of Sema3G at exactly the same kinetics as in the untreated cells.

To the contrary, when the cells are treated with PAN, we can observe a dose dependent and a time related response. The response at 3hours is minimal with similar levels of Sema3G expression at low and/or high dose of PAN. But after 6hours of culture, the PAN treated cells showed an accelerated decreased of Sema3G in a dose dependent manner. The results at the time point of 24hours are even more marked (Figure 52). Unfortunately none of these results are statistically significant due to high variation and thus represent just a trend.

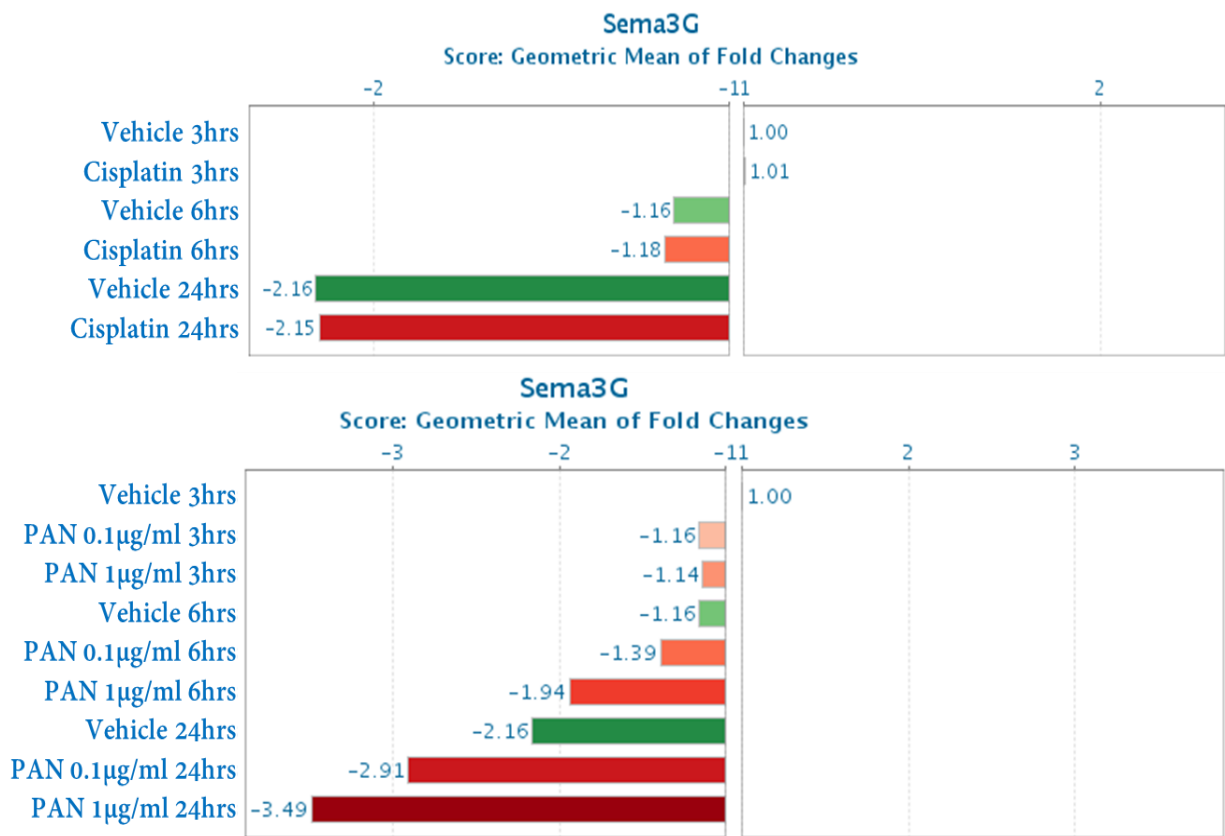


Figure 52: Sema3G expression in podocytes after treatment with Cisplatin (top graph) and PAN (0.1 and 1µg/ml) (bottom graph). Results are expressed in fold change compare to vehicle treatment at 3 hours.

The scoring results for CYTC expression after treatment with Cisplatin showed a negative expression score which do not reflect any specific effect considering that Cisplatin is a tubular specific toxicant and was used as negative control on the podocytes cells. It may just show a general cytotoxic effect on the culture even if the dosage selected should not.

But also with the treatment of the cells with PAN, CYTC was expected to be upregulated based on the *in vivo* data and surprisingly no drug specific effects were seen, without time related effect (see Figure 53). The expressions of CYTC stays stable in the cells until 6 hours and suddenly dramatically fall down at 24hours.

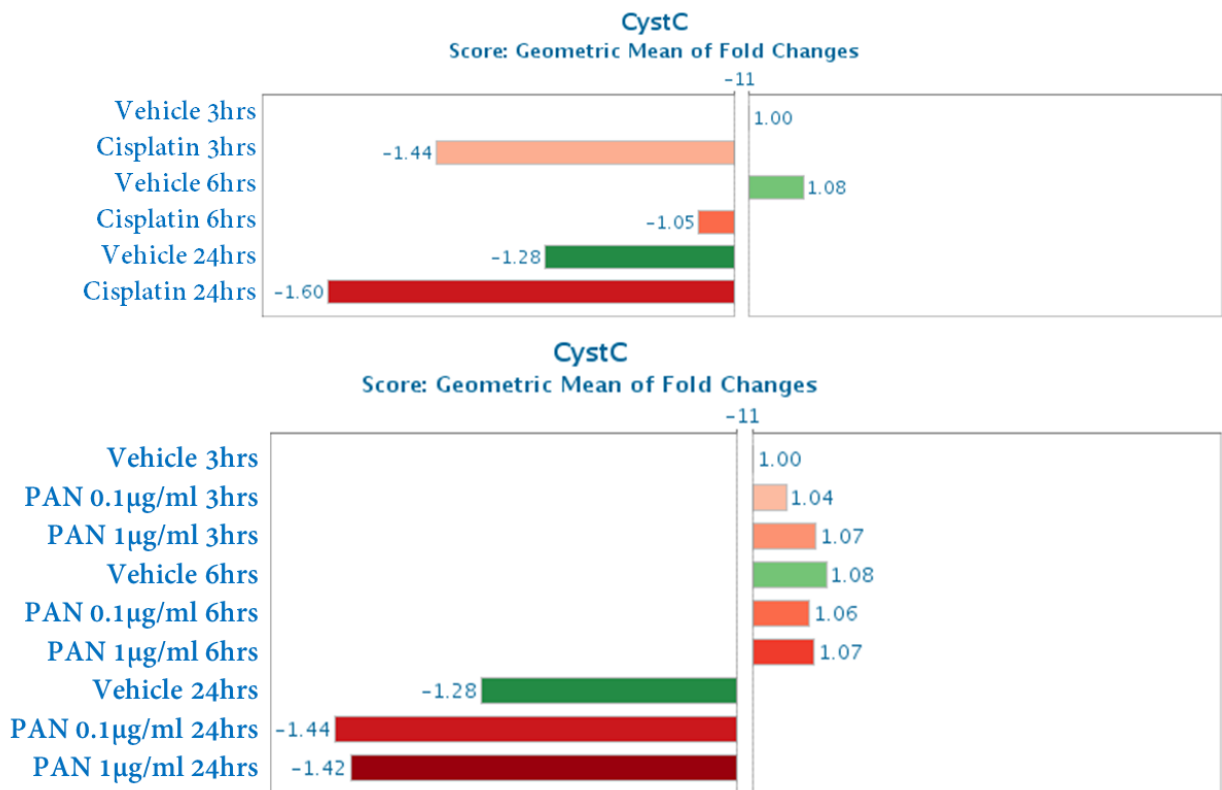


Figure 53: CYTC expression in podocytes after treatment with Cisplatin or PAN (0.1 and 1µg/ml)

Summary of the nephrotoxicant model results: in vitro data

A primary culture of rat podocytes could be established and tested for toxicity reaction with PAN and cisplatin.

Overall, very few genes were affected by the treatment.

Sema3G was down regulated in vitro in a dose and time dependent manner mirroring the in vivo findings

The results were not statistically significant and could be interpreted only as a trend.

The second marker CYTC didn't reproduce the in vivo figure.

4.20 Comparative summary of the animal models results

The results for the expression of Sema3G, CYTC and KIM-1 in the different animal models are summarized in the Table 5. The *in vitro* results for Sema3G and CYTC are summarized in Table 6.

This summary gives an overview of the reactivity of these 3 markers assessed in different situation of podocyte adaption and injury and shows that each marker had a different reactivity according to the type and/or the intensity of the injury.

Table 5 (Top): Summary of the in vivo results and Table 6 (Bottom): Summary of the in vitro results (Legend: + or – refer to expression; ↓ or ↑ refer to down and up regulation).

In vivo Model / type	Podocytes	Sema3G	CYTC	KIM-1 outer medulla	KIM-1 cortex
Normal kidney	Healthy	+	+	–	–
Albumin overload <i>Functional model</i>	No injury	+	+	+	++
PHN Structural model (alteration of GBM)	Stress leading to podocyte adaption (reversible injury)	↓	+	+	-
PAN <i>Glomerular toxicity model</i>	Toxicity leading to podocyte injury	↓↓	↑↑↑	+	+++
Cisplatin <i>Tubular toxicity model</i>	No podocyte injury	+	+	+++	++

In vitro model	Sema3G	CYTC
Primary rat podocytes		
Untreated	-	+
PAN 0.1µg/ml	↓	↓↑
PAN 1 µg/ml	↓↓	↓↑
Cisplatin	-	↓

6. Discussion

The goal of these investigations was to identify podocytes specific markers that could be used to characterize and differentiate early podocyte adaption (reversible injuries) from podocyte irreversible injury. Furthermore we wanted to verify the possible integration of these podocytes markers with a tubular injury marker in order to define patterns of tissue injury. The hope is to use this pattern of injury to identify early signs of glomerular dysfunction/damage in toxicology studies, preclinical models of diseases and possibly clinical case series. After experimental validation, this pattern could be applied in drug discovery and development to better characterize early glomerular toxic injury and support the development of new drugs. Depending of translatability to human, this injury pattern may be considered for potential clinical application and an improved evaluation of glomerular diseases.

To reach the goal we started by identifying podocytes specific markers, tested them in different animal models of podocyte injury, and integrate these markers with a well-known tubular injury marker, KIM-1, to define the different patterns of nephron injury. The genomic analysis of laser captured microdissected glomeruli identified Sema3G and CYTC as potential interesting candidates. Using molecular localization, we demonstrated that the expression of these markers in the glomerulus is podocyte specific. We also proved that Sema3G expression is specific to the podocyte in glomeruli for several other species, including human. CYTC expression in podocytes is instead rat specific, or below the level of detection by IHC.

By testing the expression of Sema3G in different models of podocyte stress and injury, we found that Sema3G was down-regulated in the model of PHN and drug-induced toxicity with PAN. These models are representing situation of podocyte adaption and damage, respectively. On the other hand, Sema3G expression remains unchanged in a model of albumin overload which with the protocol used, represent a reversible functional alteration without podocyte injury. In addition, Sema3G expression did not vary in a model of tubular toxicity induced by cisplatin. In conclusion, Sema3G is downregulation in case of both

reversible and irreversible injury but not in case of functional impairment without injury.

In the opposite, the marker CYTC normally expressed by the podocytes of the rat, was upregulated only upon PAN toxicity but not in models of albumin overload and PHN. Therefore we conclude that the upregulation of CYTC potentially represent a marker of irreversible podocyte injury.

4.21 Sema3G as marker of podocyte adaption and injury

Sema3G has been mainly studied for its autocrine effect on endothelial cells and its paracrine effect on smooth muscle cells (Kutschera, Weber et al. 2011), as well as for its function as repulsive axon guidance signalling molecule (Yu and Moens 2005) . In our studies, we found expression of Sema3G and its receptor NRP2 in the endothelial cells of the kidney cortex vascular bed, as expected by their known expression and function in the endothelial cells. However, Sema3G was absent in the endothelial cells of the glomerulus but present at high levels in the specialized epithelial cells. The presence of Sema3G in the podocytes represents a new finding.

At the moment, the significance of Sema3G expression in podocyte is not clear. Considering Sema3G function as repulsive axon guidance signalling molecule, it may be secreted by the podocytes in the Bowman's space and interact with NRP2 present on the parietal cells of the Bowman's capsule (vis-à-vis the podocyte). Sema3G could act as a repulsive signalling molecule helping to maintain the appropriate distance between the parietal layer and visceral layer of the capsule.

In addition to this potential function to maintain the Bowman's capsule space, Sema3G could be implicated in the maintenance of the glomerular filtration barrier and/or in podocyte protection, together with VEGF. In fact NRP2 is not exclusively binding Sema3G but is part of the entire complex of NRPs-plexins receptor family, which also binds VEGF (Schramek, Sarkozi et al. 2009). High expression levels of VEGF are present in the

podocytes and are playing a key role for the establishment and maintenance of the glomerular filtration barrier (Eremina, Sood et al. 2003, Eremina, Baelde et al. 2007). The podocyte is responsible to provide migratory cues to glomerular endothelial cells to establish the renal filtration barrier and because VEGF is still expressed by mature podocytes, it is often considered to play this role. VEGF has been also suggested to function in an autocrine fashion that is required for podocyte survival and that podocyte survival is diminished upon inhibition of VEGF receptor (Foster, Hole et al. 2003). Similarly to Sema3G, the expression of VEGF has been shown to be down regulated in podocytes upon treatment with PAN in the rat kidney (Fan, Wakayama et al. 2002). Therefore it is entirely possible that the presence of Sema3G in podocytes may be involved in similar processes. Sema3G could represent a redundant or a synergic molecule to VEGF that insure a function in the maintenance of the filtration barrier and/or podocyte protection.

Very recently, Sema3G has also been described as a novel podocyte expressed gene which protects the podocyte from inflammatory kidney disease and diabetic nephropathy (Ishibashi, Takemoto et al. 2016). These data confirm our findings on Sema3G podocyte expression and reinforce the potential importance of this molecule in podocyte biology. The authors have demonstrated a role for Sema3G as inhibitor of basal inflammatory cytokine expression through the ERK and NF- κ B signaling, acting therefore as kidney inflammation protector.

Our results suggest that Sema3G downregulation represent a general marker of podocyte stress while its expression remains unchanged without podocytes adaption or injury. During the heterologous phase of the PHN model, the podocytes are lifted from the glomerular basal membrane by the deposition of anti-FxA1 antibodies and stimulated by the deposition of complement. We hypothesize that this indirectly a source of cellular stress and the podocyte start repressing Sema3G mRNA expression. PAN is causing direct toxic injury and we see repression of Sema3G expression concomitantly with the morphological alteration of the podocytes.

On the opposite, in presence of a functional impairment (reversible injury) where the podocyte is undamaged, the podocytes remains able to maintain Sema3G expression. These results based on *in vivo* model were also confirmed *in vitro* using a primary culture of rat podocytes. After treatment with toxicants, a time and dose dependent decrease of Sema3G could be reproduced while its expression remains unchanged after Cisplatin treatment.

In the literature, Sema3G itself has never been associated to podocyte stress or injury. But in diabetic nephropathies which are also associated to podocytes adaption/injury and proteinuria, some data showed that the expression of both isoforms of neuropilin receptor (NRP1 and NRP2) as well as the entire signaling complex involving another Semaphorin family member, semaphoring-3A is significantly reduced in the context of this pathology (Bondeva, Ruster et al. 2009).

In summary, our work demonstrates that Sema3G downregulation is a valuable marker of podocyte injury, allowing to discriminate irreversible injuries due to structural damage and/or toxic damages from reversible podocytes injury. Furthermore the specific expression of Sema3G in podocytes of several species, as demonstrated earlier in this work, warrant future investigations to assess its potential as podocyte injury markers in human diseases.

4.22 Cystatin C as marker of podocyte injury

The second podocyte specific marker assessed in this study, Cystatin C, was also localized in the rat kidney and was shown to be highly expressed in podocytes at the mRNA as wells as at the protein level. This indicates that, on the contrary of what was described so far, podocytes are an intrarenal source of cystatin C. This implies that cystatin C could have a function in these cells.

The result of the CYTC expression in podocyte injury models seems in relation to podocyte

injury only. This was demonstrated by the time dependent increase of CYTC expression upon PAN treatment. The increase of CYTC compared to Sema3G downregulation strengthens the Sema3G results. In fact, it confirms that the reduction of Sema3G in the same sample is the result of an active cellular process in relation to podocyte injury, and not a general toxic effect of the PAN treatment on podocytes. The final outcome of these investigations is that the expression of CYTC is modulated *in vivo* only in case of podocyte toxicity but not in case of functional impairment (albumin overload model) or structural impairments (PHN model). Therefore we conclude that the modulation of CYTC is restricted to situations with major morphological changes of the podocyte (e.g. podocytes effacement due to cytoskeleton changes) and cell death induced by the toxic effect of PAN.

When the podocytes are injured due to toxicants, the most characteristic change observed is the reorganization of actin skeleton that leads to foot process effacement. Within many others, one cause of foot process effacement is the activation of the cathepsin L-mediated proteolysis and more generally an enzymatic cleavage of essential podocytes actin dynamics by cytosolic cathepsin-L (Mundel and Reiser 2010). The increase of the protease inhibitor CYTC observed in podocytes could be a reaction to limit and/or compensate the cathepsin-L activity and avoid or reduce proteinuria.

The function of CYTC is not limited to protease inhibition activity only and CYTC can be regulated by several stimuli and is susceptible to chemical insult. The roles of CYTC as a disease-associated protein, subjected to multiple regulations, has recently been reviewed (Xu, Ding et al. 2015). In this review, the authors linked CYTC to several pathological processes through various mechanisms, independently from its function as protease inhibitor.

As example, some very high levels of CYTC are present in brain of patients with epilepsy, in animal models of neurodegenerative conditions and in response to injury. It was demonstrated in mouse cortical neurons that CYTC plays a protective role by inducing autophagy and is neuroprotective in neurodegenerative diseases (Tizon, Sahoo et al. 2010). Now, the podocyte is a cell that exhibits an unusually high level of constitutive autophagy

(Hartleben, Godel et al. 2010) and share this specificity with the neuronal cells. Knowing that the cellular response to stress through autophagy has been identified as a major pathway to maintain cellular homeostasis, the autophagy regulation into these two cells types is crucial and could be an important task for CYTC in the podocytes of the rat. The induction of autophagy by CYTC in podocytes has not been demonstrated yet but need further investigations.

In summary, our data indicate that CYTC, independently from its function, is a specific marker of podocyte toxic injury only and not of functional (albumin overload model) or structural impairments (PHN model) of podocytes.

Unfortunately, our data cannot currently address the potential use of CYTC as marker of podocyte toxicity in other species. The basal expression of CYTC in podocytes seems to be rat specific, but this does not means that following exposure to specific toxicants, the podocytes of other species could start expressing CYTC or increase the expression up to levels detectable by in situ hybridization.

4.23 A tubular injury marker associated to podocyte injury evaluation

When the podocytes are injured, the foot processes simplify or lose their normal interdigitating pattern and the slit diaphragm is disrupted. With a damaged filtration barrier, some high molecular weight proteins are reaching the proximal tubule and are damaging the cells. Considering that the protein KIM-1 is localized in the apical brush border of the proximal tubule cells and is a very sensitive indicator of many type of tubular injury (Ichimura, Bonventre et al. 1998, Bailly, Zhang et al. 2002), including protein overload (van Timmeren, Bakker et al. 2006), KIM-1 can be expected to react to all the situations of barrier impairment tested in this work.

KIM-1 increased expression in response to a tubular toxicant like Cisplatin is well-known. Independently from his well-known role as tubular injury biomarker measurable in the urine, KIM-1 can also be use at the mRNA level as tissue biomarker for detection of early

injury events in the proximal tubule cells. Having the possibility to study KIM-1 localization during a time course study with a tubular toxicant, can give a sequential picture of toxicity McDuffie and colleagues (McDuffie, Ma et al. 2013) studied the time course of renal proximal tubule injury following cisplatin administration but focused more on the correlation of temporal expression versus the histopathology and urinary biomarker. The spatial distribution in tissue was not evaluated.

Therefore, we investigated the spatial expression of KIM-1 to verify where its upregulation starts and how it evolves along the proximal tubule in relation to treatment time. With this approach, we were able to identify a pattern of spatial progression along the proximal tubule. In fact, it appears that KIM-1 expression follows precisely the drug toxic effect along the proximal tubule, starting from the descending portion of the proximal tubule (S3) which is the most sensitive portion of the tubule to injury and over time is expanding toward the convoluted part of the proximal tubule (S1). This expression pattern follows the accumulation of Cisplatin in the proximal tubule by organic cation transporter uptake (Pabla and Dong 2008). Our results show that KIM-1 is a good indicator of the topography of injury related to Cisplatin toxicity. In our hands KIM-1 *in situ* hybridization created a visual pattern of tubular toxicity reflecting the spatial and temporal progression of the lesions. This work demonstrated the validity of KIM-1 spatial localization as a method to follow toxicity along the tubule in a case of primary tubular toxicity.

As next step we proceed testing the spatial localization of KIM-1 as indicator of secondary tubular injury associated to a podocyte “primary” injury. We reasoned that if the podocyte is the primary target of an injury located at the beginning of the nephron, the proximal tubule will indirectly suffer and should show some “secondary” injury. When assessing KIM-1 expression in the time course study with PAN treatment, we were able to detect KIM-1 positivity in the proximal tubule and in the parietal epithelium of Bowman’s capsule before detecting KIM-1 in the descending portion. The fingerprint analysis and quantification reflects perfectly this pattern with KIM-1 expression starting first in the cortex region in a patchy way. It reveals a feature completely different from the one observed with the sample in the Cisplatin study. In fact, our results are in keeping with the

description of KIM-1 expression in glomeruli of a rat diabetic model (Zhao, Zhang et al. 2011), where the authors demonstrated a correlation between the level of glomerular KIM-1 expression and the degree of proteinuria, proving that KIM-1 is a sensitive marker that correlate with the extent of loss of podocytes differentiation markers in the damaged glomeruli. These results demonstrate that KIM-1 can also be used as a local tissue marker of injury, independently from the cause of the injury (glomerulus versus tubular). The observation of KIM-1 positivity either in parietal epithelia cells of the Bowman's capsule, in the proximal epithelial cells directly after the glomeruli or in the descending portion of the proximal tubule, can help to understand the site of initiation of toxicity and its evolution.

Looking now at the animal models non related to drug-induced injury, it appears interestingly that a pattern of KIM-1 expression similar to the PAN model was observed in the case of albumin overload, while KIM-1 expression in the PHN model was much lower (almost undetectable) but more similar to Cisplatin pattern. These differences are probably reflecting the filtration barrier capacity of the glomerulus and the consequent injury related to the flow of protein. From the functional point of view, the albumin overload model determines a stronger functional impairment of the filtration barrier capacity of the glomerulus and higher flow of protein in the tubule inducing injury than the PHN model.

4.24 A pattern of tissue injury to explore glomerular damages?

Podocyte stress and/or injury is not a phenomenon that can be assessed using a single marker and as recently reviewed by Braun et al. in 2016 (Braun, Becker et al. 2016), there are long-standing debate on the underlying mechanisms responsible for podocyte depletion, ranging for necrosis and apoptosis to detachment of viable cells from the glomerular basement membrane.

Viable podocytes can be isolated from the urine of healthy as well as glomerular disease samples (Vogelmann, Nelson et al. 2003) and represents an interesting source of

information. Many approaches are attempting to take advantage of these isolated cells to characterize and evaluate podocyte injury. As example Sato et al. (Sato, Wharram et al. 2009) monitored podocyte loss by detecting nephrin and podocin mRNA in urine of diaphtheria toxin receptor transgenic rat and consider that it could be a useful clinical tool for diagnostic and monitoring of glomerular diseases. Using the same strategy , Lioudaki (Lioudaki, Stylianou et al. 2015) measured the presence of mRNA for podocin, nephrin and synaptopodin in urine of patients with diabetes mellitus (DM) and demonstrate that DM is the only significant determinant of the presence of nephrin and/or podocin mRNA in urine in this population.

Our goal is different from these efforts and we are not attempting to develop accessible biomarkers to identify podocytes specific injuries. The goal of our research is to develop tissue markers able to discriminate different categories of podocytes injuries, to understand transient versus permanent injury, and through the use of a tubular damage marker, the consequences in terms of filtration impairment. It is the integration of these different markers together (and not from the analysis of each of them separately) that generate an added value in understanding the consequences on the kidney functionality. The proposed combination is composed of a molecule (Sema3G) that reflect the podocyte injury level, with the expression of CYTC that indicate situations of morphological changes (e.g. podocytes effacement due to cytoskeleton changes), with finally a third marker (KIM-1) helping to determine the toxic effect on tubule resulting from podocyte injury and consequent flow of protein.

By testing this combination of markers in several model of injury, we revealed a differential expression pattern specific to each injury type and/or effect on glomerular protein filtration:

- The functional impairment of podocytes (absence of adaption or injury) is characterized by an absence of modulation of the podocyte markers although tubular injury is present due to the excessive flow of proteins in the tubule.
- The podocytes adaption (structural impairment of GBM) is characterized by a

specific downregulation of Sema3G and is accompanied by a weak tubular injury.

- The podocytes injury (drug-induced toxicity) is characterized by a downregulation of Sema3G and an upregulation of CYTC accompanied by a strong tubular injury similar to functional impairment toxicity.

The classification detailed above demonstrate that the combination of these 3 markers represents a valuable tool for determining effect of drugs or diseases, on podocyte integrity and the consequences on tubular functions.

7. Future outlook

This work could identify useful podocyte markers and could demonstrate that combining *in-situ* glomerular and tubular injury markers enables a more, sensitive detection of podocyte injury.

This combination of markers can be used for direct toxicity assessment on podocytes in investigative rat toxicology study. Detection of the two markers Sema3G and CYTC on tissue sections is complementary to classical clinical pathology and urinary biomarker and will contribute to their interpretation. This will provide information about the “degree” of injury of the podocyte. By localizing KIM-1 direct or indirect tubular toxicity of the drug compound can be predicted.

Furthermore, such a combination of markers can be applied to animal models of kidney disease, as screening tool for drug selection. Hence, it can also be used as a pharmacodynamic readout of drug efficacy.

An interesting aspect to further explore would be the reversibility of the Sema3G downregulation. In the present studies, all animal models were assessed during the treatment period no recovery arm were included in the study design. Normalization of Sema3G expression levels would imply that podocytes have a certain capacity of regeneration. As proliferation of podocytes is very unusual in the majority of the glomerular diseases, the remaining adult podocytes are unable to replace the depleted or injured ones. However, parietal epithelial cells are often proposed as potential progenitors for podocytes but also the Cells of Renin Lineage (CoRL) exhibit marked plasticity (review of (Shankland, Pippin et al. 2014) giving some hope of potential restoration.

Equally interesting it will be to further explore reversibility of KIM-1 downregulation during a recovery phase. It was shown, in a case of adriamycin-induced nephropathy (Kramer, van Timmeren et al. 2009), that KIM-1 downregulation was reversible and proportional to proteinuria reduction indicating reversibility of early tubular injury.

Expression of Sema3G and CYTC in podocytes of other species has been assessed in mouse, dog and monkey by *in-situ* hybridization. The presence of Sema3G in other species opens perspective for applying this marker as screening marker for podocytes injury. As glomerulonephritis in dogs and cats have been clearly described (Slauson and Lewis 1979), measurement of Sema3G expression in podocytes in these species could guide to discriminate between immune versus non-immune glomerulopathies and improve the diagnosis as well as guide therapy.

Finally, the ultimate goal would be assess Sema3G expression in different types of human glomerulus pathology and investigate if the animal models results could be translated.

In summary, the markers explored in the present work give very precise and local information about the sequence of the pathological events, starting at the level of the glomerulus in the podocyte cells and extending to the tubular cells injury. Overall, this will contribute to further elucidate the pathogenesis of glomerulopathies.

8. Conclusion

The maintenance of the glomerular filtration barrier integrity is a mandate for the proper functionality of the kidney and podocyte injury is playing a central role in kidney dysfunction.

Two novel markers Sema3G and CYTC highly expressed in podocytes could be identified and tested in several type of podocyte injury (e.g. functional or structural impairment and drug-induced toxicity) and showed some differential expression according to the type and intensity of the injury. In combination with the tubular injury marker KIM-1, an integrated tissue injury pattern tool could be proposed.

As each member of this panel of markers has a different behavior according to the type of podocyte injury, it became possible not only to identify earlier podocyte injury but also to describe the sequence of the injury events, including the indirect toxicity related to the protein outflow into the proximal tubules.

Such a panel of markers requires the availability of tissue section or biopsy but has the advantage to give an “*in situ*” picture with a resolution at the cellular level.

9. Supplementary data

Supplementary data Table 1: Primer sequences for Sema3G, CYTC and KIM-1 riboprobes generation.

Gene name	Accession number	Forward primer sequence	Reverse primer sequence	Amplicon size and position
Rat Sema3G	NM_001100882	GGCTCAGCCGCCTTGAT	CGAAACCAGTGAGCTGAAGGAT	219 bp (1968-2186)
Rat Cst3	NM_012837	CTCCGCAGGAGGCAGATG	ACAAGTAAGGGACCATTGGC	371 bp (164-535)
Rat KIM-1	NM_173149	TTGCCCTCATAGATAAGTAGAAGAAGAG	GAAGGAAACCCGTGGTAGTCC	401 bp (1992-2392)
Mouse Sema3G	NM_001025379	GACGCAGGAAACTACACTTGCA	CCCCTGAGCTGAAGGATGTC	200 bp (1983-2182)
Mouse Cst3	NM_009976	CGCTGTGAGCGAGTACAACAA	CAGGGAGTGTGTGCCTTTCC	241 bp (282-531)
Dog Sema3G	XM_541852	CCGACCAGGTAAGACAGATGAG	TGCGCCCGGCTCTTC	406bp (1958-2363)
Dog Cst3	XM_003639821	ACAACCGGGCGAGCAA	TCTGGAAAGAGCAGAGCGTTTT	200 bp (327-527)
Human Sema3G	NM_020163	TCGAGGTGTACGCGCTGTT	CAGGAAAATGACATCGTAGGTCC	401bp (1026-1427)
Human Cst3	NM_000099	CCTGGTGGGAGGCCCATGGACG	GTGCATAAGAGGTGATAGGC	383 bp (288-671)

Supplementary data Table 2: Detailed probes concentrations and hybridization conditions

Probe name	Probe quantity/ per slide	Hybridization temperature	Stringency wash conditions
Rat Sema3G	20ng	65°C	3 times 2xSSC at 60°C
Rat Cst3	2ng	65°C	3 times 0.1xSSC at 70°C
Rat KIM-1	20ng	65°C	3 times 0.1xSSC at 70°C
Mouse Sema3G	50ng	65°C	3 times 2xSSC at 60°C
Mouse Cst3	50ng	70°C	3 times 2xSSC at 65°C
Dog Sema3G	50ng	70°C	3 times 2xSSC at 65°C
Dog Cst3	50ng	65°C	3 times 2xSSC at 60°C
Monkey Sema3G (using the human probe)	150ng	65°C	3 times 2xSSC at 60°C
Monkey Cst3 (using the human probe)	50ng	70°C	3 times 2xSSC at 65°C
Human Sema3G	75ng	55°C	3 times 2xSSC at 50°C
Human Cst3	50ng	65°C	3 times 2xSSC at 60°C

Supplementary data Table 3: Gene list of the gene expression analysis results from laser capture microdissected glomeruli versus cortex without glomeruli

Probe Set ID	Gene Symbol	Gene Name	Cortex [mean expression]	Glomeruli [mean expression]	Glomeruli [mean fold change (FC)]	Glomeruli mean expression (log2)	Glomeruli mean fold change (log2)	FC glomeruli vs. cortex	P Value	1/(p-value)
1367562_at	Sparc	secreted protein, acidic, cysteine-rich (osteonectin)	3181	14589	4.59	13.83	2.20	4.59	1.04E-05	96107.418
1391856_at	Sema3g	sema domain, immunoglobulin domain (Ig), short basic domain, secreted, (semaphorin) 3G	777	11138	14.33	13.44	3.84	14.33	9.24E-06	108238.947
1369895_s_at	Podxl	podocalyxin-like	1011	10732	10.61	13.39	3.41	10.61	3.79E-06	263651.824
1370855_at	Cst3	cystatin C	1276	10373	8.13	13.34	3.02	8.13	0.0001039	9628.055
1393368_at	Osbpl5	oxysterol binding protein-like 5	1050	8367	7.97	13.03	2.99	7.97	1.29E-05	77584.571
1368412_a_at	Ptpro	protein tyrosine phosphatase, receptor type, O	343	7849	22.90	12.94	4.52	22.90	6.37E-06	156969.239
1388786_at	Synpo	synaptopodin	696	6705	9.64	12.71	3.27	9.64	7.59E-05	13170.219
1385788_at	Ephb3	Eph receptor B3	603	6232	10.33	12.61	3.37	10.33	0.0027464	364.108
1387146_a_at	Ednrb	endothelin receptor type B	898	6023	6.71	12.56	2.75	6.71	6.78E-06	147522.735
1398827_at	Cd81	Cd81 molecule	918	5535	6.03	12.43	2.59	6.03	0.0001567	6381.122
1398333_at	Epas1	endothelial PAS domain protein 1	1301	5518	4.24	12.43	2.08	4.24	2.65E-05	37696.577
1381548_at	Golim4	golgi integral membrane protein 4	677	5395	7.97	12.40	2.99	7.97	0.0003924	2548.126
1390119_at	Sfrp2	secreted frizzled-related protein 2	389	4874	12.52	12.25	3.65	12.52	4.08E-05	24500.828
1385823_s_at	Podxl	podocalyxin-like	223	4809	21.54	12.23	4.43	21.54	0.0001367	7316.018
1367568_a_at	Mgp	matrix Gla protein	1030	4777	4.64	12.22	2.21	4.64	1.36E-06	734485.145
1384509_s_at	Pcdh17	protocadherin 17	722	4715	6.53	12.20	2.71	6.53	0.0003773	2650.168
1385243_at	Maf	v-maf avian musculoaponeurotic fibrosarcoma oncogene homolog	995	4346	4.37	12.09	2.13	4.37	0.0007528	1328.337
1367816_at	Hopx	HOP homeobox	339	4185	12.34	12.03	3.63	12.34	5.90E-05	16944.945
1367574_at	Vim	vimentin	683	4143	6.06	12.02	2.60	6.06	0.000256	3906.809
1369008_a_at	Olfm1	olfactomedin 1	154	4070	26.39	11.99	4.72	26.39	0.0001666	6002.742
1370254_at	Clic5	chloride intracellular channel 5	247	4065	16.49	11.99	4.04	16.49	0.0001265	7902.948
1373657_at	Slc31a2	solute carrier family 31 (copper transporter), member 2	677	4059	6.00	11.99	2.58	6.00	0.0014231	702.713

1368860_at	Phlda1	pleckstrin homology-like domain, family A, member 1	419	3997	9.55	11.96	3.26	9.55	0.0007331	1364.085
1368858_at	Ugt8	UDP glycosyltransferase 8	481	3905	8.12	11.93	3.02	8.12	6.03E-06	165832.443
1385540_at	Pias1	protein inhibitor of activated STAT, 1	939	3764	4.01	11.88	2.00	4.01	1.18E-05	84581.369
1369961_at	Ppap2a	phosphatidic acid phosphatase type 2A	502	3706	7.38	11.86	2.88	7.38	9.39E-05	10648.246
1367948_a_at	Kdr	kinase insert domain receptor	644	3692	5.73	11.85	2.52	5.73	5.06E-05	19774.191
1372299_at	Cdkn1c	cyclin-dependent kinase inhibitor 1C	278	3662	13.18	11.84	3.72	13.18	3.04E-05	32849.347
1368842_at	Tcf4	transcription factor 4	867	3607	4.16	11.82	2.06	4.16	0.0014157	706.375
1393454_at	Pcdh17	protocadherin 17	734	3600	4.90	11.81	2.29	4.90	4.24E-05	23566.955
1388453_at	Myadm	myeloid-associated differentiation marker	555	3522	6.34	11.78	2.67	6.34	6.27E-05	15944.579
1394907_at	Synpo	synaptopodin	89	3493	39.23	11.77	5.29	39.23	0.0016678	599.575
1371354_at	Tnnc1	troponin C type 1 (Winslow, Swenberg et al.)	89	3467	39.15	11.76	5.29	39.15	0.0003325	3007.403
1376102_at	Tmbim1	transmembrane BAX inhibitor motif containing 1	504	3333	6.62	11.70	2.73	6.62	2.61E-05	38251.027
1391406_at	Degs1	delta(4)-desaturase, sphingolipid 1	439	3296	7.50	11.69	2.91	7.50	0.0001125	8885.761
1379713_at	LOC102557211	uncharacterized LOC102557211	122	3256	26.69	11.67	4.74	26.69	0.0003357	2978.600
1372947_at	Pls3	plastin 3	605	3241	5.36	11.66	2.42	5.36	0.0001756	5695.005
1372473_at	Tjp1	tight junction protein 1	416	3206	7.70	11.65	2.94	7.70	0.0008439	1185.023
1373613_at	Slc48a1	solute carrier family 48 (heme transporter), member 1	401	3175	7.92	11.63	2.98	7.92	0.0012297	813.221
1372587_at	Emcn	endomucin	515	3084	5.99	11.59	2.58	5.99	1.86E-05	53845.999
1372064_at	Cxcl16	chemokine (C-X-C motif) ligand 16	575	3023	5.25	11.56	2.39	5.25	0.000663	1508.409
1369153_at	Nphs1	nephrosis 1, congenital, Finnish type (nephrin)	82	2964	36.33	11.53	5.18	36.33	1.45E-06	690711.065
1388831_at	Slc9a3r2	solute carrier family 9, subfamily A (NHE3, cation proton antiporter 3), member 3 regulator 2	326	2892	8.86	11.50	3.15	8.86	0.0013201	757.520
1367800_at	LOC100910418	tissue-type plasminogen activator-like plasminogen activator, tissue	237	2849	12.01	11.48	3.59	12.01	8.42E-05	11882.718
1367563_at	Sparc	secreted protein, acidic, cysteine-rich (osteonectin)	692	2770	4.00	11.44	2.00	4.00	0.0005487	1822.500
1371430_at	Dag1	dystroglycan 1 (dystrophin-associated glycoprotein 1)	550	2736	4.98	11.42	2.32	4.98	0.0011119	899.373
1371702_at	Tspan7	tetraspanin 7	453	2577	5.69	11.33	2.51	5.69	0.0001904	5253.099
1390207_at	Lats2	large tumor suppressor kinase 2	555	2554	4.60	11.32	2.20	4.60	0.000599	1669.518

1395754_at	Frem2	Fras1 related extracellular matrix protein 2	226	2475	10.94	11.27	3.45	10.94	0.0051024	195.987
1395408_at	Nostrin	nitric oxide synthase trafficking	98	2471	25.29	11.27	4.66	25.29	0.0004495	2224.857
1387995_a_at	Ifitm3	interferon induced transmembrane protein 3	559	2457	4.40	11.26	2.14	4.40	0.0082016	121.927
1387122_at	Plagl1	pleiomorphic adenoma gene-like 1	540	2438	4.52	11.25	2.18	4.52	0.0008974	1114.278
1380544_at	Foxp1	forkhead box P1	230	2365	10.27	11.21	3.36	10.27	0.0077722	128.664
1372585_at	LOC100910973	uncharacterized LOC100910973	457	2315	5.07	11.18	2.34	5.07	0.0050478	198.108
1371356_at	Tenc1	tensin like C1 domain containing phosphatase (tensin 2)	448	2250	5.02	11.14	2.33	5.02	0.0005484	1823.361
1372564_at	Ets2	v-ets avian erythroblastosis virus E26 oncogene homolog 2	418	2234	5.35	11.13	2.42	5.35	0.002735	365.626
1387933_s_at	Podxl	podocalyxin-like	172	2210	12.88	11.11	3.69	12.88	0.0016032	623.760
1376782_at	Cdc14a	cell division cycle 14A	417	2200	5.28	11.10	2.40	5.28	0.0047175	211.977
1367648_at	Igfbp2	insulin-like growth factor binding protein 2	63	2179	34.57	11.09	5.11	34.57	0.0018372	544.304
1369476_at	Efnb1	ephrin B1	173	2178	12.56	11.09	3.65	12.56	0.0035968	278.024
1373403_at	LOC100910163 LOC684871	uncharacterized LOC100910163 similar to Protein C8orf4 (Thyroid cancer protein 1) (TC-1)	534	2154	4.03	11.07	2.01	4.03	8.49E-07	1178367.516
1368884_at	Entpd1	ectonucleoside triphosphate diphosphohydrolase 1	205	2140	10.45	11.06	3.39	10.45	0.0002764	3617.727
1368473_at	Gja5	gap junction protein, alpha 5	227	2060	9.09	11.01	3.18	9.09	0.0012216	818.604
1379443_at	Hps3	Hermansky-Pudlak syndrome 3 homolog (human)	385	2054	5.33	11.00	2.41	5.33	0.0085174	117.407
1388837_at	Slc44a2	solute carrier family 44 (choline transporter), member 2	282	2000	7.10	10.97	2.83	7.10	0.0043618	229.264
1377286_at	Gimap4	GTPase, IMAP family member 4	161	1985	12.30	10.96	3.62	12.30	0.0006026	1659.523
1368901_at	Thbd	thrombomodulin	128	1979	15.51	10.95	3.96	15.51	0.0006995	1429.578
1386921_at	Cpe	carboxypeptidase E	232	1979	8.53	10.95	3.09	8.53	2.47E-05	40439.957
1369793_a_at	Mcam	melanoma cell adhesion molecule	361	1919	5.31	10.91	2.41	5.31	0.0089169	112.146
1395516_at	Arglu1	arginine and glutamate rich 1	441	1918	4.35	10.91	2.12	4.35	0.0005196	1924.444
1374630_at	Clic3	chloride intracellular channel 3	61	1879	30.85	10.88	4.95	30.85	6.91E-05	14472.947
1373541_at	Arhgef17	Rho guanine nucleotide exchange factor (GEF) 17	254	1810	7.12	10.82	2.83	7.12	0.0017859	559.954
1389282_at	Itga3	integrin, alpha 3	130	1802	13.82	10.82	3.79	13.82	0.0006072	1646.867
1369273_a_at	Npr3	natriuretic peptide receptor 3	81	1801	22.31	10.81	4.48	22.31	0.0073782	135.534
1373357_at	Foxd2	forkhead box D2	69	1794	25.89	10.81	4.69	25.89	0.0014121	708.172

1388177_at	Ddn	dendrin	89	1775	19.87	10.79	4.31	19.87	7.52E-05	13303.948
1376150_at	S1pr3	sphingosine-1-phosphate receptor 3	393	1755	4.46	10.78	2.16	4.46	0.0001634	6120.475
1374704_at	Kdelc2	KDEL (Lys-Asp-Glu-Leu) containing 2	227	1753	7.74	10.78	2.95	7.74	0.0006907	1447.845
1395078_at	Sema3g	sema domain, immunoglobulin domain (Ig), short basic domain, secreted, (semaphorin) 3G	56	1598	28.65	10.64	4.84	28.65	0.0006905	1448.182
1370933_at	Myo1e	myosin IE	301	1575	5.24	10.62	2.39	5.24	0.0195424	51.171
1395166_at	Ehd2	EH-domain containing 2	331	1574	4.76	10.62	2.25	4.76	2.61E-05	38321.115
1374403_at	Efnb1	ephrin B1	210	1534	7.30	10.58	2.87	7.30	0.0009158	1091.981
1374774_at	Ptpn14	protein tyrosine phosphatase, non-receptor type 14	234	1478	6.32	10.53	2.66	6.32	0.0054033	185.073
1393160_at	Tbx3	T-box 3	105	1467	13.90	10.52	3.80	13.90	0.0119452	83.715
1370893_at	Acaca	acetyl-CoA carboxylase alpha	306	1467	4.79	10.52	2.26	4.79	0.018403	54.339
1388920_at	Bmp6	bone morphogenetic protein 6	194	1454	7.51	10.51	2.91	7.51	0.0033929	294.734
1398275_at	Mmp9	matrix metalloproteinase 9	48	1421	29.45	10.47	4.88	29.45	2.23E-05	44803.336
1379742_at	Sp100	SP100 nuclear antigen	282	1337	4.74	10.38	2.24	4.74	0.0055695	179.549
1369154_at	Nphs1	nephrosis 1, congenital, Finnish type (nephrin)	134	1336	10.00	10.38	3.32	10.00	0.0001086	9211.672
1387588_at	Ehd3	EH-domain containing 3	268	1330	4.97	10.38	2.31	4.97	0.0028579	349.911
1367850_at	Fcgr2a	Fc fragment of IgG, low affinity IIa, receptor low affinity immunoglobulin gamma Fc region receptor III-like low affinity immunoglobulin gamma Fc region receptor III-like low affinity immunoglobulin gamma Fc region receptor III-like Fc gamma receptor II beta	281	1297	4.61	10.34	2.21	4.61	0.0171063	58.458
1369949_at	Bcam	basal cell adhesion molecule (Lutheran blood group)	158	1293	8.19	10.34	3.03	8.19	0.0103792	96.346
1370402_at	Egfl7	EGF-like-domain, multiple 7	317	1293	4.07	10.34	2.03	4.07	0.0013017	768.215
1391499_at	LOC100909676	uncharacterized LOC100909676	70	1288	18.53	10.33	4.21	18.53	0.0005037	1985.324
1368513_at	Enpep LOC100910501	glutamyl aminopeptidase glutamyl aminopeptidase-like	249	1254	5.05	10.29	2.34	5.05	0.0001084	9228.042
1370406_at	Cd55	Cd55 molecule	86	1248	14.47	10.28	3.85	14.47	0.0012972	770.880
1383155_at	Fam117b	family with sequence similarity 117, member B	230	1242	5.39	10.28	2.43	5.39	6.42E-05	15566.282
1379604_at	Apol3	apolipoprotein L, 3	162	1229	7.59	10.26	2.92	7.59	0.0021724	460.312

1393401_at	Eccscr	endothelial cell surface expressed chemotaxis and apoptosis regulator	68	1215	17.93	10.25	4.16	17.93	0.0037 415	267.27 1
1373036_at	lqgap2	IQ motif containing GTPase activating protein 2	260	1214	4.67	10.25	2.22	4.67	0.0001 047	9554.0 94
1389913_at	Lrrfip1	leucine rich repeat (in FLII) interacting protein 1	205	1210	5.90	10.24	2.56	5.90	0.0009 574	1044.5 27
1390437_at	Sema5a	sema domain, seven thrombospondin repeats (type 1 and type 1-like), transmembrane domain (TM) and short cytoplasmic domain, (semaphorin) 5A	191	1199	6.28	10.23	2.65	6.28	0.0018 761	533.01 1
1370287_a_at	Tpm1	tropomyosin 1, alpha	179	1189	6.64	10.21	2.73	6.64	0.0030 244	330.64 7
1391435_at	Pltp	phospholipid transfer protein	107	1188	11.15	10.21	3.48	11.15	0.0033 624	297.40 4
1390389_at	Mertk	c-mer proto-oncogene tyrosine kinase	114	1182	10.36	10.21	3.37	10.36	0.0002 476	4039.2 29
1369651_at	Thy1	Thy-1 cell surface antigen	109	1175	10.83	10.20	3.44	10.83	0.0034 901	286.52 7
1388848_at	Inf2	inverted formin, FH2 and WH2 domain containing	100	1142	11.41	10.16	3.51	11.41	0.0010 367	964.63 4
1384558_at	Plac9	placenta-specific 9	61	1137	18.74	10.15	4.23	18.74	0.0003 533	2830.4 28
1371627_at	Amotl1	angiomin-like 1	152	1135	7.47	10.15	2.90	7.47	0.0004 716	2120.5 68
1387165_at	Maf	v-maf avian musculoaponeurotic fibrosarcoma oncogene homolog	275	1131	4.12	10.14	2.04	4.12	0.0137 978	72.475
1386282_x_at	Snrk	SNF related kinase	223	1131	5.07	10.14	2.34	5.07	0.0212 992	46.950
1382732_at	Lyve1	lymphatic vessel endothelial hyaluronan receptor 1	156	1130	7.23	10.14	2.85	7.23	2.47E- 05	40479. 024
1388763_at	Cnn2	calponin 2	266	1119	4.21	10.13	2.07	4.21	0.0003 467	2884.6 86
1377223_at	Wt1	Wilms tumor 1	49	1119	22.86	10.13	4.51	22.86	0.0016 841	593.77 3
1385354_at	Itga8	integrin, alpha 8	136	1117	8.20	10.13	3.04	8.20	0.0013 056	765.94 3
1387976_at	Slc9a3r2	solute carrier family 9, subfamily A (NHE3, cation proton antiporter 3), member 3 regulator 2	178	1115	6.25	10.12	2.64	6.25	0.0026 025	384.24 9
1390606_at	Hhip	Hedgehog-interacting protein	35	1102	31.31	10.11	4.97	31.31	0.0017 23	580.38 6
1372583_at	Tmtc1	transmembrane and tetratricopeptide repeat containing 1	128	1065	8.34	10.06	3.06	8.34	0.0001 293	7734.3 39
1389617_at	Elk3	ELK3, member of ETS oncogene family	176	1049	5.96	10.03	2.58	5.96	0.0031 35	318.97 5
1395978_at	Clec1a	C-type lectin domain family 1, member A	121	1033	8.50	10.01	3.09	8.50	0.0004 152	2408.5 76
1369968_at	Ptn	pleiotrophin	154	1031	6.68	10.01	2.74	6.68	0.0004 269	2342.2 80
1371527_at	Emp1	epithelial membrane protein 1	196	1023	5.22	10.00	2.39	5.22	0.0013 466	742.59 2
1376858_at	Exoc3l2	exocyst complex component 3-like 2	186	1021	5.50	10.00	2.46	5.50	5.75E- 05	17383. 458

1383372_at	Ptafr	platelet-activating factor receptor	158	1021	6.44	10.00	2.69	6.44	2.40E-06	416325.766
1369779_at	Myo1d	myosin ID	234	1016	4.34	9.99	2.12	4.34	0.0003167	3157.930
1385226_at	Kctd11	potassium channel tetramerization domain containing 11	127	1015	7.97	9.99	2.99	7.97	0.0254865	39.236
1383273_a_at	Pcbp3	poly(rC) binding protein 3	245	1002	4.08	9.97	2.03	4.08	0.0656498	15.232

Supplementary data Table 4: Gene list of Gene expression analysis from rat podocytes primary culture treated with PAN and cisplatin

Probe Set	Gene Symbol	Gene	Vehicle FC	Cisplatin 50 uM FC	Puromycin 0.1 mg/ml FC	Puromycin 1 mg/ml FC
1370912_at	Hspa1a	heat shock 70kD protein 1A	1	9.3672	1.8340	8.3946
1368247_at	Hspa1a Hspa1b	heat shock 70kD protein 1A heat shock 70kD protein 1B (mapped)	1	5.4542	1.4256	5.6690
1373767_at	Zfand2a	zinc finger, AN1-type domain 2A	1	3.2439	1.9577	2.8396
1386321_s_at	Trib3	tribbles pseudokinase 3	1	2.1687	1.3338	1.8518
1369590_a_at	Ddit3	DNA-damage inducible transcript 3	1	1.4230	1.0692	2.0800
1385620_at	Hsph1	heat shock 105/110 protein 1	1	1.5590	1.0883	1.6830
1395680_at	Sh3gl1	SH3-domain GRB2-like 1	1	1.6718	1.1442	1.3394
1394100_at	Ffar2	free fatty acid receptor 2	1	1.6514	1.2473	1.0352
1376504_at	Bai1	brain-specific angiogenesis inhibitor 1	1	1.2693	1.6322	1.0797
1388898_at	Hsph1	heat shock 105/110 protein 1	1	1.5595	1.0978	1.6016
1387434_at	Slc22a4	solute carrier family 22 (organic cation/zwitterion transporter), member 4	1	1.2432	1.2804	1.6011
1390332_at	Zfp692	zinc finger protein 692	1	1.5999	1.1073	-1.0315
1378560_at	Per2	period circadian clock 2	1	1.1268	1.5999	1.5254
1370695_s_at	Trib3	tribbles pseudokinase 3	1	1.5105	1.1495	1.4798

1370970_at	Kcnj14	potassium inwardly-rectifying channel, subfamily J, member 14	1	1.1789	-1.0063	1.5091
1377702_at	Lpar6	lysophosphatidic acid receptor 6	1	-1.1746	-1.0889	-1.5009
1370842_at	Bckdk	branched chain ketoacid dehydrogenase kinase	1	-1.1145	-1.5014	-1.1301
1368109_at	St3gal5	ST3 beta-galactoside alpha-2,3-sialyltransferase 5	1	-1.2052	-1.1150	-1.5135
1388600_at	Paqr8	progesterone and adipoQ receptor family member VIII	1	-1.1237	-1.0475	-1.5466
1373288_at	St5	suppression of tumorigenicity 5	1	-1.1701	-1.0881	-1.5545
1385969_at	Adamts16	ADAM metalloproteinase with thrombospondin type 1 motif, 16	1	-1.0155	-1.0548	-1.6276
1379026_at	Rhbdl3	rhomboid, veinlet-like 3 (Drosophila)	1	1.0166	-1.2699	-1.6370
1393762_at	Kat2b	K(lysine) acetyltransferase 2B	1	-1.5308	-1.2714	-1.6457
1390931_at	Adamts15	ADAM metalloproteinase with thrombospondin type 1 motif, 15	1	1.0200	1.0150	-1.7764
1377336_at	Sema3b	sema domain, immunoglobulin domain (Ig), short basic domain, secreted, (semaphorin) 3B	1	-1.4284	-1.0729	-1.7919
1371286_at	Plaur	plasminogen activator, urokinase receptor	1	-1.2973	-1.1181	-2.1228
1392647_at	Saal1	serum amyloid A-like 1	1	-1.4974	-1.3127	-2.2034

10. Bibliography

- Bailly, V., et al. (2002). "Shedding of kidney injury molecule-1, a putative adhesion protein involved in renal regeneration." J Biol Chem **277**(42): 39739-39748.
- Baines, R. J. and N. J. Brunskill (2008). "The molecular interactions between filtered proteins and proximal tubular cells in proteinuria." Nephron Exp Nephrol **110**(2): e67-71.
- Baston-Buest, D. M., et al. (2010). "The embryo's cystatin C and F expression functions as a protective mechanism against the maternal proteinase cathepsin S in mice." Reproduction **139**(4): 741-748.
- Behar, O., et al. (1999). "Semaphorin 3A growth cone collapse requires a sequence homologous to tarantula hanatoxin." Proc Natl Acad Sci U S A **96**(23): 13501-13505.
- Bokenkamp, A., et al. (2001). "Fetal serum concentrations of cystatin C and beta2-microglobulin as predictors of postnatal kidney function." Am J Obstet Gynecol **185**(2): 468-475.
- Bondeva, T., et al. (2009). "Advanced glycation end-products suppress neuropilin-1 expression in podocytes." Kidney Int **75**(6): 605-616.
- Bonventre, J. V. (2014). "Kidney injury molecule-1: a translational journey." Trans Am Clin Climatol Assoc **125**: 293-299; discussion 299.
- Boron, WF. and Boulapep, E.(2012). "Medical Physiology, 2nd edition." Publisher: Saunders. ISBN-13: 978-1437717532.
- Braun, F., et al. (2016). "Live or Let Die: Is There any Cell Death in Podocytes?" Semin Nephrol **36**(3): 208-219.
- Chen, S., et al. (2013). "Role of NADPH oxidase-mediated reactive oxygen species in podocyte injury." Biomed Res Int **2013**: 839761.
- Davies, D. J. and D. B. Brewer (1977). "Irreversible glomerular damage following heterologous serum albumin overload." J Pathol **123**(1): 45-52.
- Diamond, J. R., et al. (1986). "A role for oxygen free radicals in aminonucleoside nephrosis." Kidney Int **29**(2): 478-483.
- Dieterle, F., et al. (2010). "Urinary clusterin, cystatin C, beta2-microglobulin and total protein as markers to detect drug-induced kidney injury." Nat Biotechnol **28**(5): 463-469.
- Eddy, A. A. and C. M. Giachelli (1995). "Renal expression of genes that promote interstitial inflammation and fibrosis in rats with protein-overload proteinuria." Kidney Int **47**(6): 1546-1557.
- Edgington, T. S., et al. (1968). "Autologous immune complex nephritis induced with renal tubular antigen. I. Identification and isolation of the pathogenetic antigen." J Exp Med **127**(3): 555-572.
- Edgington, T. S., et al. (1967). "Characterization and isolation of specific renal tubular epithelial antigens." J Immunol **99**(6): 1199-1210.

- Eremina, V., et al. (2007). "Role of the VEGF--a signaling pathway in the glomerulus: evidence for crosstalk between components of the glomerular filtration barrier." Nephron Physiol **106**(2): p32-37.
- Eremina, V., et al. (2003). "Glomerular-specific alterations of VEGF-A expression lead to distinct congenital and acquired renal diseases." J Clin Invest **111**(5): 707-716.
- Eriksen, B. O., et al. (2012). "The role of cystatin C in improving GFR estimation in the general population." Am J Kidney Dis **59**(1): 32-40.
- Fan, L., et al. (2002). "Downregulation of vascular endothelial growth factor and its receptors in the kidney in rats with puromycin aminonucleoside nephrosis." Nephron **90**(1): 95-102.
- Flower, D. R. (1996). "The lipocalin protein family: structure and function." Biochem J **318 (Pt 1)**: 1-14.
- Foster, R. R., et al. (2003). "Functional evidence that vascular endothelial growth factor may act as an autocrine factor on human podocytes." Am J Physiol Renal Physiol **284**(6): F1263-1273.
- Fougeray, S. and N. Pallet (2015). "Mechanisms and biological functions of autophagy in diseased and ageing kidneys." Nat Rev Nephrol **11**(1): 34-45.
- Greka, A. and P. Mundel (2012). "Cell biology and pathology of podocytes." Annu Rev Physiol **74**: 299-323.
- Guan, F., et al. (2006). "Autocrine class 3 semaphorin system regulates slit diaphragm proteins and podocyte survival." Kidney Int **69**(9): 1564-1569.
- Hartleben, B., et al. (2010). "Autophagy influences glomerular disease susceptibility and maintains podocyte homeostasis in aging mice." J Clin Invest **120**(4): 1084-1096.
- Herrmann, A., et al. (2012). "Semi-automated quantitative image analysis of podocyte desmin immunoreactivity as a sensitive marker for acute glomerular damage in the rat puromycin aminonucleoside nephrosis (PAN) model." Exp Toxicol Pathol **64**(1-2): 45-49.
- Heymann, W., et al. (1959). "Production of nephrotic syndrome in rats by Freund's adjuvants and rat kidney suspensions." Proc Soc Exp Biol Med **100**(4): 660-664.
- Hogan, J. J., et al. (2015). "Drug-induced glomerular disease: immune-mediated injury." Clin J Am Soc Nephrol **10**(7): 1300-1310.
- Ichimura, T., et al. (1998). "Kidney injury molecule-1 (KIM-1), a putative epithelial cell adhesion molecule containing a novel immunoglobulin domain, is up-regulated in renal cells after injury." J Biol Chem **273**(7): 4135-4142.
- Inker, L. A. and A. Okparavero (2011). "Cystatin C as a marker of glomerular filtration rate: prospects and limitations." Curr Opin Nephrol Hypertens **20**(6): 631-639.
- Ishibashi, R., et al. (2016). "A novel podocyte gene, semaphorin 3G, protects glomerular podocyte from lipopolysaccharide-induced inflammation." Sci Rep **6**: 25955.

- Izzedine, H., et al. (2006). "Drug-induced glomerulopathies." Expert Opin Drug Saf **5**(1): 95-106.
- Kaplan, G., et al. (1996). "Identification of a surface glycoprotein on African green monkey kidney cells as a receptor for hepatitis A virus." EMBO J **15**(16): 4282-4296.
- Karayan-Tapon, L., et al. (2008). "Semaphorin, neuropilin and VEGF expression in glial tumours: SEMA3G, a prognostic marker?" Br J Cancer **99**(7): 1153-1160.
- Kaseda, R., et al. (2007). "Megalin-mediated endocytosis of cystatin C in proximal tubule cells." Biochem Biophys Res Commun **357**(4): 1130-1134.
- Katsuya, K., et al. (2006). "An improved method for primary culture of rat podocytes." Kidney Int **69**(11): 2101-2106.
- Kramer, A. B., et al. (2009). "Reduction of proteinuria in adriamycin-induced nephropathy is associated with reduction of renal kidney injury molecule (Kim-1) over time." Am J Physiol Renal Physiol **296**(5): F1136-1145.
- Kumar, V., et al. (2009). "Robin & Cotran Pathologic basis of disease (8th edition)." Publisher: Saunders, ISBN-13: 978-1416031215
- Kutschera, S., et al. (2011). "Differential endothelial transcriptomics identifies semaphorin 3G as a vascular class 3 semaphorin." Arterioscler Thromb Vasc Biol **31**(1): 151-159.
- Lawrence, G. M. and D. B. Brewer (1981). "Effect of strain and sex on the induction of hyperalbuminaemic proteinuria in the rat." Clin Sci (Lond) **61**(6): 751-756.
- Li, J. S., et al. (2015). "Angiopietin-Like-4, a Potential Target of Tacrolimus, Predicts Earlier Podocyte Injury in Minimal Change Disease." PLoS One **10**(9): e0137049.
- Lioudaki, E., et al. (2015). "Increased Urinary Excretion of Podocyte Markers in Normoalbuminuric Patients with Diabetes." Nephron **131**(1): 34-42.
- Liu, W., et al. (2015). "PPAR-gamma promotes endothelial cell migration by inducing the expression of Sema3g." J Cell Biochem **116**(4): 514-523.
- Luo, Y., et al. (1993). "Collapsin: a protein in brain that induces the collapse and paralysis of neuronal growth cones." Cell **75**(2): 217-227.
- Markowitz, G. S., et al. (2015). "Drug-induced glomerular disease: direct cellular injury." Clin J Am Soc Nephrol **10**(7): 1291-1299.
- McDuffie, J. E., et al. (2013). "Time course of renal proximal tubule injury, reversal, and related biomarker changes in rats following cisplatin administration." Int J Toxicol **32**(4): 251-260.
- Medic, B., et al. (2015). "Kidney Injury Molecule-1 and Cardiovascular Diseases: From Basic Science to Clinical Practice." Biomed Res Int **2015**: 854070.
- Mizushima, N., et al. (2004). "In vivo analysis of autophagy in response to nutrient starvation using transgenic mice expressing a fluorescent autophagosome marker." Mol Biol Cell **15**(3): 1101-1111.

- Mundel, P. and J. Reiser (2010). "Proteinuria: an enzymatic disease of the podocyte?" Kidney Int **77**(7): 571-580.
- Mussap, M. and M. Plebani (2004). "Biochemistry and clinical role of human cystatin C." Crit Rev Clin Lab Sci **41**(5-6): 467-550.
- Nagata, M. (2016). "Podocyte injury and its consequences." Kidney Int **89**(6): 1221-1230.
- Nejat, M., et al. (2012). "Albuminuria increases cystatin C excretion: implications for urinary biomarkers." Nephrol Dial Transplant **27 Suppl 3**: iii96-103.
- Niranjan, T., et al. (2008). "The Notch pathway in podocytes plays a role in the development of glomerular disease." Nat Med **14**(3): 290-298.
- Pabla, N. and Z. Dong (2008). "Cisplatin nephrotoxicity: mechanisms and renoprotective strategies." Kidney Int **73**(9): 994-1007.
- Pabla, N., et al. (2009). "The copper transporter Ctr1 contributes to cisplatin uptake by renal tubular cells during cisplatin nephrotoxicity." Am J Physiol Renal Physiol **296**(3): F505-511.
- Patrakka, J. and K. Tryggvason (2010). "Molecular make-up of the glomerular filtration barrier." Biochem Biophys Res Commun **396**(1): 164-169.
- Pippin, J. W., et al. (2009). "Inducible rodent models of acquired podocyte diseases." Am J Physiol Renal Physiol **296**(2): F213-229.
- Rahier, J., et al. (1989). "Determination of antigen concentration in tissue sections by immunodensitometry." Lab Invest **61**(3): 357-363.
- Ricono, J. M., et al. (2003). "Morphological insights into the origin of glomerular endothelial and mesangial cells and their precursors." J Histochem Cytochem **51**(2): 141-150.
- Ruifrok, A. C. and D. A. Johnston (2001). "Quantification of histochemical staining by color deconvolution." Anal Quant Cytol Histo **23**(4): 291-299.
- Sato, S., et al. (2006). "Autophagy by podocytes in renal biopsy specimens." J Nippon Med Sch **73**(2): 52-53.
- Sato, Y., et al. (2009). "Urine podocyte mRNAs mark progression of renal disease." J Am Soc Nephrol **20**(5): 1041-1052.
- Schramek, H., et al. (2009). "Neuropilin-1 and neuropilin-2 are differentially expressed in human proteinuric nephropathies and cytokine-stimulated proximal tubular cells." Lab Invest **89**(11): 1304-1316.
- Shankland, S. J. (2006). "The podocyte's response to injury: role in proteinuria and glomerulosclerosis." Kidney Int **69**(12): 2131-2147.
- Shankland, S. J., et al. (2014). "Progenitor cells and podocyte regeneration." Semin Nephrol **34**(4): 418-428.

- Shi, G. P., et al. (1999). "Cystatin C deficiency in human atherosclerosis and aortic aneurysms." J Clin Invest **104**(9): 1191-1197.
- Shimojo, H. (1998). "Adaptation and distortion of podocytes in rat remnant kidney." Pathol Int **48**(5): 368-383.
- Slauson, D. O. and R. M. Lewis (1979). "Comparative pathology of glomerulonephritis in animals." Vet Pathol **16**(2): 135-164.
- Suckow, M.A., et al. (2005). "The laboratory rat". Publisher: Academic Press. ISBN-13: 978-0120749034.
- Swenberg, J. A., et al. (1989). "The comparative pathobiology of alpha 2u-globulin nephropathy." Toxicol Appl Pharmacol **97**(1): 35-46.
- Takemoto, M., et al. (2006). "Large-scale identification of genes implicated in kidney glomerulus development and function." EMBO J **25**(5): 1160-1174.
- Taniguchi, M., et al. (2005). "Identification and characterization of a novel member of murine semaphorin family." Genes Cells **10**(8): 785-792.
- Tizon, B., et al. (2010). "Induction of autophagy by cystatin C: a mechanism that protects murine primary cortical neurons and neuronal cell lines." PLoS One **5**(3): e9819.
- Togashi, Y., et al. (2013). "Urinary cystatin C as a renal biomarker and its immunohistochemical localization in anti-GBM glomerulonephritis rats." Exp Toxicol Pathol **65**(7-8): 1137-1143.
- Togashi, Y. and Y. Miyamoto (2013). "Urinary cystatin C as a biomarker for diabetic nephropathy and its immunohistochemical localization in kidney in Zucker diabetic fatty (ZDF) rats." Exp Toxicol Pathol **65**(5): 615-622.
- Turk, V., et al. (2012). "Cysteine cathepsins: from structure, function and regulation to new frontiers." Biochim Biophys Acta **1824**(1): 68-88.
- van Timmeren, M. M., et al. (2006). "Tubular kidney injury molecule-1 in protein-overload nephropathy." Am J Physiol Renal Physiol **291**(2): F456-464.
- Vogelmann, S. U., et al. (2003). "Urinary excretion of viable podocytes in health and renal disease." Am J Physiol Renal Physiol **285**(1): F40-48.
- Weide, T. and T. B. Huber (2011). "Implications of autophagy for glomerular aging and disease." Cell Tissue Res **343**(3): 467-473.
- Wiggins, J. E., et al. (2005). "Podocyte hypertrophy, "adaptation," and "decompensation" associated with glomerular enlargement and glomerulosclerosis in the aging rat: prevention by calorie restriction." J Am Soc Nephrol **16**(10): 2953-2966.
- Winslow, R. M., et al. (1989). "Gas exchange properties of goat hemoglobins A and C." J Biol Chem **264**(9): 4812-4817.
- Xu, Y., et al. (2015). "Cystatin C is a disease-associated protein subject to multiple regulation." Immunol Cell Biol **93**(5): 442-451.

Xu, Y., et al. (2014). "Developmental regulation of synthesis and dimerization of the amyloidogenic protease inhibitor cystatin C in the hematopoietic system." J Biol Chem **289**(14): 9730-9740.

Yonezawa, A., et al. (2005). "Association between tubular toxicity of cisplatin and expression of organic cation transporter rOCT2 (Slc22a2) in the rat." Biochem Pharmacol **70**(12): 1823-1831.

Yoshida, S., et al. (2008). "Podocyte injury induced by albumin overload in vivo and in vitro: involvement of TGF-beta and p38 MAPK." Nephron Exp Nephrol **108**(3): e57-68.

Yu, H. H. and C. B. Moens (2005). "Semaphorin signaling guides cranial neural crest cell migration in zebrafish." Dev Biol **280**(2): 373-385.

Zhang, Z., et al. (2007). "Shedding of the urinary biomarker kidney injury molecule-1 (KIM-1) is regulated by MAP kinases and juxtamembrane region." J Am Soc Nephrol **18**(10): 2704-2714.

Zhao, X., et al. (2011). "Glomerular expression of kidney injury molecule-1 and podocytopenia in diabetic glomerulopathy." Am J Nephrol **34**(3): 268-280.

11. Curriculum Vitae of Valérie DUBOST

Work experience

Novartis Institute for Biomedical Research (Basel) – Preclinical Safety- Discovery and Investigative Pathology

2011-present: Lab Head - Molecular Histology Lab

2001-2011: Laboratory Associate - Molecular Histology Lab

Novartis Pharma (Basel) – Biomarker Development- RNA Analytics

1999 – 2001: Laboratory Associate - RNA Analytics Lab

Novartis Pharma (Basel) – Preclinical Safety – Experimental Toxicology

1995 – 1999: Laboratory associate - Dermatotoxicology Lab

Sandoz Pharma (Basel) – Drug Delivery System

1988 – 1995: Laboratory associate - *in vitro* and *in vivo* Drug Absorption Lab

Education

2016: PhD in Pharmaceutical Sciences at University of Basel (Switzerland)

2002: Master's degree in Pharmacology: "Drug metabolism and mechanism of action – Clinical pharmacology" at University of Sciences - Nancy (France).

2000 –2001: Bachelor's degree in Cell biology and physiology at University of Sciences - Besançon (France)

1984 –1986: Associate's degree in Biology at University of Sciences - Clermont-Ferrand (France).

Publications

First author / equal first author

Dubost V. et al.: Semaphorin 3G and Cystatin C are expressed in podocytes of rat and are differentially regulated upon injury (manuscript in preparation)

Pantano S, **Dubost V**, Darribat K, Couttet P, Grenet O, Busch S, Moulin P: Differential expression of dipeptidyl peptidase IV in human versus cynomolgus monkey skin eccrine sweat glands. *J Mol Histol.* (2013) 44(6):733-47.

V. Picarles-Dubost, K.Laurent, O.Grenet : De l'expression des gènes à la visualisation sur coupes : principe et technique de l'hybridation *in situ*. *Rev. Fr. Histotechnol.* (2004) , vol 17, n°1, p.85-93.

Additional publications

Vitobello A., Pouche L., Romer M., Glogovac M., MacLeod K., Ellinger-Ziegelbauer H., Westphal M., **Dubost V.**, Stiehl D., Dumotier B., Fekete A., Moulin P., Zell A., Schwarz M., Moreno R., Huang J., Elcombe C., Henderson C., Wolf R. Moggs J., Terranova R.: Xenobiotic CAR activators induce Dlk1-Dio3 locus non-coding RNA expression in mouse liver. (manuscript submitted)

Uteng, M., Mahl, A., Beckmann, N., Piaia, A., Ledieu, D., **Dubost, V.**, Tritto, E., Wolf, A., Moulin, P., Li, L., Chibout, S. Pognan, F.: Comparative renal safety assessment of the hepatitis B drugs, adefovir, tenofovir, telbivudine and entecavir in rats. *Toxicol. Sci.* (2017) 155 (1): 283-297.

Luisier R, Lempiäinen H, Scherbichler N, Braeuning A, Geissler M, **Dubost V**, Müller A, Scheer N, Chibout SD, Hara H, Picard F, Theil D, Couttet P, Vitobello A, Grenet O, Grasl-Kraupp B, Ellinger-Ziegelbauer H, Thomson JP, Meehan RR, Elcombe CR, Henderson CJ, Wolf CR, Schwarz M, Moulin P, Terranova R, Moggs JG. : Phenobarbital induces cell cycle transcriptional responses in mouse liver humanized for constitutive androstane and pregnane x receptors. *Toxicol Sci.* (2014) Jun;139(2):501-11

Kinzel B, Pikiólek M, Orsini V, Sprunger J, Isken A, Zietzling S, Desplanches M, **Dubost V**, Breustedt D, Valdez R, Liu D, Theil D, Müller M, Dietrich B, Bouwmeester T, Ruffner H, Tchorz JS.: Functional roles of Lgr4 and Lgr5 in embryonic gut, kidney and skin development in mice. *Dev Biol.* (2014) Jun 15;390(2):181-90

Vliegenthart AD, Starkey Lewis P, Tucker CS, Del Pozo J, Rider S, Antoine DJ, **Dubost V**, Westphal M, Moulin P, Bailey MA, Moggs JG, Goldring CE, Park BK, Dear JW.: Retro-orbital blood acquisition facilitates circulating microRNA measurement in zebrafish with paracetamol hepatotoxicity. *Zebrafish*. (2014) Jun;11(3):219-26

Hoffmann P, Bentley P, Sahota P, Schoenfeld H, Martin L, Longo L, Spaet R, Moulin P, Pantano S, **Dubost V**, Lapadula D, Burkey B, Kaushik V, Zhou W, Hayes M, Flavahan N, Chibout SD, Busch S.: Vascular origin of vildagliptin-induced skin effects in Cynomolgus monkeys: pathomechanistic role of peripheral sympathetic system and neuropeptide Y. *Toxicol Pathol*. (2014) Jun;42(4):684-95

Vacchi-Suzzi C, Hahne F, Scheubel P, Marcellin M, **Dubost V**, Westphal M, Boeglen C, Büchmann-Møller S, Cheung MS, Cordier A, De Benedetto C, Deurinck M, Frei M, Moulin P, Oakeley E, Grenet O, Grevot A, Stull R, Theil D, Moggs JG, Marrer E, Couttet P : Heart structure-specific transcriptomic atlas reveals conserved microRNA-mRNA interactions. *PLoS One*. (2013) 8(1):e52442. doi: 10.1371/journal.pone.0052442.

Lempiäinen H, Couttet P, Bolognani F, Müller A, **Dubost V**, Luisier R, Del Rio Espinola A, Vitry V, Unterberger EB, Thomson JP, Treindl F, Metzger U, Wrzodek C, Hahne F, Zollinger T, Brasa S, Kalteis M, Marcellin M, Giudicelli F, Braeuning A, Morawiec L, Zamurovic N, Längle U, Scheer N, Schübeler D, Goodman J, Chibout SD, Marlowe J, Theil D, Heard DJ, Grenet O, Zell A, Templin MF, Meehan RR, Wolf RC, Elcombe CR, Schwarz M, Moulin P, Terranova R, Moggs JG: Identification of Dlk1-Dio3 imprinted gene cluster noncoding RNAs as novel candidate biomarkers for liver tumor promotion. *Toxicol Sci*. (2013) 131(2):375-86.

J. Medina, **V. Picarles**, B. Greiner, C. Elsaesser, M. Kolopp, A. Mahl, D. Roman, B. Vogel, P. Nussbaumer, A. Winiski, J. Meingassner, A. de Brugerolle de Fraissinette: LAV694, a new antiproliferative agent showing improved skin tolerability vs. clinical standards for the treatment of actinic keratosis. *Biochem Pharmacol*. (2003) 15;66(10): 1885-95.

Chibout SD, De Brugerolle De Fraissinette A, Hartmann N, **Picarles V**, Grenet O, Cordier A, Molloy S, Medina J: Vitamin D(3) 24-hydroxylase mRNA expression in the skin of calcipotriol-treated psoriatic patients correlates with clinical efficacy. *Arch Dermatol Res*. (2003) Sep 23.

Medina J, Elsaesser C, **Picarles V**, Grenet O, Kolopp M, Chibout SD, de Brugerolle de Fraissinette A: Assessment of the phototoxic potential of compounds and finished topical products using a human reconstructed epidermis. *In Vitro Mol Toxicol*, (2001) 14(3):157-68.

A. de Brugerolle de Fraissinette, **V. Picarles**, S. Chibout, M. Kolopp, J. Medina, P. Burtin, M.E. Ebelin, S. Osborne, F.K. Mayer, A. Spake, M. Rosdy, B. De Wever, R.A. Ettlin and A. Cordier : Predictivity of an in vitro model for acute and chronic skin irritation (SkinEthic®) applied to the testing of topical vehicles. *Cell Biology and Toxicology*, (1999) 15: 121-135.

Fricker G, **Dubost V**, Schwab D, Bruns C, Thiele C: Heterogeneity in hepatic transport of somatostatin analog octapeptides. *Hepatology*, (1994) 20(1 Pt 1):191-200.

Fricker G, **Dubost V**, Finsterwald K, Boyer JL: Characteristics of bile salt uptake into skate hepatocytes. *Biochem J*, (1994) 299 (Pt 3):665-70.